THE UNIVERSITY OF MICHIGAN

INDUSTRY PROGRAM OF THE COLLEGE OF ENGINEERING

THE CONSTANT VOLUME HEAT CAPACITIES OF GASEOUS PERFLUOROCYCLOBUTANE AND PROPYLENE

Noel H. de Nevers

A dissertation submitted in partial fulfillment
of the requirements for the degree of
Doctor of Philosophy in the
University of Michigan
1958

December, 1958
IP-342

erm

UMRC790

ACKNOWLEDGEMENTS

Numerous people and groups have helped the author immensely; to them he would like to express his gratitude.

Professor Joseph J. Martin, his committee chairman, first interested him in this research, and helped him over many of the difficulties in it. The other members of his committee, Professors Banchero, Ragone, Thatcher and Westrum gave freely of their advice and help.

Mr. Yu-Tang Hwang assisted in the construction and operation of the experimental equipment. Assistant Professor James R. Black of the Electrical Engineering Department helped in the design and fabrication of the electrical lead seals. Various members of the staff of the Chemical and Metallurgical Engineering Department helped on many details of the project.

The Faculty Research and Equipment Fund of the University of Michigan provided most of the necessary funds for this research. The National Science Foundation supported the author by means of fellowships during his tenure as a graduate student. The Industry Program of the College of Engineering assisted in the figure preparation, typing and printing of this dissertation. The following companies supplied materials at no cost: E. I. du Pont de Nemours & Co., The General Motors Corporation, The Anaconda Wire & Cable Co., Chemo-Textiles Incorporated.

TABLE OF CONTENTS

TABLE OF CONTENTS (CONT'D)

LIST OF TABLES

LIST OF FIGURES

LIST OF FIGURES (CONT'D)

INTRODUCTION

Masi[22] has succinctly introduced the field of gas calorimetry as follows:

> "The specific heat is one of the most important thermodynamic properties of pure substances, and at the same time it is one of those measurable in the laboratory to a degree of confidence proportional to the expenditure of care and the refinement of technique. In the particular case of gases, accurate heat-capacity measurements, at several pressures and over a range of temperatures, are valuable in at least two ways: (a) They may be extrapolated to zero pressure at the several temperatures to obtain a set of values of the ideal-gas heat capacities. For gases of any complexity the heat capacities thus obtained frequently may be used to decide questions of structure or vibrational frequency. Once a reliable set of molecular constants is available, the zero-pressure thermodynamic properties may be calculated over a temperature range far larger than that of the heat-capacity experiments. (b) The values obtained for the change of heat capacity with pressure may be an order of magnitude more accurate than the same quantity calculated from data of state of good accuracy. Thus there is provided an opportunity to check or modify existing equations of state."

Comparison of Constant-Pressure and Constant-Volume Calorimetry

Flow calorimetry, the measurement of the constant-pressure heat capacity of gases, C_p, at various temperatures and pressures has reached a high state of development. As early as 1924, a flow calorimeter was built by Osborne, Stimson and Sligh[27] which produced heat capacity data reliable to plus or minus 0.1%. Constant-volume calorimetry, the measurement of the heat capacity of gases at constant volume, C_v, has not been equally well developed.

The fundamental problem which has hindered progress in constant-volume calorimetry may be illustrated by briefly considering the direct methods for measuring C_p and C_v. A flow calorimeter, for measuring C_p,

consists in principle of a tube, in which a measured, steady flow of gas is maintained. The temperature of the gas is determined at two points of the tube, between which points the temperature of the gas is raised by adding a known amount of heat. The apparatus operates at steady state, i.e., measurements are made when temperature is not changing with respect to time at any place in the system. Because only the gas is changing temperature, the heat capacity of the tube and accessory apparatus does not enter the calculations, nor affect the accuracy of the results. Constant-volume calorimetry, however, must be carried out in a closed vessel of fixed volume. The method is applied to liquids and solids by placing a container of sample, together with a heater and a thermometer, in adiabatic surroundings. The temperature is measured, a known amount of heat is added, and the temperature is again measured. This method requires that the heat capacity of the container and accessory apparatus be known, since this must be subtracted from the measured heat capacity to obtain the heat capacity of the substance under investigation. When the method of constant-volume calorimetry has been applied to gases at low pressures the heat capacity of the container and accessory apparatus has been many times that of the contained gas. When the heat capacity of the container, etc., is twenty times that of its contents - see for example Hoge[14] - an error of 1% in the overall heat capacity of the calorimeter plus its contents leads to an error of 20% in the heat capacity of the gas. As the pressure of the gas is increased, the mass of the contained gas increases; so does the mass of the container, designed to withstand the pressure with an adequate margin of safety. One obvious way to improve existing C_V calorimetry is to find ways of lowering the

heat capacity of the calorimeter and accessory apparatus without sacrificing overall accuracy.

The zero-pressure heat capacity at constant volume, C_v^*, is readily calculated from the corresponding zero-pressure heat capacity at constant pressure C_p^* by the relation $C_v^* = C_p^* - R$, where R is the universal gas constant. Since C_p^* can be determined in a flow calorimeter to an accuracy of about 0.1%, there has never existed much interest in direct measurement of C_v^*. However, as a criterion for the accuracy of an equation of state, or as a check on state data, C_v data over a range of temperatures and densities are more useful than C_p data.

The Objectives of this Research

The purpose of this research was to explore the possibility of directly measuring C_v as a function of temperature and density. The method chosen was adiabatic calorimetry. All efforts were directed toward having the lowest possible calorimeter heat capacity, for a given volume and pressure rating. The objectives were:

1. to design, build, and test an accurate, adiabatic C_v calorimeter of the lowest possible heat capacity;
2. to collect data on C_v as a function of temperature and density over as wide a range of these variables as practical, for several gases; in particular data were to be collected as near to the critical state as possible; and
3. to compare these data with the available state data and the available equations of state.

THEORETICAL BACKGROUND

The Relation Between the Constant Volume Heat Capacity and State Behavior

The following is an exact thermodynamic relation for a single phase of a pure substance. From it stems the great utility of C_v as a check on state data and equations of state:

$$\left(\frac{dC_v}{dV}\right)_T = -\rho^2\left(\frac{dC_v}{d\rho}\right)_T = T\left(\frac{d^2P}{dT^2}\right)_V \qquad (1)$$

where V is the specific volume, T is the absolute temperature, P is the pressure and ρ is the density. This relation is derived in Appendix D, page 132.

The significance of Equation (1) is best explained with reference to the state data for a single pure substance, as shown on a pressure-temperature plot. A typical plot of this type is shown in Figure 1, page 5. On this plot PVT (pressure-specific volume-temperature) data are shown by drawing lines of constant specific volume (or constant density), on a pressure-temperature plane. These lines of constant specific volume, called isochores (or isometrics) all end in the vapor-pressure curve, which represents the states of equilibrium between liquid and vapor. For a single phase of one component, fixing any two independent variables fixes the state completely, so that for a fixed specific volume, P can be represented as function of T alone. The isochores represent this function.

Equations of state are algebraic relations between P, V and T. They are constructed to represent the experimental PVT data as accurately

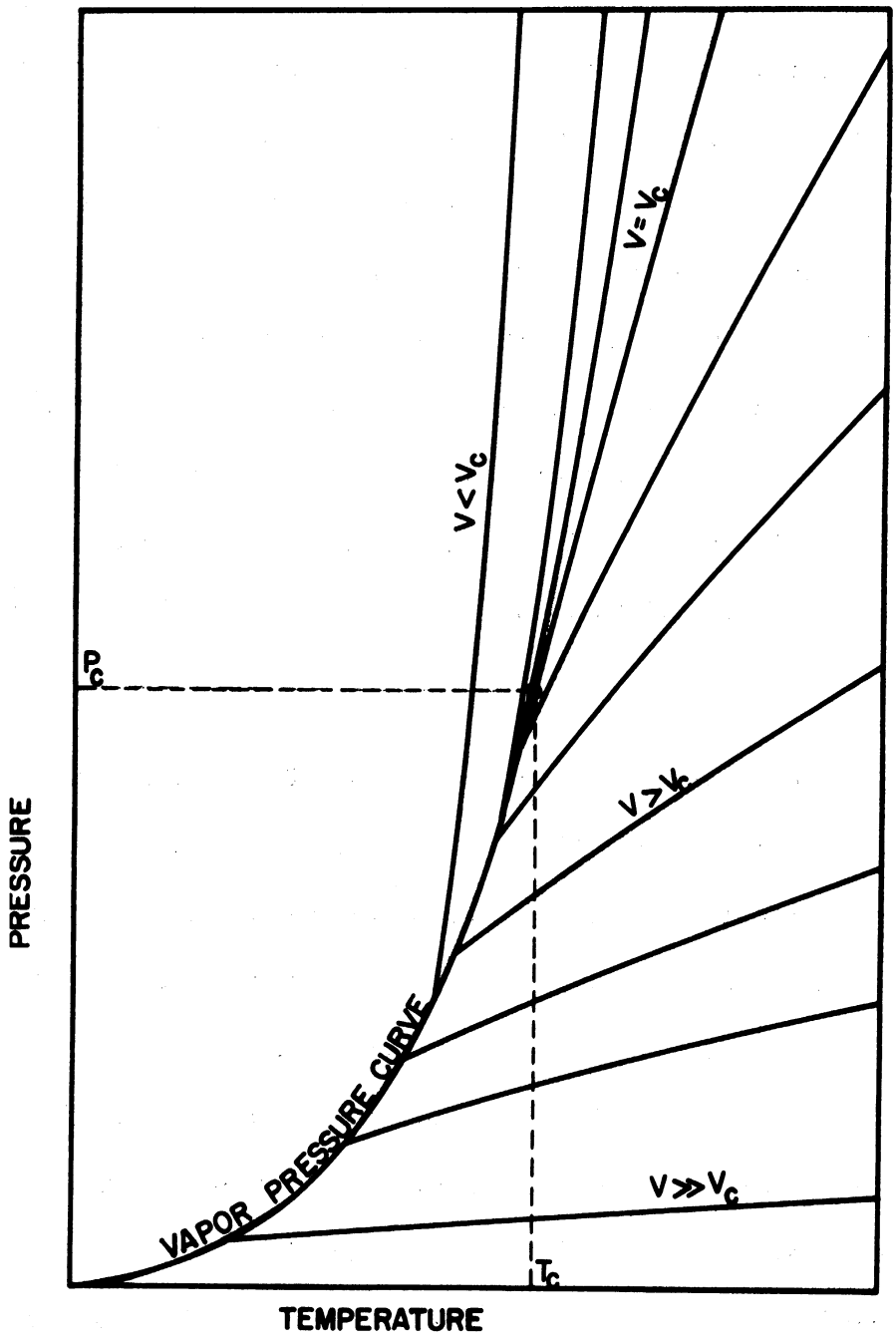

Figure 1. A Typical Pressure-Temperature Plot

as possible. When such an equation has been constructed, it may be used to interpolate accurately between measured PVT points, and to compute the various partial derivatives of P, V and T with respect to one another. Furthermore, because of the similarity between various substances, an equation which satisfactorily represents the PVT relations of one substance can be adjusted to represent the PVT relations of similar substances, or in some cases of quite dissimilar substances. Thus equations of state may be used to predict PVT data which have not been measured.

Two common forms of equations of state are $P = f(V,T)$ and $V = f(P,T)$. For either of these forms, when V is held constant, i.e., for an isochore, a relation $P = f(T)$ results. The earliest equations of state used a linear relation, e.g.,

$$P = A + BT \quad \text{or} \quad P = BT \tag{2}$$

where A and B are constants. Using relations of this sort it is possible to represent wide ranges of PVT data with errors no greater than plus or minus several percent. The most accurate PVT data, however, show that most of the isochores are not straight, but slightly curved. (Very low specific volume isochores, very high specific volume isochores and isochores very near to the critical density appear to be straight or nearly so - all other isochores appear to be slightly curved.) This curvature is borne out by the available C_v data. If the isochores were all straight, $(d^2P/dT^2)_V$ would be zero, as would $(dC_v/dV)_T$. Hence C_v would not be a function of specific volume; experimental data show that C_v varies with varying specific volume. Modern equations of state represent most of the isochores as being curved. Three relations which have been used to

represent $P = f(T)$ for an isochore are:

$$P = A + BT + \frac{C}{T^2} \tag{3}$$

$$P = A + BT + \frac{C}{T^4} \tag{4}$$

and

$$P = A + BT + C \exp(-DT) \tag{5}$$

where A, B, C and D are arbitrary constants. All of these forms show increasing curvature with decreasing temperature, which is in accord with the PVT data.

Determining the proper curvature of an isochore from the PVT data is difficult; it requires two differentiations of state data. According to Equation (1) the same curvature can be determined by a single differentiation of C_v data. If the available PVT data and C_v data are of the same order of accuracy, then the latter method should yield more accurate results.

The heat capacity at constant pressure, C_p, is also useful in checking state data, by means of the relation

$$\left(\frac{dC_p}{dP}\right)_T = -T\left(\frac{d^2V}{dT^2}\right)_p \tag{6}$$

However, $(d^2V/dT^2)_p$ is not as directly applicable to the problems of constructing an equation of state as is $(d^2P/dT^2)_V$. Furthermore, near the critical state C_p increases without limit, so that it cannot be used to check state data in this region. C_v remains finite in the region near

the critical point, so that its utility for checking state data and equations of state is greater than that of C_p.

Using Equation (1) and the fact that C_v is equal to C_v^* at zero density it is possible to calculate $C_v - C_v^*$ from state data or equations of state. In Appendix F, page 139, the representation of $C_v - C_v^*$ by several equations of state is shown. All but one of the equations considered represent $C_v - C_v^*$ as the product of two functions, one of which is dependent only on density, and the other of which is dependent only on temperature, i.e.,

$$C_v - C_v^* = f(T) \cdot f(\rho) \tag{7}$$

Thus, according to these equations of state, the various isotherms on a $C_v - C_v^*$ vs. density plot must be a series of similar curves; given any isotherm it must be possible to construct any other isotherm by multiplying the ordinates of the first isotherm by a constant multiplier. If one isotherm is linear, all must be linear; if one is parabolic, all must be parabolic, etc.

The form of the density function in Equation (7) determines the shape of the isotherms on a $C_v - C_v^*$ vs. density plot. The types of density functions used by several equations are; Berthelot equation

$$C_v - C_v^* = f(T) \cdot \rho \tag{8}$$

Beattie-Bridgeman equation

$$C_v - C_v^* = f(T) \cdot (A\rho + B\rho^2 - C\rho^3) \tag{9}$$

Benedict-Webb-Rubin equation

$$C_V - C_V^* = f(T)\cdot\left[A\rho + B\left\{2\exp(-C\rho^2) - 2 + C\rho^2\exp(-C\rho^2)\right\}\right] \quad (10)$$

and Martin-Hou equation

$$C_V - C_V^* = f(T)\cdot\left[\frac{A\rho}{(1-\rho B)} - \frac{C\rho^2}{(1-\rho B)^2} + \frac{D\rho^4}{(1-\rho B)^4}\right] \quad (11)$$

where in the above A, B, C, and D are arbitrary constants all of which are positive. Here and in the remainder of this section, A, B, C, etc., have been used for simplicity in place of more complicated expressions using the nomenclature peculiar to each equation. In Appendix F, these relations are written out in the nomenclature of each equation.

The Berthelot equation predicts that on a C_V-C_V^* vs. density plot the isotherms must be straight lines through the origin. The Beattie-Bridgeman equation predicts each isotherm by the cubic equation shown. The shape of the isotherms predicted by the Benedict-Webb-Rubin and Martin-Hou equations is not obvious, but may be seen from the following analysis. The direction of curvature, upward or downward, of an isotherm is determined by the sign of $(d^2C_V/d\rho^2)_T$ at that density. Using Equation (1)

$$\left(\frac{d^2C_V}{d\rho^2}\right)_T = \frac{d}{d\rho_T}\left[\frac{-T}{\rho^2}\left(\frac{d^2P}{dT^2}\right)_\rho\right] = T\left[\frac{2}{\rho^3}\left(\frac{d^2P}{dT^2}\right)_\rho - \frac{1}{\rho^2}\left(\frac{d^3P}{dT^2 d\rho_T}\right)\right] \quad (12)$$

The Benedict-Webb-Rubin equation predicts

$$\left(\frac{d^2C_v}{d\rho^2}\right)_T = f(T)\cdot\left[A\left\{\exp(-B\rho^2)\right\}(-1-C\rho^2+D\rho^4)\right] \qquad (13)$$

where A, B, C, and D are positive constants. Equation (13) is negative at low densities and positive at high densities, so that the Benedict-Webb-Rubin equation predicts isotherms which curve downward at low densities and upward at high densities. The Martin-Hou equation predicts

$$\left(\frac{d^2C_v}{d\rho^2}\right)_T = f(T)\cdot\left[\frac{-A}{(1-\rho B)^3} + \frac{C\rho^3}{(1-\rho B)^5} - \frac{D\rho}{(1-\rho B)^4} + \frac{E\rho^3}{(1-\rho B)^6}\right] \qquad (14)$$

where A, B, C, D, and E are positive constants. Equation (14) also is negative at low densities and positive at high densities, so that the Martin-Hou equation predicts isotherms which have the same general curvature as those predicted by the Benedict-Webb-Rubin equation.

As mentioned previously, the best available state data indicates that for densities near the critical density, $(d^2P/dT^2)_V$ is zero, so that $(dC_v/d\rho)_T$ must also be zero and the isotherms on a C_v-C_v^* vs. density plot must have a horizontal tangent at or near the critical density. The latter three equations mentioned predict that $(d^2P/dT^2)_V$ is zero at or near the critical density[3,4,19]. Using the curvatures at low density and at high density, and the horizontal tangent at or near the critical density, it is possible to sketch a typical C_v-C_v^* vs. density isotherm for the Martin-Hou equation, and the Benedict-Webb-Rubin equation. This has been done in Figure 2, page 11. Also shown in this

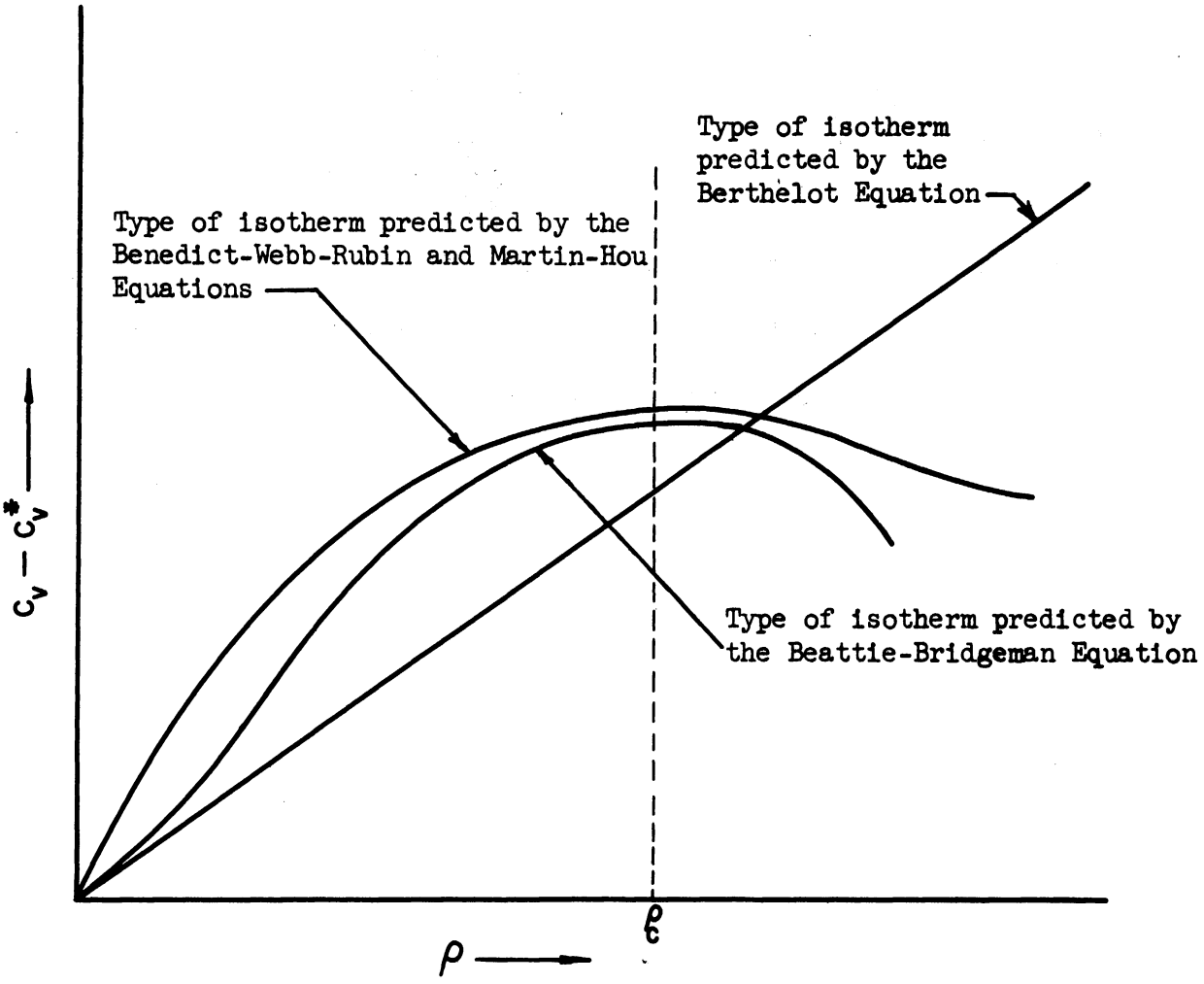

Figure 2. Types of Isotherm on a C_v-C_v^* vs. Density Plane Predicted by Several Equations of State

figure are typical isotherms predicted by the Berthelot and Beattie-Bridgeman equations.

The Relation Between the Constant Volume Heat Capacity and the Speed of Sound

The following is an exact thermodynamic relation for a single phase of one component

$$c = V\left(\frac{dP}{dT}\right)_V \left(\frac{T}{C_V}\right)^{1/2} \left\{1 - \frac{\left(\frac{C_V}{T}\right)\left(\frac{dP}{dV}\right)_T}{\left(\frac{dP}{dT}\right)_V^2}\right\}^{\frac{1}{2}} \qquad (15)$$

where c is the speed of sound. This relation is derived in Appendix D, page 132. Equation (15) makes it possible to determine C_V from measurements of the speed of sound and state data.

PRIOR WORK IN CONSTANT VOLUME CALORIMETRY

Calorimetric Measurements of the Constant Volume Heat Capacity

In 1894, Joly[15] made the first recorded measurements of C_v. Working with a differential steam calorimeter, he measured the C_v of carbon dioxide over the range of temperatures from room temperature to 100°C and over a low pressure range. While his data are only of historical interest, he did correctly conclude that for the range he considered, C_v increased with increasing temperature and increased with increasing density.

Dieterici[8] measured the heat capacities of carbon dioxide and isopentane. His measurements were made on a two-phase system, so that his experimental results were the two-phase saturated heat capacity, $C_{sat}^{g,l}$. His work was done with a Bunsen ice calorimeter. By means of the PVT data of Young[40] he made the necessary calculational corrections to his experimental data so that he was able to present it in the form of the heat capacity of the saturated liquid C_{sat}^{l} and as C_v.

Reinganum[33] compared Dieterici's measured C_v values with those calculated from the PVT data of Amagat[1] and Young[40]. He found that the agreement was good except near the critical point. He postulated from the available data that C_v as a function of density for a constant temperature would exhibit a maximum near the critical density. Examination of the best available PVT data has led all subsequent investigators to agree with this postulate. Most modern equations of state (see Figure 2) show this behavior.

As is seen from Figure 1, in the region near the critical state, the rate of change of density with temperature and pressure is very great,

so that many isochores crowd into a very small area on a P-T plot. In order to clarify the PVT behavior of substances in this region, several attempts have been made to measure C_v near the critical state.

Bennewitz and Splittgerber[5] constructed a calorimeter to measure the C_v of carbon dioxide near the critical point. The calorimeter was a steel vessel placed in an evacuated space and surrounded by a water bath of constant, fixed temperature. The temperature of the calorimeter was measured by resistance thermometry, and heat was added electrically. The heat capacity of the calorimeter was about 18 calories/degree C, while that of the contents varied from 7 to 29 calories/degree C. Most of Bennewitz and Splittgerber's data were taken in the two-phase region below the critical temperature. By means of the available PVT data the C_v of the liquid and the C_v of the gas were computed from the experimental data. The conclusions of the research were that $(dC_v/dV)_T$ is zero at the critical point, and that just below the critical temperature both the C_v of the liquid phase and the C_v of the gas phase have negative values. No subsequent workers have observed negative values of C_v. Keenan[16] points out why negative values of C_p are impossible in a stable system. His reasoning applies equally well to C_v, which implies that Bennewitz and Splittgerber's work must be in error.

Pall, Broughton and Maass[29] used an adiabatic calorimeter to measure the C_v of ethylene. They were interested in "hysteresis" effects near the critical state. Using only one density (the critical density) they measured C_v as a function of temperature. They found a difference of up to 3% between the heat capacity measured when the gas had been heated from below the critical state before a heat capacity experiment,

and the heat capacity measured at the same temperature when the gas had been cooled from well above the critical temperature before an experiment. Their results are shown in Figure 3, page 16 . Although the "hysteresis" effect appears small, Pall et al., insisted that it was real, and not the result of scatter, or experimental errors. The heat capacity of their calorimeter was about 40 calories/degree C, while that of its contents was 5 to 8 calories/degree C.

Michels and Strijland[24] constructed a differential calorimeter, and measured the C_v of carbon dioxide over a considerable range of temperatures and densities. Theirs has been the only research to date which has presented a comprehensive picture of the relations between C_v, temperature and density for any substance. Their calorimeter consisted of two identical containers, of which only one was filled with gas. To each of the containers was supplied an identical amount of heat in the form of electrical energy, and from the resulting difference in their temperature rise the heat capacity of the contents of the filled container was computed. They compared the measured C_v of carbon dioxide with that computed from PVT data. (Their method of computing C_v from PVT data is discussed in Appendix F, page 139). For temperatures and densities well removed from the critical temperature and density, the agreement was satisfactory. For the critical temperature they found that near the critical density C_v increased to values far in excess of those predicted from the PVT data. Their results are shown in Figure 4, page 17 .

This high value of C_v near the critical point is of great interest. First, it must be noted that it is extremely difficult to determine the heat capacity accurately in this region, and the possibility

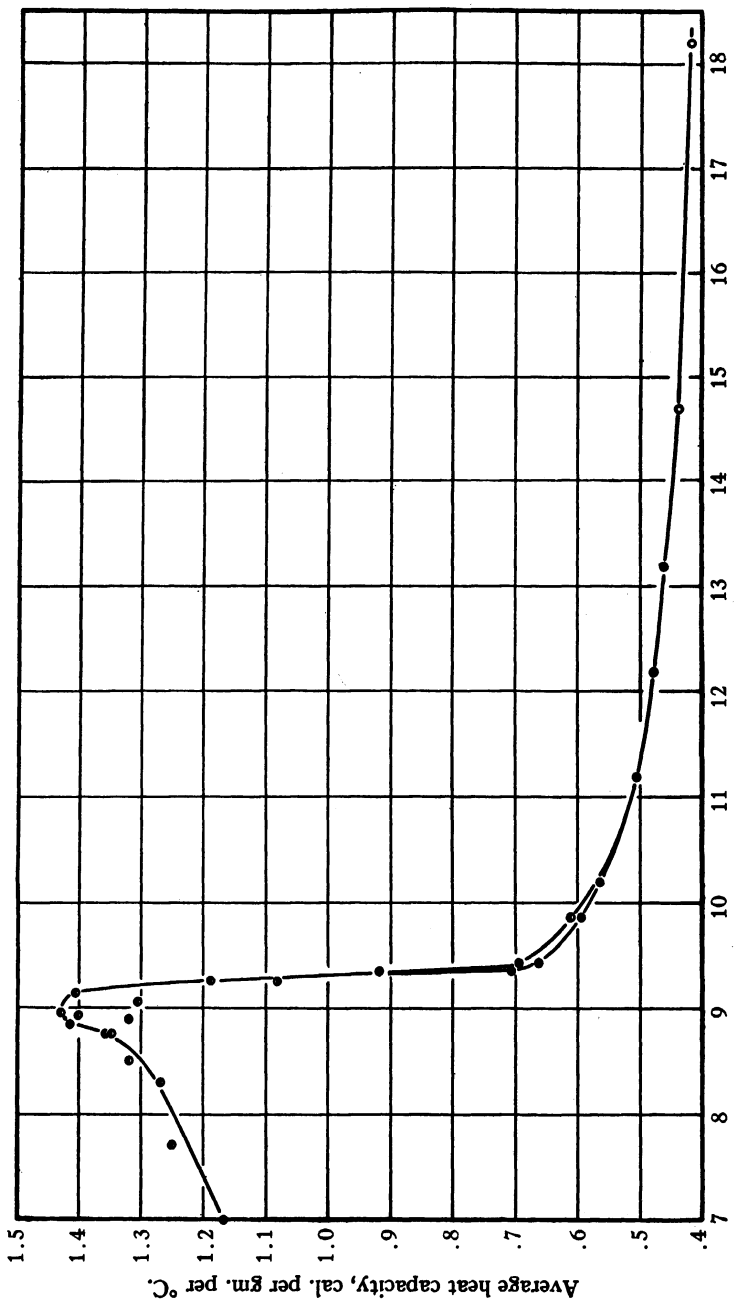

Heat capacity of ethylene, 7 to 18° C. Average density, 0.2255. ●, Temperature brought up from 8° or below before run started. ◒, Temperature brought down from above 15° before run started.

Figure 3. Pall, Broughton and Maass' C_v Data

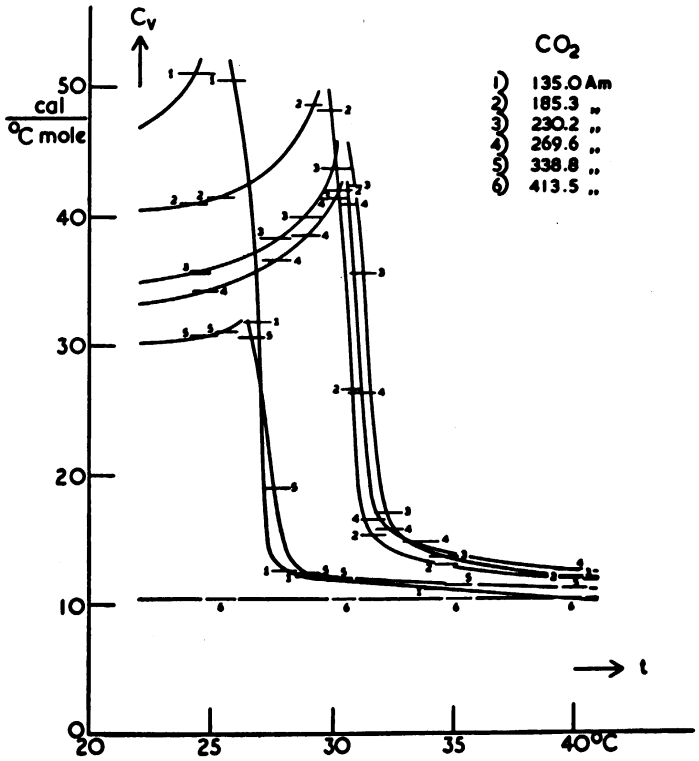

Specific heat of carbon dioxide as a function of temperature for six different densities.

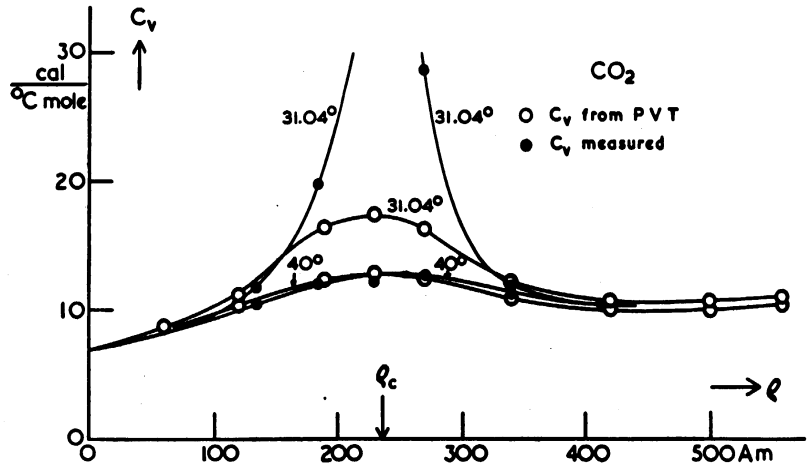

Specific heat of carbon dioxide as a function of density.

Figure 4. Michels' and Strijland's C_v Data
Density is given in Amagat units. (1 Am = 0.0019768 gm/cc)

exists that Michels and Strijland's data are in error just as those of Bennewitz and Splittgerber[5] must be. If Michels and Strijland's data are correct, then either:

1. the isochores on a P-T plot (Figure 1) in the region near the critical are much more strongly curved than the PVT measurements of them have indicated, or

2. one phase thermodynamic relations do not hold in this region. (The work of Pall et al.,[29] suggests this.)

Hoge[14] measured the $C_{sat}^{g,l}$ and C_v of oxygen, in an apparatus designed for vapor pressure measurements. He was primarily interested in determining if $C_{sat}^{g,l}$ and C_v measurements could be used to determine the boundary of the two-phase region more accurately than the boundary can be determined by PVT measurements. His suggestion was based on the fact that for a given mass of substance contained in a fixed volume container $C_{sat}^{g,l}$ is much larger than C_v. Hence, the measured heat capacity undergoes a marked drop when the substance passes from two phases to one. This effect is well illustrated in Figures 3 and 4. In view of the exploratory nature of his work, he did not feel that he had answered the question completely; his tentative answer was that near the critical density, $C_{sat}^{g,l}$ and C_v measurements should be as reliable as PVT measurements for determining the boundary of the two-phase region, and that the former should be easier to carry out. The heat capacity of Hoge's calorimeter was about twenty times that of its contents.

Eucken and Hauck[10] have made some C_{sat}^{l} and C_v measurements on argon, carbon dioxide, ethane and air in the liquid and supercritical region, using an adiabatic calorimeter. The heat capacity of the

calorimeter was five to eight times that of its contents. Eucken and Hauck stated that the purpose of their work was "to increase our deficient knowledge of heat capacities" in this region.

Sage et al.,[6] have made numerous measurements of $C_{sat}^{g,l}$ in order to determine the heat capacity of the saturated liquid. In their work the density of the two-phase mixture was chosen so that the overwhelming majority of the heat added was expended in heating the liquid phase. The corrections for the gas phase heat capacity and for the heat of vaporization, made from available PVT data were small. In the work of Sage et al., the heat capacity of the calorimeter was about one-half that of its contents. The two calorimeters used by Sage et al., for $C_{sat}^{g,l}$ measurements were the only constant-volume calorimeters to date which used mechanical stirring to obtain temperature uniformity; all others relied upon conduction of heat through their heavy metal walls. In one calorimeter used by Sage et al., this stirring was provided by rocking the entire calorimeter, so that the liquid moved about within it, in the other an internal stirrer was driven by an external motor, whose shaft entered the calorimeter through a rotary shaft seal. The energy input due to the stirrer was accounted for in calculating the heat capacity of the calorimeter plus contents.

Constant Volume Heat Capacity from Speed of Sound Measurements

The high values of C_v at the critical point, which had been determined calorimetrically led Curtiss, Boyd and Palmer[7], to attempt to verify these values by measurements of the speed of sound at the critical point. The relation between C_v and the speed of sound is given

by Equation (15), page 12 . At the critical state $(dP/dV)_{T_C}$ is zero, so that Equation (15) may be simplified to:

$$c = V_c \left(\frac{dP}{dT}\right)_{V_c} \left(\frac{T_c}{C_v}\right)^{\frac{1}{2}} \qquad (16)$$

If the critical volume, critical temperature, and the slope of the vapor pressure curve at the critical point are known, then a measurement of c determines C_v. Curtiss et al., measured the speed of sound at the critical point for carbon dioxide and ethylene. Their computed value for the C_v of carbon dioxide at the critical point was 18.2 cal./gm mole °C, compared with Michels and Strijland's calorimetric value of about 50 cal./gm mole °C. Their value for the C_v of ethylene at the critical point was 17.2 cal./gm mole °C, compared with the calorimetric value of Pall et al., about 39 cal./gm mole °C.

Schneider and Chynoweth[35], noting the above results, stated that the determination of C_v by speed of sound measurements at the critical point could not be made correctly. They maintained that although $(dP/dV)_{T_C}$ is indeed zero at the critical temperature for static measurements, it is not zero for the small adiabatic pressure changes caused by the movement of a sound wave. Hence, they claimed that although Equation (15) is true, the substitution of $[(dP/dV)_{T_C} = 0]$ at the critical point is not justified, and that Equation (16) cannot be relied upon. If $(dP/dV)_{T_C}$ were non-zero, it would be negative, so that for a given c, a non-zero $(dP/dV)_{T_C}$ would imply a higher value of C_v than that corresponding to a zero value of $(dP/dV)_{T_C}$.

Methods of Measuring the Constant Volume Heat Capacity at Low Pressure

Two methods of measuring C_v have been proposed which could only be applied at low pressures. Schaefer[34] proposed a method based on measuring the rate of heat loss from an electrically heated wire at sub-atmospheric pressures. He showed theoretically that this heat loss rate was a function of $\alpha(C_v + R/2)$ where α is the accommodation coefficient and R is the universal gas constant. His experimental device was designed to measure accommodation coefficients, but he claimed that it would also produce C_v values as a by-product. No values have been published, nor compared with those obtained from C^*_p measurements. Trautz and Grosskinsky[38] proposed a method based on measuring the increase in pressure of a gas with an input of heat, as compared with the increase in pressure of a gas of known heat capacity for the same heat input. This method depends on numerous questionable assumptions; a critique of it is given by Partington and Shilling[28].

EXPERIMENTAL APPARATUS AND MATERIALS

In all previous C_v calorimetry the gas container has been very heavy relative to the mass of substance contained. This is the normal consequence of the high pressure of gases at high densities. The novel idea of this research has been to construct a calorimeter whose container would have as low a heat capacity as possible. Normal design procedures require that the highest expected wall stress in a pressure vessel should not exceed 1/3 to 1/5 of the yield stress of the material used. In this research a calorimeter was designed in which, at the maximum contemplated pressure, the wall stress would equal the yield stress of the material. Under these conditions it was necessary to provide shielding to prevent injuries and damage in the case of rupture of the calorimeter. Thus, the heat capacity of the calorimeter was limited to about 110 calories/degree C; the heat capacity of the contents of the calorimeter was a minimum of 80 calories/degree C and a maximum of 610 calories/degree C.

Because the calorimeter had a fixed heat capacity, while the heat capacity of the contents was variable, the accuracy of the calorimeter, which was a function of the ratio of heat capacity of calorimeter to heat capacity of contents, was variable. In principle, it would be desirable to have an infinite number of calorimeters, one for each infinitesimal pressure range, so that each measurement could be made just below the bursting pressure of the calorimeter. In this way, all the data would be taken under conditions of optimum accuracy. In practice, it may be desirable to have several calorimeters with different rated pressures; for this research only one was used. Its design pressure was arbitrarily set at 1000 psi.

The lower working temperature limit was chosen as room temperature, so that no refrigeration equipment would be necessary. There is no reason why lower temperatures may not be used, if the experimenters are willing to face the added complexities involved. The upper temperature limit was originally chosen as 250°C. The availability of higher-temperature gasketing materials was considered the limiting factor. Later, when it was found necessary to include a motor-stirrer in the calorimeter, the upper working temperature limit of the motor, 150°C, became the upper working temperature limit of the calorimeter. A motor with an upper working temperature limit of 200°C has been procured for future work; it was not available when the calorimeter used for this research was constructed.

The Calorimeter

The calorimeter itself was a gas container, inside of which were placed a thermometer-heater and a motor-stirrer. Figure 5, page 24, is a cross section of the calorimeter, adiabatic shield and vacuum container. Many of the details described below are illustrated on it.

The calorimeter shell was a sphere; the spherical shape was chosen because it is the most efficient, on the basis of lowest mass of container material for a given volume and pressure. The sphere was made of two hemispheres, Aro Equipment Corporation #13577. These hemispheres had an inside diameter of 8.015 inches and a wall thickness of 0.031 inches. They were cold drawn from sheets of type 304 extra low carbon stainless steel. The hemispheres were joined by Heliarc fusion welding. After assembly the exterior of the sphere was copper plated to reduce heat transfer by radiation. The welding and plating were done by the Aro

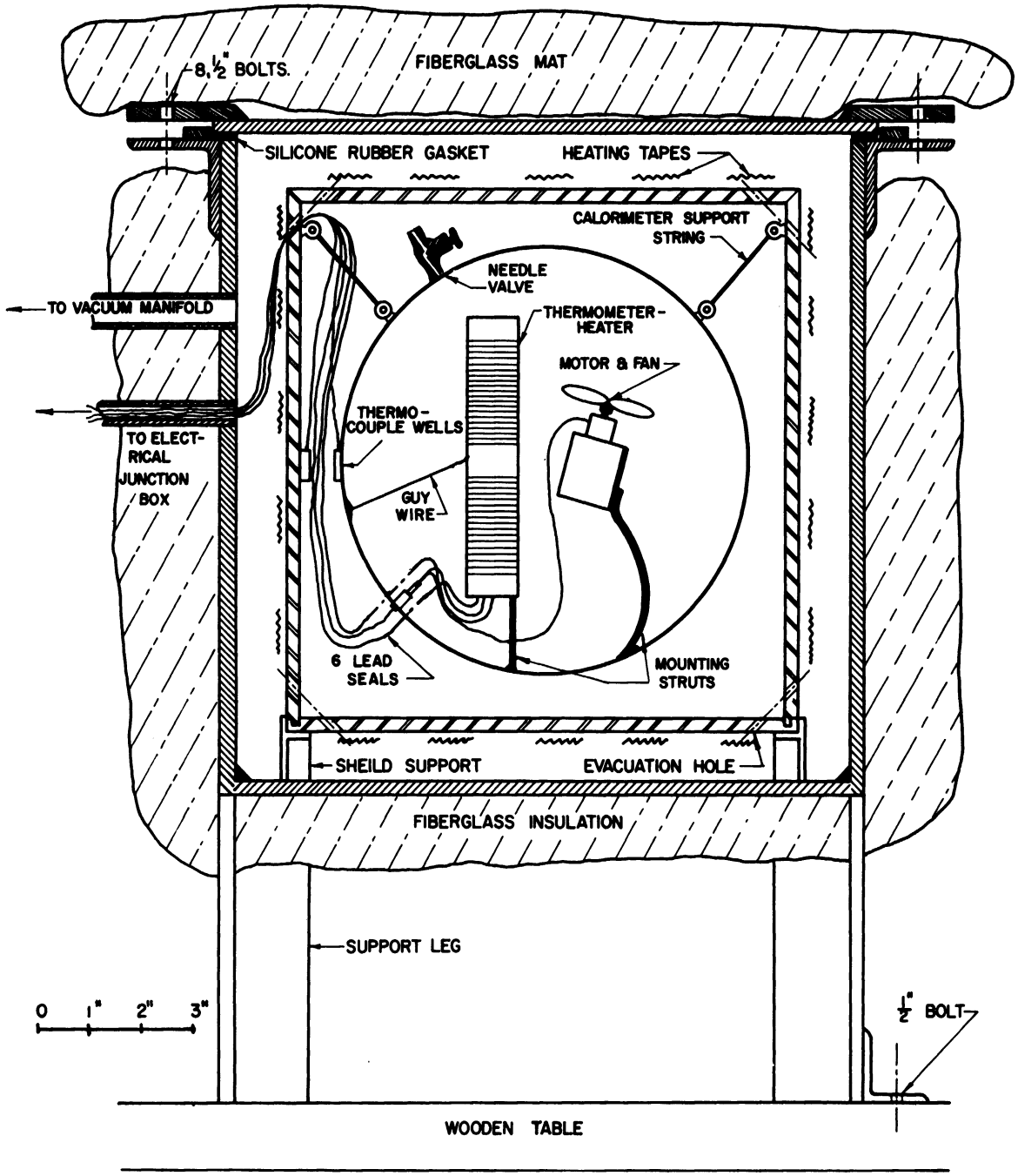

Figure 5. Cross-Section of the Calorimeter Assembly

Equipment Corporation. According to the standard formula for the wall stress in a thin-walled spherical pressure vessel, under internal pressure

$$\text{stress} = (\text{pressure})(\text{diameter})/4\ (\text{wall thickness}). \qquad (17)$$

For a pressure of 1000 psi, a diameter of 8.015 inches and a wall thickness of 0.031 inches, the resulting stress is 64,500 psi. This was considered a good estimate of the yield stress of the steel used. In the fully work-hardened condition it could have a yield stress of up to 200,000 psi, but considering the annealing effects of the weld, 64,500 psi seemed a reasonable figure.

For loading and unloading the calorimeter a stainless steel needle valve, Hoke #321, was silver-soldered into the wall of the calorimeter. Three small brass rings were silver-soldered to the top of the calorimeter for mounting purposes.

The first calorimeter had no motor-stirrer; natural convection was relied upon to produce uniform temperatures. Temperature differences of up to 5 degrees C were measured on the surface of this calorimeter. These temperature differences made it impossible to control the heat leakage from the calorimeter to its surroundings. The final calorimeter had a motor-stirrer, which limited these measured temperature differences to 0.2 degrees C, under which conditions heat transfer to the surroundings could be controlled. The motor was Delco #5067043. It operated on 3 to 12 volts D.C. The motor speed varied with voltage, gas density and gas viscosity; it was always sufficient to keep the temperature differences on the surface of the calorimeter below 0.2 degrees C. Six 1/8 inch diameter holes were drilled in the outer shell of the motor to improve its

cooling, and to speed the attainment of thermal equilibrium between the motor and the gas. The stirrer was a propeller 2-1/2 inches long, made of 3/32 inch thick stainless steel sheet, with a 1/4 inch diameter stainless steel rod for a hub.

During heating periods the motor and the thermometer-heater were connected electrically in series. About 3/4 of the energy input was dissipated by the thermometer-heater, and about 1/4 of the energy input was dissipated by the motor.

The motor was mounted on a 1/16 inch thick brass plate, which was silver-soldered to two 1/8 inch diameter copper wires, which in turn were silver-soldered to the inside of the sphere. The thermometer was mounted on a strut made of the same 1/8 inch diameter copper wire; and was protected from lateral movement by three 30 gauge Chromel guy wires. Both the strut and the three guy wires were silver-soldered to the inside of the sphere. Figure 6, page 27 , shows the lower half of the calorimeter before the joining of the two hemispheres. The guy wires to the thermometer, and the heavy copper lead wires to the motor are visible, as are two of the motor cooling holes mentioned previously.

All electrical wiring inside the calorimeter was made of 20 gauge copper wire, so that the wires would be stiff enough to avoid contacting one another or the side of the sphere. This eliminated the need for insulation. All internal wiring connections were made either with silver solder or with Belmont #5951 lead-silver alloy. The latter has a melting range of 306-365°C. This solder was also used for all connections within the vacuum container.

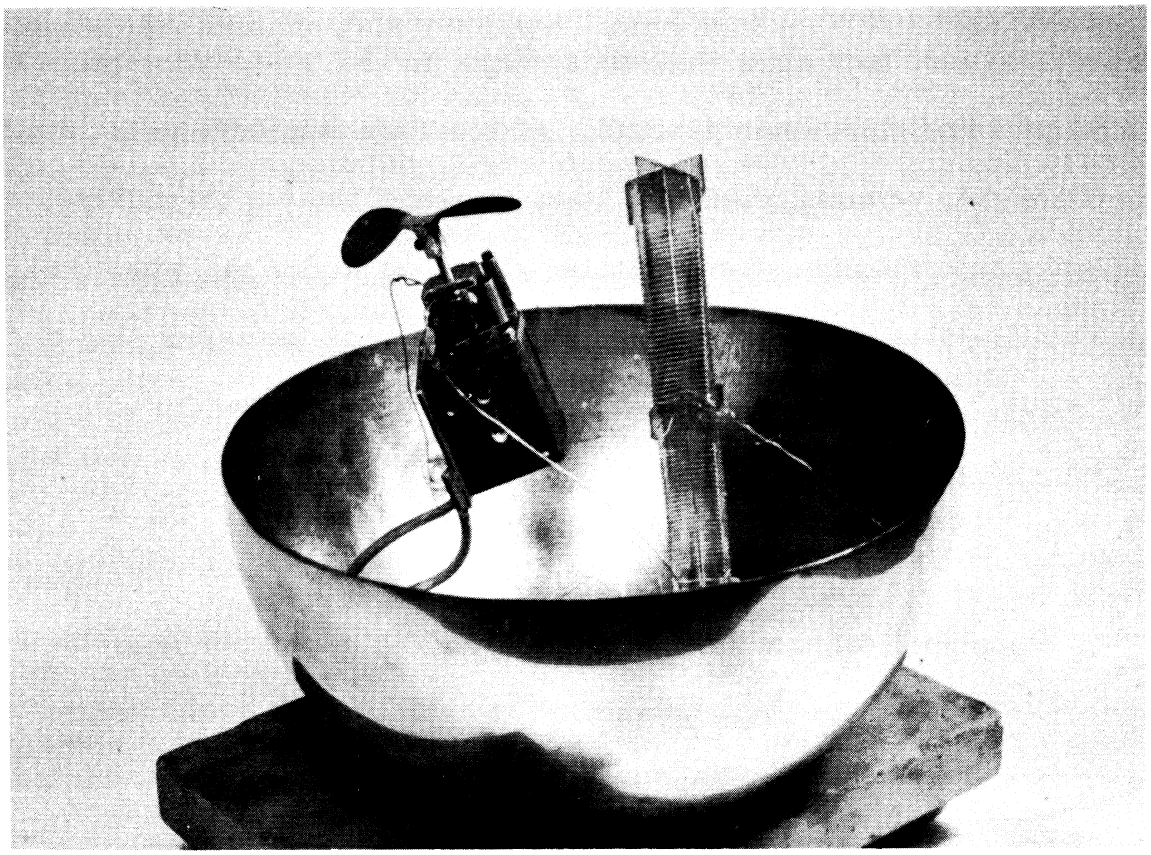

Figure 6. View of Lower Half of the Unassembled Calorimeter

The six electrical leads (4 from the thermometer, 2 from the motor) left the calorimeter through kovar-glass seals. These seals were made by the Electron Tube Laboratory of the University of Michigan. Figure 7, page 29, is a cross section of one of these seals. The seals were silver-soldered into the wall of the calorimeter. The long part of the seal was inside the calorimeter; the pressure within the calorimeter produced a compressive stress in the glass. Had the seals been installed in the reverse direction, the internal pressure would have produced a tensile stress in the glass, which would have been less satisfactory. These seals were made after numerous attempts to use the readily available Stupakoff kovar glass seals #95.0001. Although the Stupakoff seals seemed ideal for this purpose, cracks and leaks developed because the silver-soldering imposed undue stresses in the glass. After the seals had been made and installed it was brought to the attention of the author that a very similar seal could be obtained from the Advanced Vacuum Products Company, Advac #ES-250.

The Thermometer-Heater

In most calorimeters the thermometer and heater are separate devices. In this calorimeter a combined thermometer-heater was used in order to simplify the design and construction of the calorimeter. The thermometer-heater was made by winding 9 feet of 36 gauge platinum wire bifilarly on a mica cross. The cross was 5-1/2 inches long, with each piece 7/8 inch wide. The winding was done on two notched sections, each 2 inches long; the notches were 1/16 inch deep. The notches were made by clamping the mica sheet between two notched brass templates, and filing away the excess mica. The mica cross was made of two pieces 3

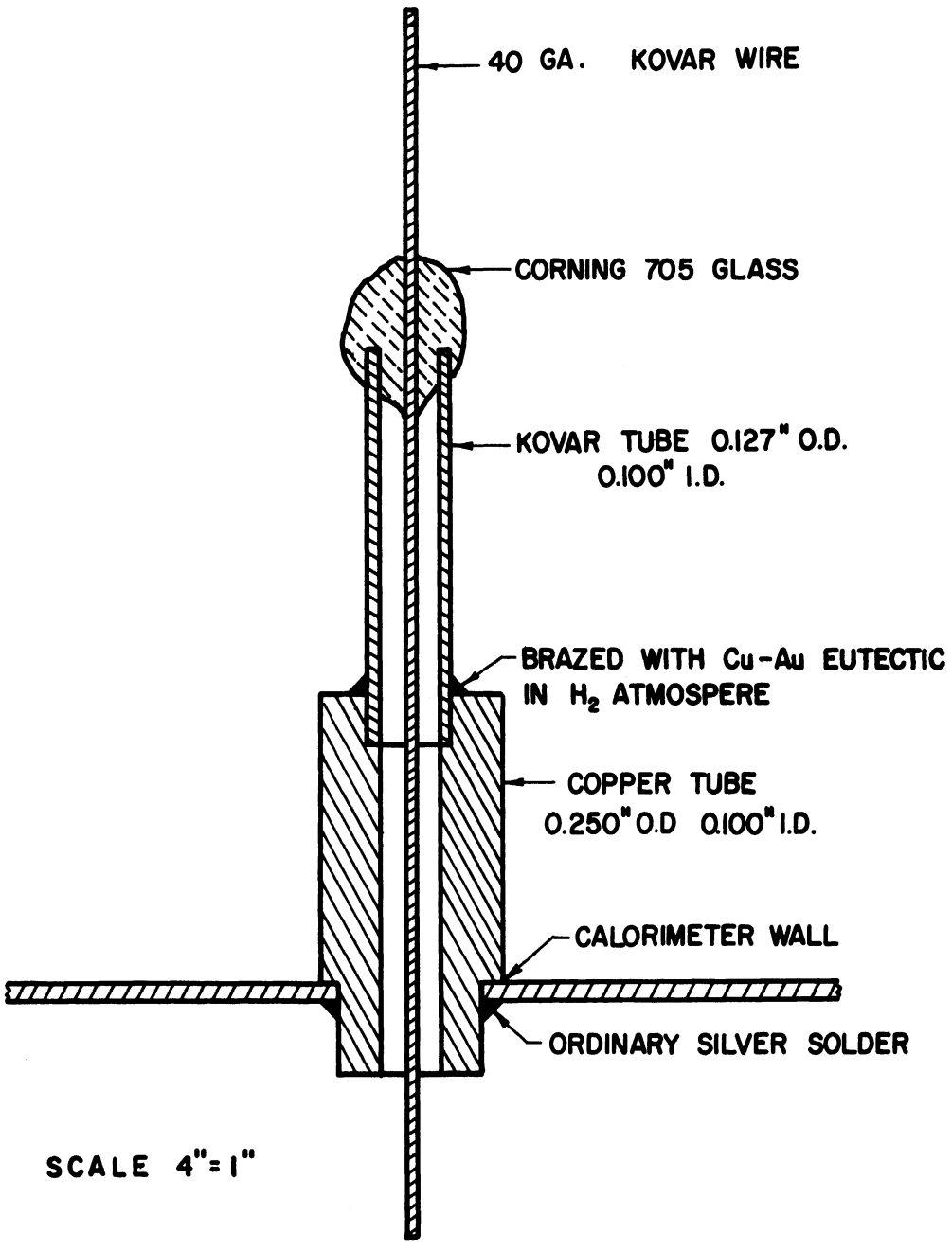

Figure 7. Cross-Section of a Lead Seal

inches long, slotted, and inserted into matching slots in the ends of one piece of mica 5-1/2 inches long. The pieces were wired together with 30 gauge Chromel wire for strength and rigidity. These construction wires did not contact the platinum wires, nor did the guy wires used for mounting. At the base of the thermometer-heater was a circular mica disc 1 inch in diameter, which was wired to the end of the cross with 30 gauge Chromel wire. To it were anchored four 24 gauge copper wires. These wires were joined, in pairs, by silver-soldering to the ends of the platinum wire, to form the four leads of the thermometer-heater. Many of these construction details are visible on Figure 6.

Before winding on the mica cross, the platinum wire was annealed, to reduce its stiffness, by connecting it across a 110 volt A.C. line for an hour. At this voltage the wire glowed a dull orange. After the wire had been wound on the mica cross, it was again annealed to remove the strains imposed by winding. This was done by again connecting it across 110 volts A.C. for 48 hours. After this treatment it was found that the resistance of the thermometer-heater at the ice point was not significantly changed by additional annealing periods of 24 hours. After the annealing the resistance as a function of temperature was calibrated: this calibration is discussed in Appendix C, page 130.

This design of thermometer-heater was chosen instead of the designs used in commercially available platinum resistance thermometers because of its open construction. It was imperative for its use as a heater that it be able to transfer large quantities of heat to the gas surrounding it, without large temperature differences. As a thermometer it had to come to rapid thermal equilibrium with the gas. None of the

commercial thermometer designs were of sufficiently open construction to meet these requirements.

The Adiabatic Shield

To reduce the heat transfer to and from the calorimeter by radiation, the calorimeter was surrounded by an adiabatic shield, whose temperature was maintained as close as possible to that of the calorimeter. This shield was a cubical box of six copper plates, each 10 inches square and 1/4 inch thick. The four side plates were silver soldered together at the corners of the box to insure good thermal contact between them. The side plates had a lip machined on their lower edge, which fitted into a matching groove in the bottom plate. The tops of the side plates were beveled, as were the edges of the top plate, so that the top plate fitted snugly into place. To the inner surface of the plates a layer of aluminum foil was attached, using a light coating of vacuum grease as an adhesive. The purpose of the foil was to lower the emissivity of the plates for radiant heat transfer. Eight 1/4 inch diameter holes were drilled in each plate near its edges, to facilitate evacuation. The electrical leads to the calorimeter were brought through these holes. The calorimeter was held in place within the adiabatic shield by three glass strings, to the ends of which steel hooks were attached. The strings ran from the three brass rings silver-soldered to the top of the calorimeter, to three rings correspondingly placed on the adiabatic shield.

The adiabatic shield was heated by "Briskeat" brand electrical heating tapes, which were attached to its outer surface. One 190 watt (at 115 volts) heating tape was attached to each of the six plates. The tapes were tied with glass string to small screws which had been inserted

into holes drilled in the outside of the plate. No attempt was made to place the tapes in thermal contact with the plates; heat transfer from the tapes to the plates was almost entirely by radiation. The four side plate heaters were controlled by supplying power to them in parallel from a "Powerstat" variable voltage transformer. The top and bottom plate heaters were controlled by separate individual "Powerstat" variable transformers. The circuit diagram of the heaters is shown in Figure 8, page 33.

The Thermocouples

The temperature differences between the plates of the adiabatic shield and corresponding points on the surface of the calorimeter were measured by means of copper-constantan differential thermocouples. These thermocouples also measured differences in temperature between various points on the surface of the calorimeter. Six thermocouples were installed, one each at the top, side and bottom of the calorimeter and in the centers of the top, bottom and one of the side plates of the adiabatic shield. The constantan wires were all brought to a common junction, at a point within the vacuum container. The six copper wires left the vacuum system through the electrical lead system. By measuring the difference in EMF between any two of the copper wires, it was possible to determine the difference in temperature between any two of the six control points. In practice, five such temperature differences were observed; top of calorimeter to top of shield, side of calorimeter to side of shield, bottom of calorimeter to bottom of shield, top of calorimeter to side of calorimeter and side of calorimeter to bottom of calorimeter.

After leaving the vacuum system, the six copper wires were brought to a junction board, from which the desired combinations were

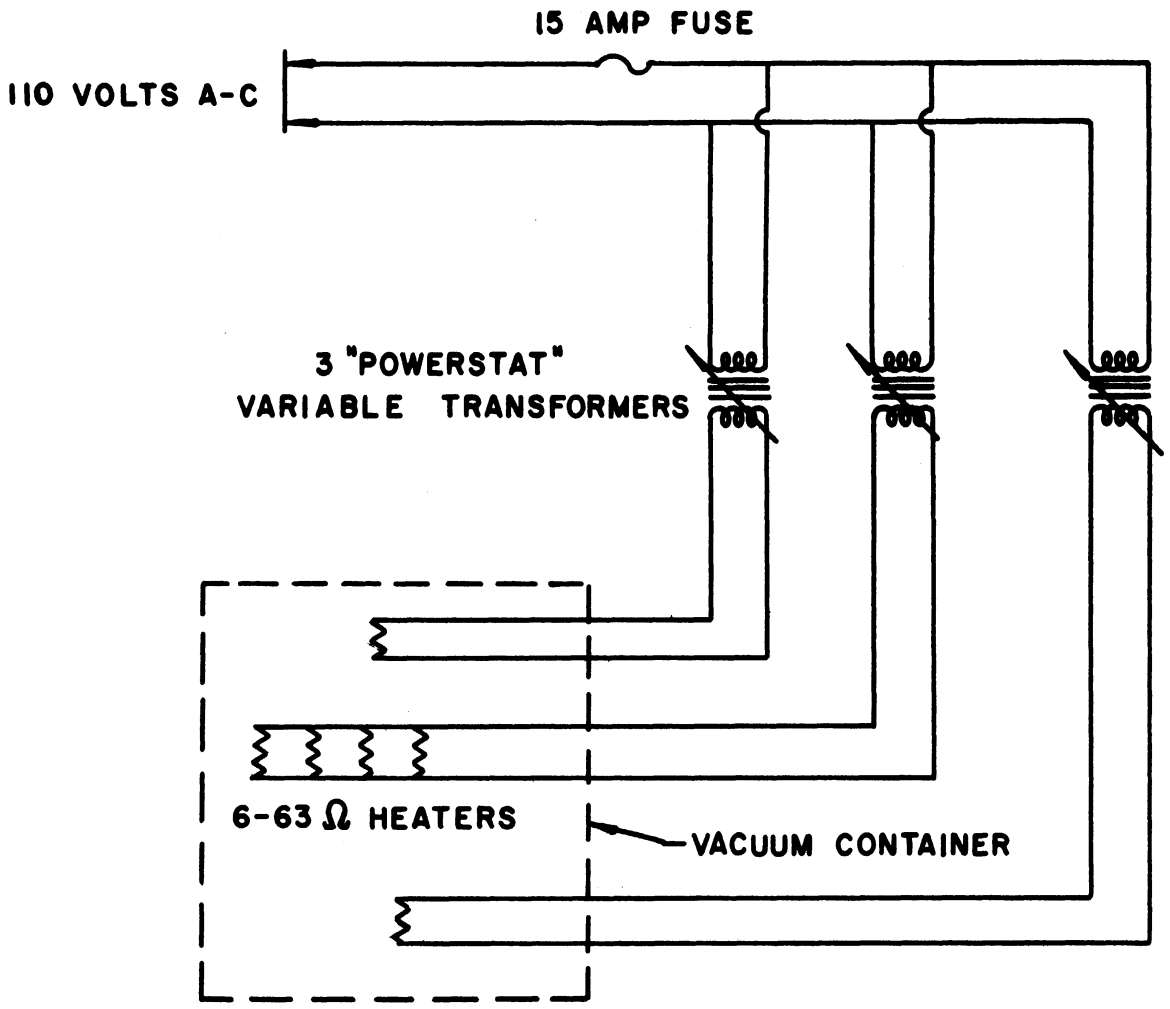

Figure 8. Circuit Diagram of Heaters

selected. These combinations were led to an eleven-point, double-pole selector switch, Leeds and Northrup type 8240, #1210525, from which the EMF of the desired combination was led to the galvanometer which is described below. Because the thermocouple EMF's were frequently too large for the galvanometer, arrangements were made to add 1,000; 10,000; and 100,000 ohm resistors in series with the galvanometer. Of these only the 1,000 ohm resistor was used frequently. Figure 9, page 35, is the circuit diagram of the thermocouple system. The circuit involved no reference junction, because only differences in temperature were measured, not temperatures themselves. Based on the published data for copper-constantan thermocouples and for the galvanometer, it was computed that one millimeter of galvonometer scale corresponded to 1/50 degree C.

Because it was necessary to place the thermocouples in thermal contact with the various surfaces, without placing them in electrical contact, insulated thermocouple wells were constructed. The wells were made of brass rods, 0.125 inches in diameter and 1/2 inch long. Axially in each rod a 0.050 inch diameter hole was drilled. One side of each rod was filed flat to within 0.010 inch of the axial hole. The rods were soft-soldered into place on their flat sides, using ample solder to insure good thermal contact. Teflon tubing 0.052 inches in outside diameter and 0.030 inches in inside diameter was coated with vacuum grease and forced into the axial holes in the rods. The insides of the tubes were filled with vacuum grease using a hypodermic syringe, and the thermocouples were forced into the tubes.

The Vacuum Container

In order to eliminate heat transfer by convection, and to minimize heat transfer by conduction, the calorimeter and adiabatic shield

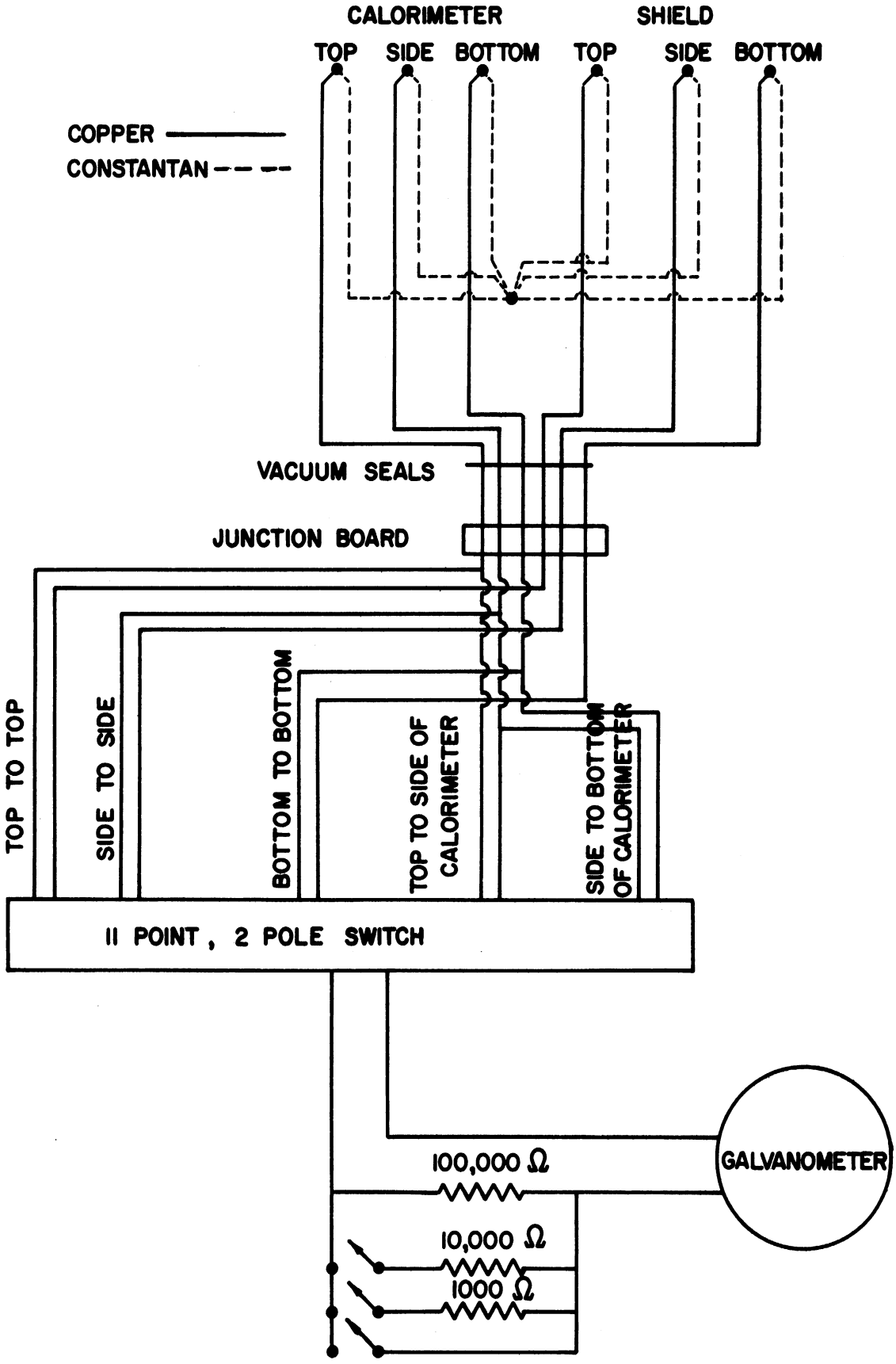

Figure 9. Circuit Diagram of Thermocouples

were placed in a vacuum container. The vacuum container was designed not only to provide an evacuated space for the calorimeter and adiabatic shield, but also to contain the contents of the calorimeter in case of rupture of the calorimeter. The vacuum container was a cubical box of six steel plates, each 12 inches square and 1/4 inch thick. Five of these were arc-welded together to form an open-topped box. A 2-inch angle iron was welded around the open end of this box to provide a gasket seat and to provide a place for the bolts which retained the top. The top was sealed to this box by a silicone rubber gasket 1/8 inch thick and 1 inch wide. The surfaces which contacted this gasket were machined flat and smooth. The top was retained by eight 1/2 inch bolts which passed through straps welded to the top and through the angle-iron flange. The container was supported on four legs, each 6 inches long, welded to its bottom corners. Two of the legs were bolted to the wooden table on which the container stood. Figure 10, page 37 , is a view looking downward at a 45 degree angle into the vacuum container with the top and top plate of the shield removed.

The entire vacuum container, except the top plate, was covered with a 4 inch thick layer of ordinary building Fiberglass insulation. Over this a layer of canvas was placed. A removable canvas-covered mat of Fiberglass 2 feet square and 4 inches thick was placed on top of the vacuum container after the cover was bolted down. This insulation lowered the heat leakage to the room, and thus lowered the power requirements of the adiabatic shield heaters. These heaters supplied not only the heat to raise the temperature of the adiabatic shield, but also the heat to raise the temperature of the vacuum container, and the heat leakage to the room.

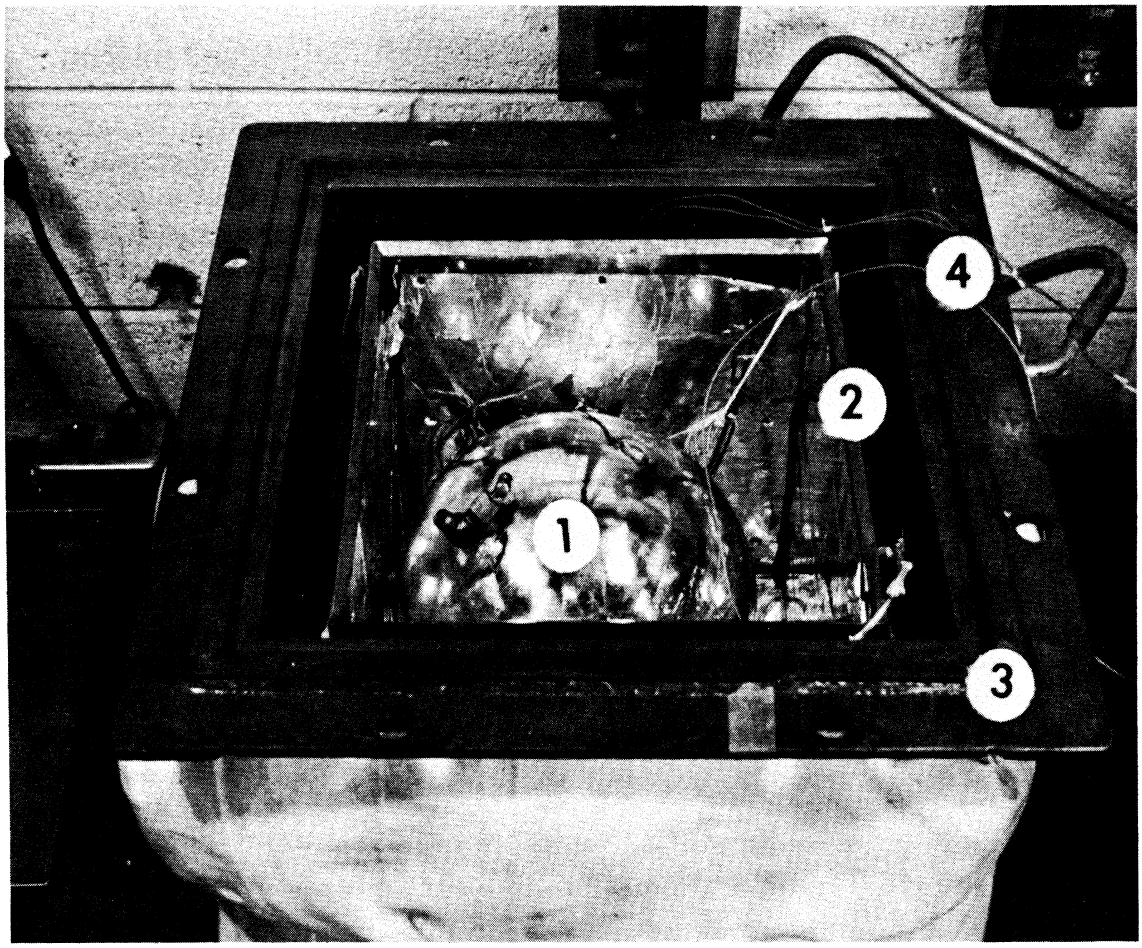

Figure 10. View into Vacuum Container with Top Removed

1. Calorimeter, showing fiberglass mounting strings, valve, and top thermocouple and thermocouple well.

2. Top of adiabatic shield, showing edge beveled to receive top plate. Note also the aluminum foil covering.

3. Top of vacuum container, showing bolt holes, and machined surfaces for gasket.

4. Couplings for top shield heater, and thermocouple for top shield.

A 1/4 inch steel pipe, welded into the side of the vacuum container made contact with the vacuum manifold. Through it the vessel was evacuated. The electrical leads left the container through a piece of steel tubing silver-soldered into its side. From this tubing they passed through a piece of Tygon tubing to the electrical lead system. An exception was made of the leads for the adiabatic shield heaters; these leads left the vacuum container through a Stupakoff kovar-glass header #95.4003, soft-soldered directly into the wall of the vacuum container. The adiabatic shield was supported by four 1 inch posts in the bottom corners of the vacuum container.

The vacuum container was designed to withstand an internal pressure of 250 psi. Its volume was roughly six times that of the calorimeter, so that if the calorimeter ruptured under a pressure of 1000 psi, the internal pressure would not be expected to exceed this value. (If the perfect gas law were obeyed, a pressure of 166 psi would be expected. Due to the increase in compressibility factor on expansion, the 250 figure seemed reasonable).

As an additional safety measure, an L-shaped plywood screen, 3 feet square on one side, and 3 feet by 6 feet on the other, made of 3/4 inch thick plywood was placed on the edge of the calorimeter table, between the vacuum container and the rest of the room. It was intended to catch any small particles which might be ejected in case of rupture of the calorimeter.

The Electrical Lead System

In the original design of the calorimeter, the electrical leads all left the vacuum container through Stupakoff kovar-glass headers soft-

soldered directly into the wall of the vacuum container. Because of the irregular temperature gradients across this wall, thermal EMF's were induced in the headers which made accurate measurements impossible. This difficulty was remedied by bringing the leads out of the vacuum system at a junction box, located several feet away from the vacuum container, where the temperature gradients were negligible. The junction box was not used for the adiabatic shield heater leads because the thermal EMF's were small compared with the heater voltages. The leads were brought to the junction box through a seven-foot long piece of Tygon tubing.

The junction box, which is shown in cross section in Figure 11, page 40, consisted of a piece of stainless steel tubing silver-soldered into the base of a 500 cc stainless steel beaker. To the top of the beaker was silver-soldered an 1/8 inch thick steel flange, to which a matching brass plate was bolted, forming a vacuum seal with an "O-ring". Three Stupakoff eight-terminal kovar-glass headers #95.4003 were soft-soldered into holes in this brass plate. These allowed 24 wires to be brought into the vacuum system at this point. Four of these wires were used for the thermometer-heater, four for the motor, six for the differential thermocouples, six for three copper-constantan thermocouples used for some preliminary work; four were spare copper wires to serve as replacements in case any of the above failed. All of the wires were 30 gauge copper Formvar- and Fiberglass-insulated.

The Vacuum System

The vacuum container was evacuated by a Cenco Hyvac #2 mechanical vacuum pump. This pump also provided the vacuum necessary for loading and unloading the calorimeter. A diagram of the vacuum manifold is shown in

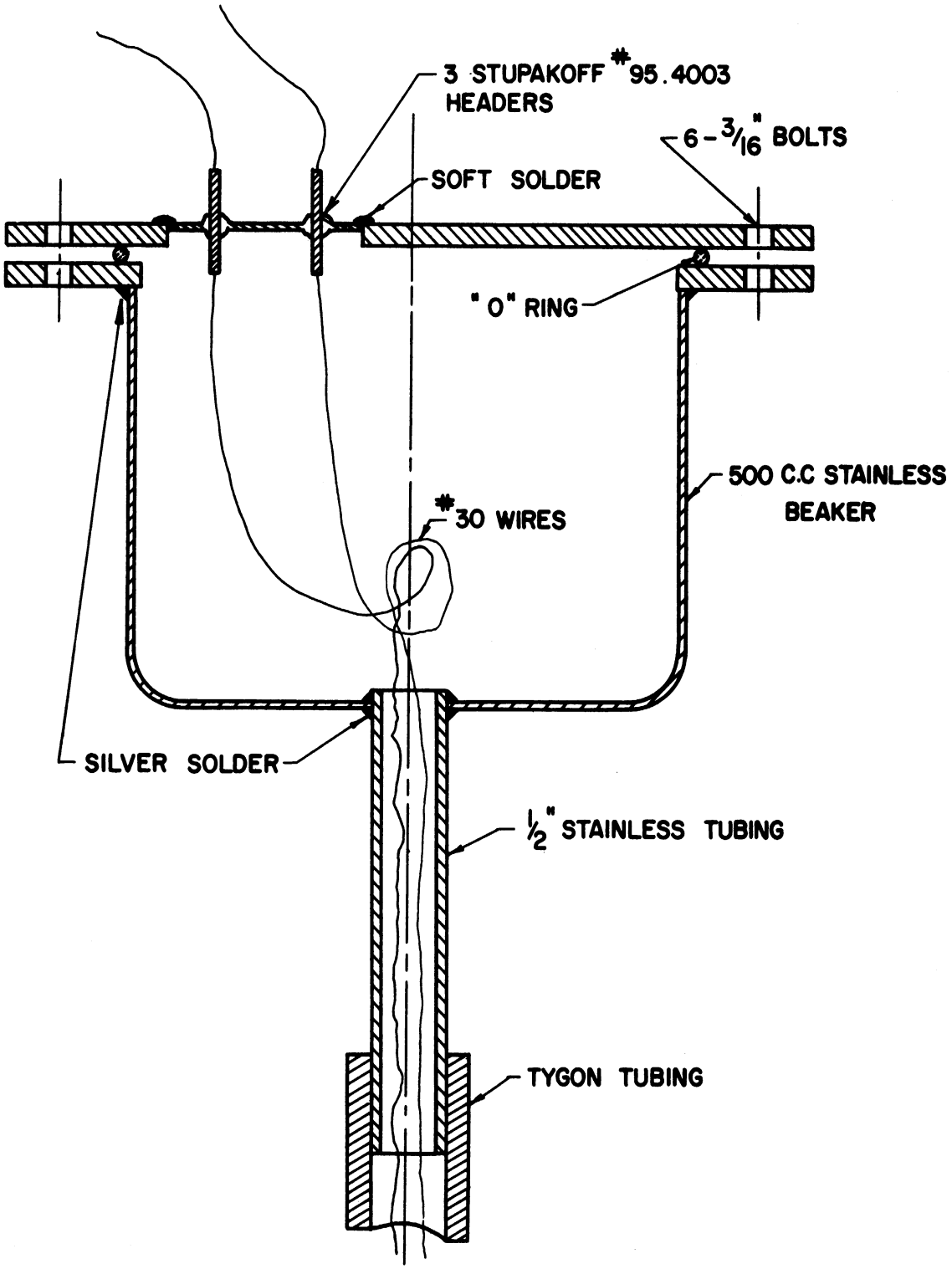

Figure 11. Cross-Section of Vacuum Junction Box

Figure 12, page 42. The manifold consisted of the various valves necessary for loading and unloading operations, a Lippincot-McLeod gauge (Kontes Glass Co. #VE - 3-a) and a cold trap. Those glass valves which would be exposed to high internal pressure by a rupture of the calorimeter were placed in a heavy wooden box, with a hinged door. This was a safety measure to prevent flying glass in case the valves shattered. Those parts of the manifold which were exposed to internal pressure during loading and unloading operations were made of copper tubing with metal needle valves. Figure 13, page 43, is a view of the vacuum system as connected to load the calorimeter. Note on this figure the angle-iron crane, with strings and pulleys, which was used to support the calorimeter during loading and unloading operations, and to lower it into place when it had been loaded.

The Measuring System

Figure 14, page 44, is a circuit diagram of the measuring system, and Figure 15, page 45, is an overall view of the measuring and control instruments.

All electrical measurements were made with a moving-coil galvanometer, Leeds and Northrup type 2284-d, serial number 1193782. The galvanometer was mounted on a wooden bracket, bolted to the wall of the room. The galvanometer stood on an 1/8 inch thick rubber sheet on this bracket, and was secured against accidental dislodgement by three short copper guy wires tied to its mounting legs. The galvanometer was read with a Leeds and Northrup light and ground glass scale, type 2100, serial number 223883. This scale was located about one meter from the galvanometer. Since only null readings were taken on this galvanometer, the

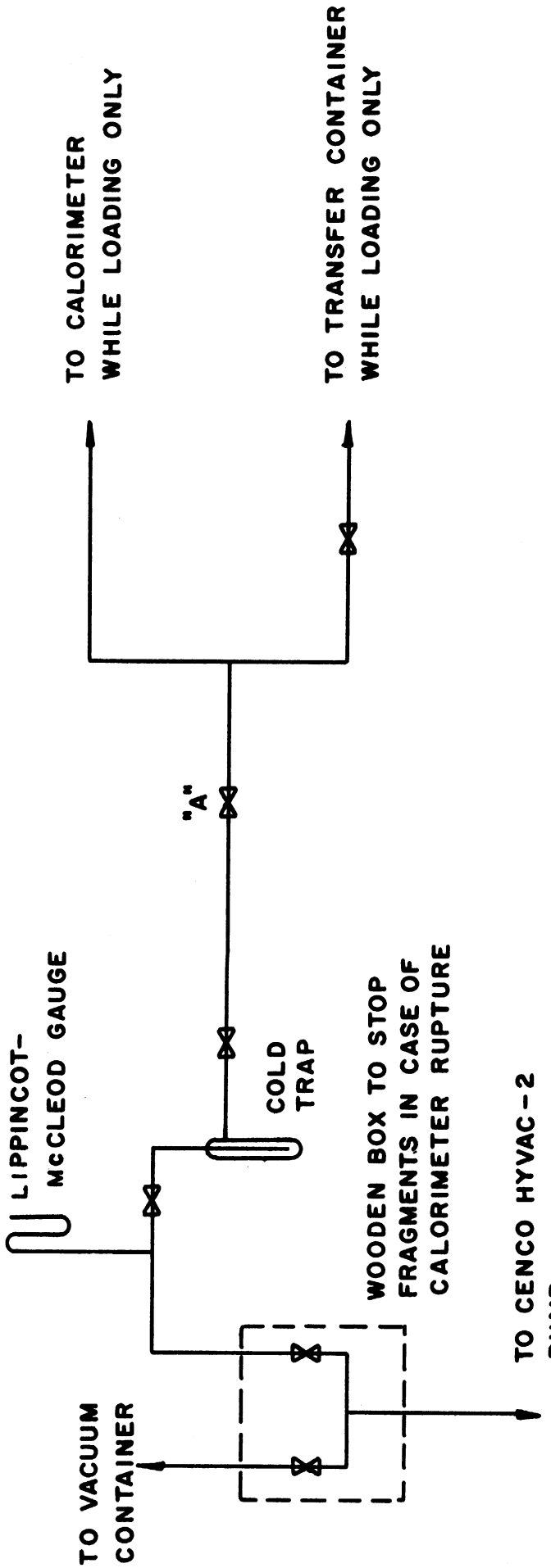

Figure 12. Vacuum System Diagram

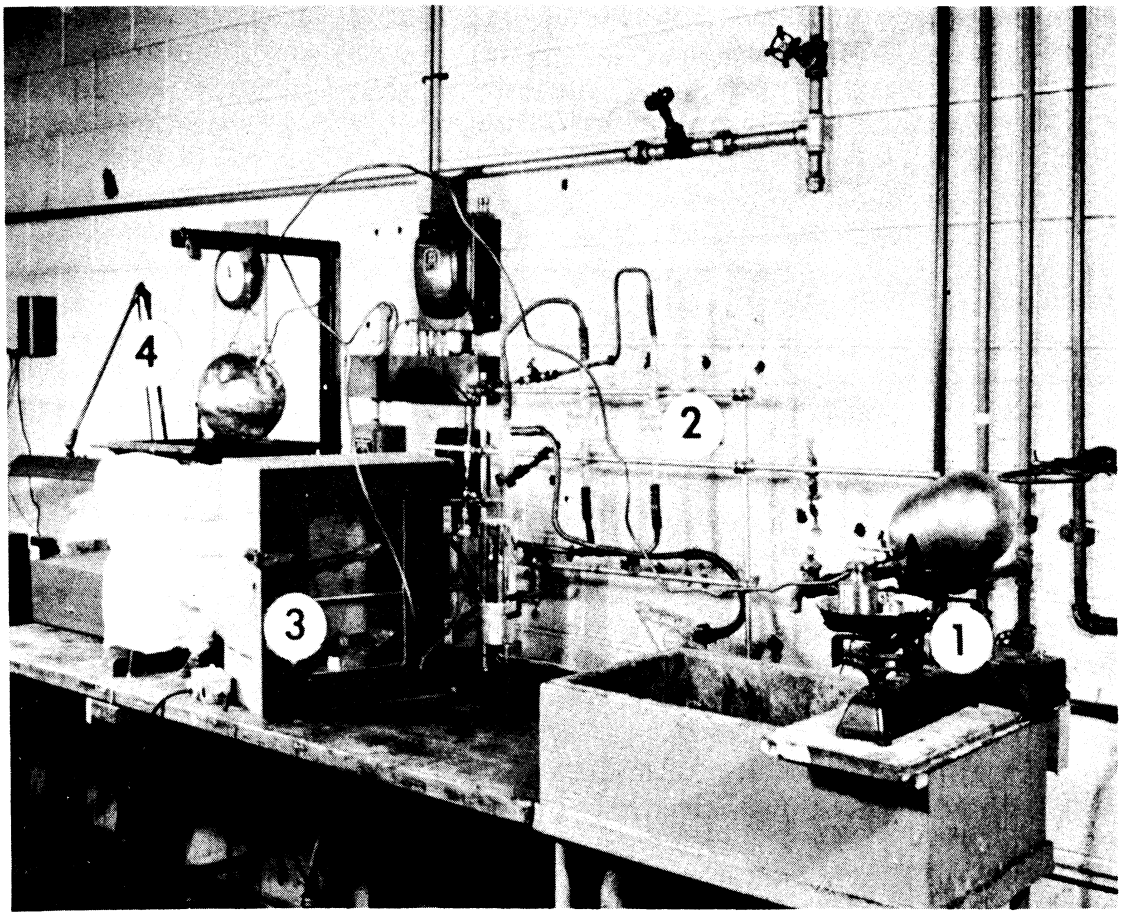

Figure 13. View of Calorimeter Loading System

1. Transfer container resting on balance pan.
2. Vacuum manifold.
3. Safety box of plywood, with Lucite window.
4. Calorimeter suspended from crane.

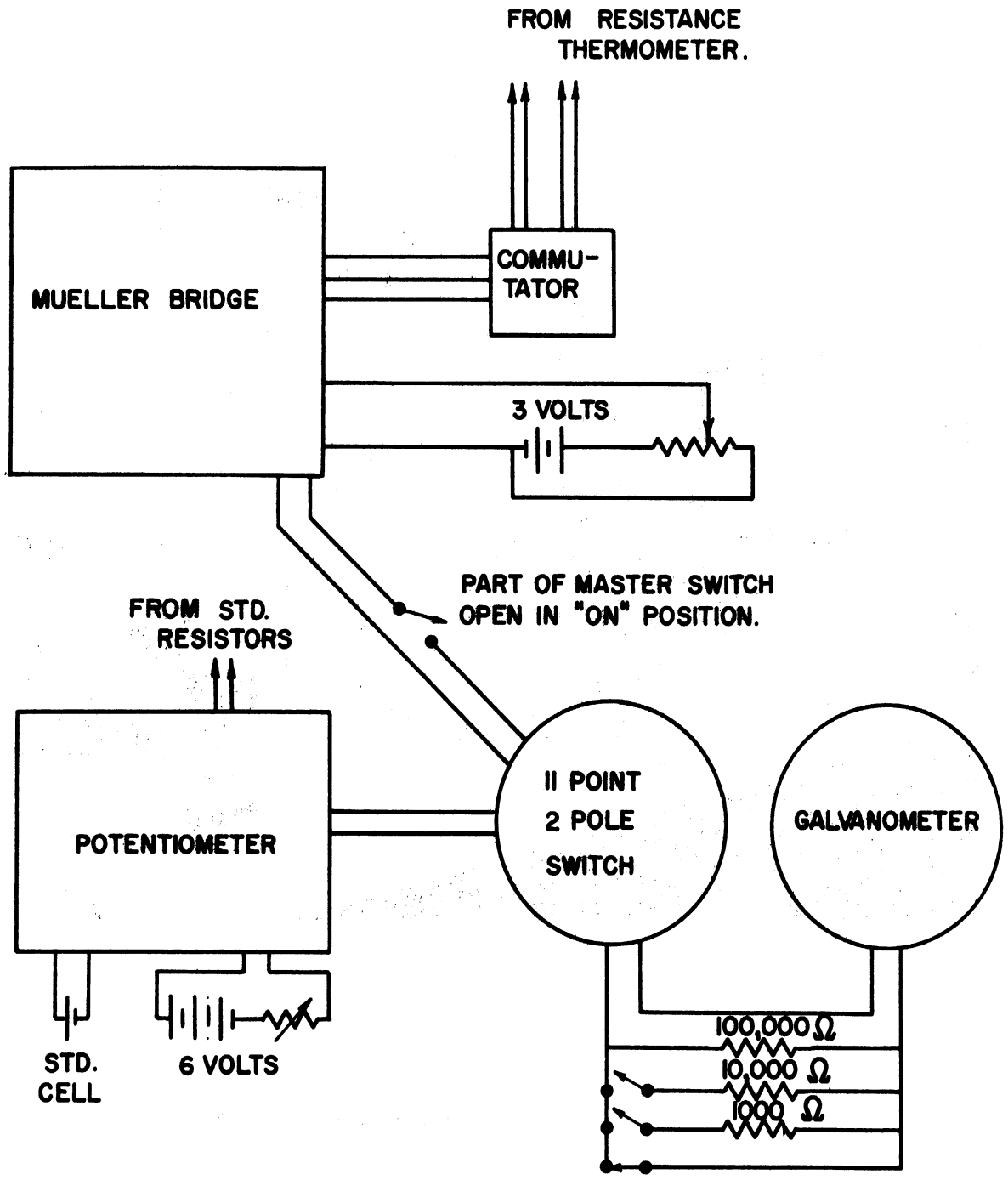

Figure 14. Circuit Diagram of Measuring System

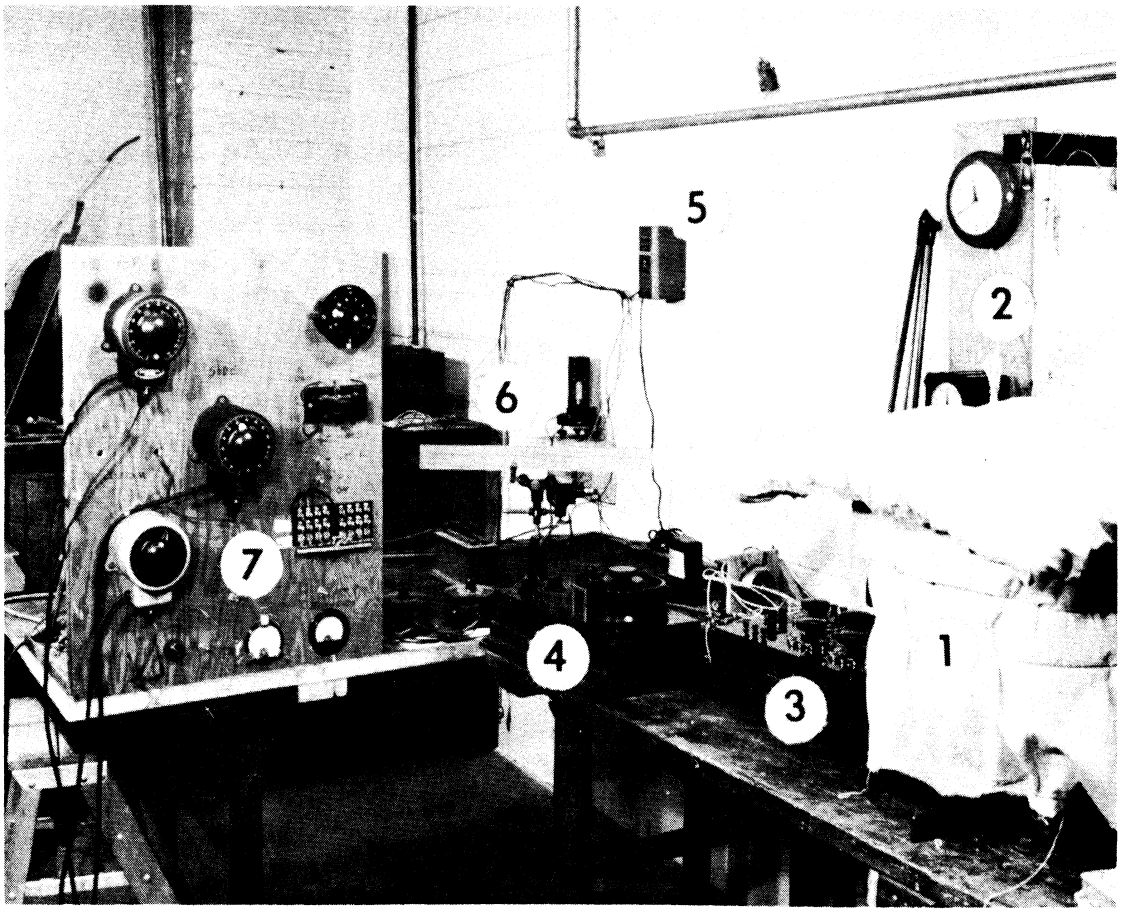

Figure 15. View of Control and Measuring Instruments

1. Vacuum container with Fiberglass insulation.
2. Clock and timer.
3. Mueller Bridge.
4. Potentiometer.
5. Battery Charger.
6. Galvanometer and light and scale.
7. Control panel with powerstats and various switches.

exact length of the light path was of no interest. Under these conditions one millimeter of scale corresponded to about 10^{-7} volts.

The signal for the galvanometer was taken from a Leeds and Northrup 11-point double-pole selector switch. For normal use the signal was transmitted directly. However, as mentioned above, resistance could be added in series with the galvanometer, when the voltage signal was too large for the galvanometer. This was done only when the thermocouples were being read.

Calorimeter temperatures were measured with the platinum resistance thermometer, using a Mueller Bridge. (Mueller[26] has described this type of bridge, which is a modified Wheatstone bridge.) The bridge was a Leeds and Northrup type C-1, serial number 1192498. The thermometer was connected in the "potential terminal" method described by Mueller, using a Leeds and Northrup mercury cup commutator, type #8068, serial number 1194595. Power for the bridge circuit was supplied by two 1-1/2 volt dry cells in series, reduced by a small rheostat used as a potential divider. (It was not necessary that this voltage be either steady or known. In practice, it was regulated to make resistance changes of the thermometer of 0.0001 ohm determinable. Such a change corresponded to a change of 0.001 degree C.)

The current through the thermometer-heater and motor was measured by measuring the voltage across a standard 0.10000 ohm resistor, Leeds and Northrup type #4221-B, serial number 1216562. This resistor was in series with the thermometer-heater and motor combination. The voltage across the thermometer-heater and motor was measured by measuring the voltage across a standard 10.000 ohm resistor, Leeds and Northrup type 4025-B,

serial number 1196149. This resistor was in series with a standard 10,000 ohm resistor, Leeds and Northrup type 4040-B, serial number 1201941. This pair of resistors was connected in parallel with the thermometer-heater and motor, at the point where the leads to the thermometer-heater and motor entered the calorimeter. All three of these standard resistors stood in an oil bath. The bath was a covered stainless steel pan, 10 inches by 7 inches by 5 inches deep, filled with 20 weight motor oil.

The voltages across these standard resistors were determined by means of a Leeds and Northrup K-2 potentiometer, serial number 227158. Power for the potentiometer was supplied by a 6 volt lead storage battery. A resistance box in series with the battery reduced the voltage to that required for the potentiometer. In order to obtain satisfactory standardization of the potentiometer working circuit, it was necessary to leave the storage battery connected to the potentiometer (i.e., the current flowing) at all times. The battery was disconnected only for re-charging at intervals of about one month. The potentiometer circuit was modified as shown in Figure 16, page 48, to adapt the potentiometer to the galvanometer. The galvanometer required an external damping resistance of about 55 ohms. The potentiometer was equipped with external damping resistances of 200 and 2000 ohms, so that the modification was necessary in order to have proper galvanometer damping. In conjunction with the potentiometer, Epply standard cell #425935 was used. Its EMF was determined to be 1.01937 volts, at 25°C.

The elapsed time of a heating period was measured by a synchronous timer with an electrically actuated clutch. The timer was Standard Electric Time Company model S-6. It was graduated in minutes and one-

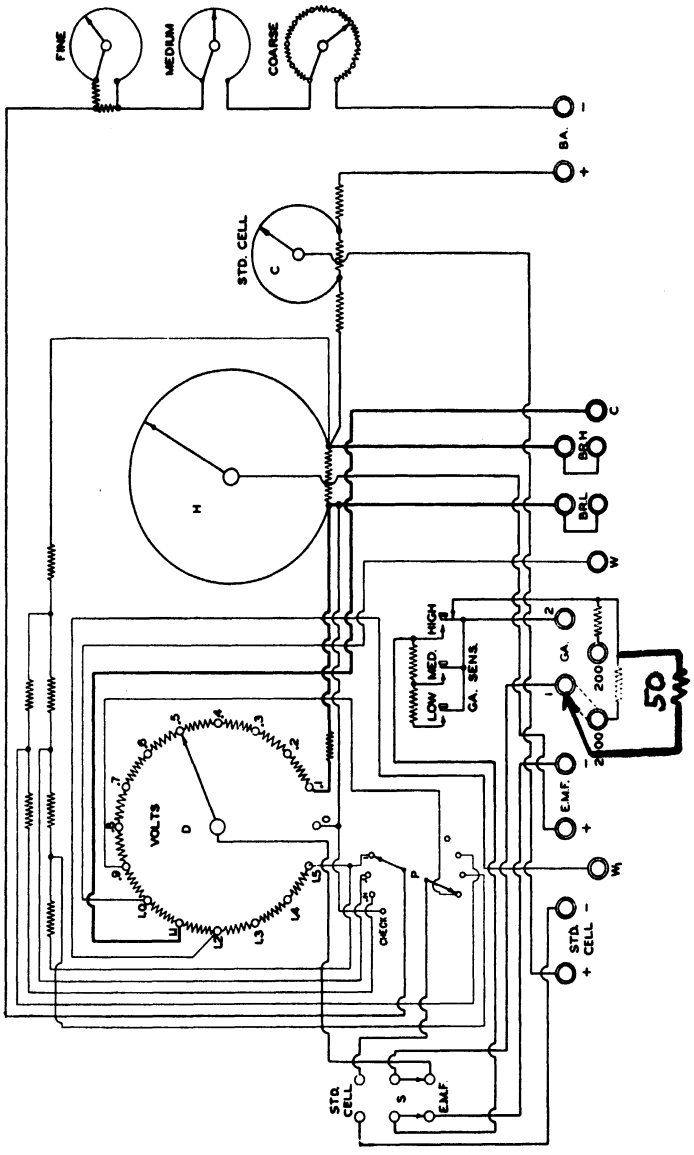

Figure 16. Modification of Potentiometer

thousandths of minutes. Its clutch was actuated by the 8 pole double-throw master switch which was used to turn on the power to the heater-thermometer and motor.

A milliammeter reading 0-800 ma. and a voltmeter reading 0-25 volts were mounted on the control panel, and connected to show the voltage across and the current through the thermometer-heater and motor combination (or the voltage across and the current through the dummy resistor). The readings of these instruments formed no part of the experimental data; they served only to help the operator of the equipment make minor adjustments, and to warn him of malfunctions of the equipment.

The Power Circuitry

Power for the calorimeter thermometer-heater and motor combination was supplied by lead storage batteries. Two six-volt and two twelve-volt batteries were combined in series to give an overall voltage of 36 volts. A charger was available to recharge the batteries when they were not in use. Before a heating period the batteries were connected to a dummy resistor, of about the same resistance as the thermometer-heater and motor combination. This insured that the battery voltage would not change rapidly at the start of a heating period.

A balancing resistor was connected in series with the thermometer-heater and motor (or in series with the dummy resistor during non-heating periods) to minimize the changes in thermometer-heater and motor power with changes in thermometer-heater and motor resistance. For a discussion of the use of the balancing resistor see Hoge[13]. In Appendix E, page 137, is a brief synopsis of Hoge's article, including a derivation of the principle formulae, showing how a balancing resistor minimizes

changes in thermometer-heater and motor power with changes in thermometer-heater and motor resistance. Both the dummy and balancing resistors were 100 ohm, sliding-contact "Ohmite" #2921 - A resistors. Figure 17, page 51, is the circuit diagram of the power circuit.

Materials Used for Investigation

In choosing materials to investigate, the following were the primary considerations:

1. the material should have a high product of heat capacity times critical density, so that near the critical state the ratio of heat capacity of contents to heat capacity of the calorimeter would be as high as possible;

2. the material should have as low a critical pressure as possible, so that the approach to the critical state could be made without exceeding the allowable pressure of the calorimeter;

3. the critical temperature should not be much higher than 100°C, so that the range of temperatures which could be investigated would extend to well above the critical temperature;

4. reliable values of C_V^* or C_p^* for the material should have been published;

5. PVT data for the material should have been published, to which a modern equation of state had been fitted, so that a meaningful comparison between the experimental C_v-C_v^* and the C_V-C_V^* predicted by the equation of state could be made; and,

6. the material should be available in high purity, so that purification problems could be avoided.

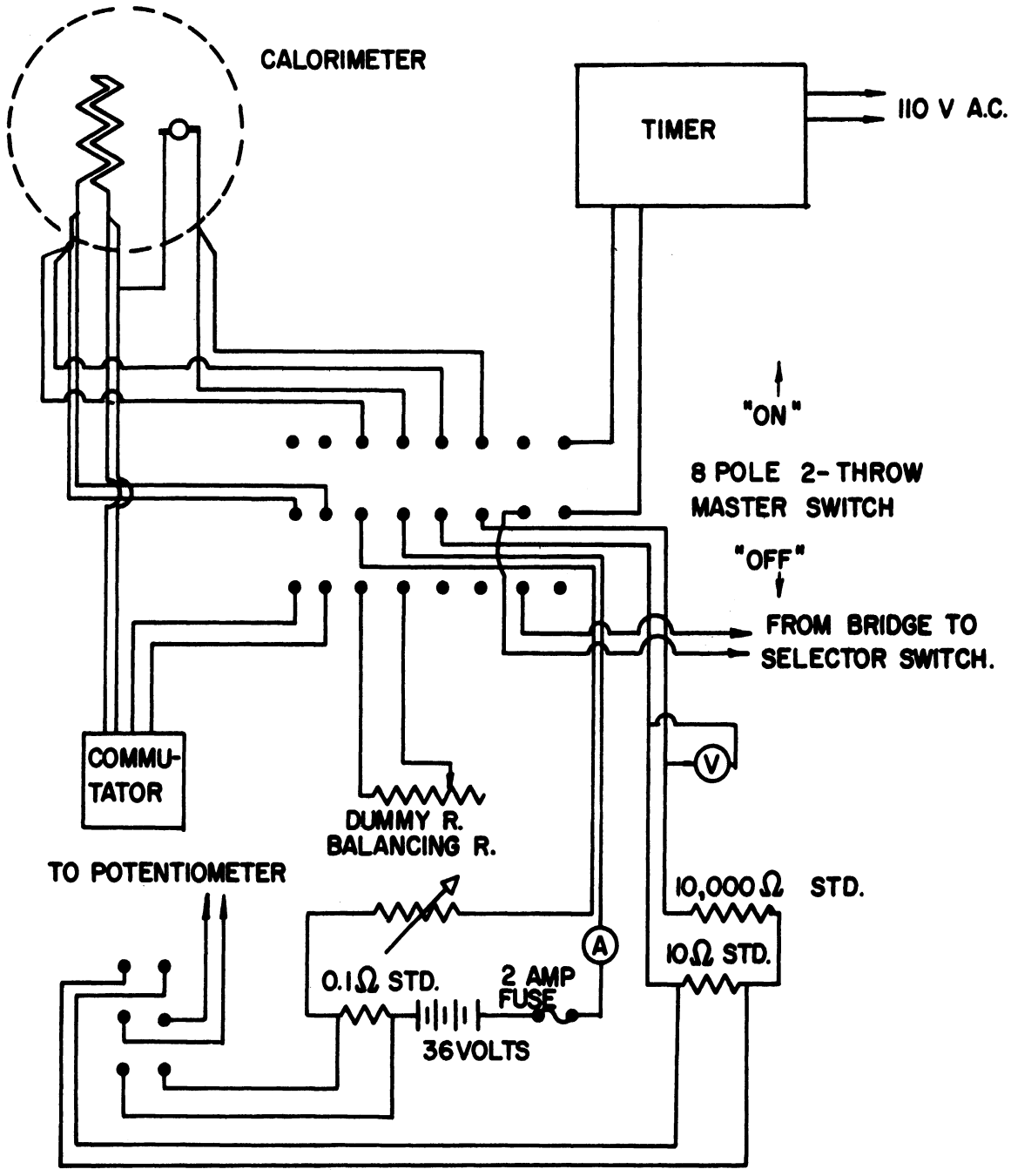

Figure 17. Circuit Diagram of Power Circuit

No single compound met all the requirements. Those chosen, perfluorocyclobutane and propylene, were good compromises. Perfluorocyclobutane has an extremely high critical density (0.6015 gm/cc) and a very low critical pressure (401 psi). PVT data have been published and fitted by the Martin-Hou equation of state. Propylene has a reasonably low critical pressure (670 psi) and a reasonably low critical temperature (91.7°C). PVT data on propylene have been fitted by the Benedict-Webb-Rubin equation of state.

The propylene used in this research was taken from a cylinder of the Matheson Co. Inc. It was their "C.P. Grade" and was specified by them to be a minimum of 99.0 mol% pure. The perfluorocyclobutane was supplied by the Freon Products Laboratory of the Du Pont Company. It was specified by them to be 99.78 weight % pure. The dichlorodifluoromethane used for calibration of the calorimeter was also supplied by the Freon Products Laboratory of the Du Pont Company. It was specified by them to be at least 99.9 mol % pure. None of these materials was subjected to additional purification on receipt from the supplier.

EXPERIMENTAL PROCEDURE

Loading the Calorimeter

Before loading the calorimeter, the material to be investigated was transferred from its shipping container to one or more light-weight transfer containers. These containers were war-surplus, stainless-steel oxygen bottles. Their volume was about two liters, and their rated pressure was 500 psi. Each was equipped with a needle valve (Hoke #321) and a permanently attached aluminum tag, on which the description of the contents was stamped. Container, valve and tag weighed about 600 grams.

To load the calorimeter the transfer container was first weighed on the "SeKo" balance in the Sohma Precision Laboratory. This balance could weigh quantities up to 3 kilograms, and could be read to 0.01 gram. Next the transfer container was connected to the calorimeter by means of the T-section of copper tubing shown in Figure 12, page 42. Figure 13, page 43, is a view of the calorimeter loading system. The transfer container was placed on one pan of a crude 2 kilogram balance, and the weights necessary to balance it were placed on the other pan. The transfer container valve was left closed, while that of the vacuum system and that of the calorimeter were opened. When the calorimeter and the transfer lines had been evacuated, the T-section of tubing was closed off, by closing valve "A" (Figure 12). Weights corresponding to the desired loading of the calorimeter were removed from the pan of the crude balance opposite the transfer container.

The valve of the transfer container was opened, allowing the contents to flow into the calorimeter. The container was normally placed on the crude balance with its valve down, so that the material was

transferred in the liquid phase. It was sometimes necessary to warm the transfer container in order to complete the transfer. When the crude balance again indicated equal mass on each pan, the valve of the transfer container was closed. The transfer lines were warmed to insure that no liquid remained in them. Then the valve of the calorimeter was closed, and that of the transfer container opened. The transfer container was immersed in a dewar of liquid nitrogen until its temperature was the same as that of the liquid nitrogen. In this way, the vapor pressure in the transfer container was reduced to a negligible value, and the material in the transfer lines was condensed back into the transfer container. The valve of the transfer container was then closed, the container was disconnected, warmed to room temperature and again weighed to 0.01 gram. From its change in mass, the mass charged to the calorimeter was computed. By means of the crude balance the mass charged could be regulated to about plus or minus 20 grams. For the highest-density perfluorocyclobutane loadings it was necessary to use the contents of more than one transfer container; this did not change the above procedure seriously.

The calorimeter was disconnected from the vacuum system. It was lowered into the adiabatic shield, and supported by the Fiberglass strings attached to the shield. The top of the adiabatic shield was installed, as were the gasket and the top of the vacuum container. The Fiberglass mat was placed over the vacuum container, and the system was evacuated.

Operating the Calorimeter

After the system had been evacuated (normally to about 0.050 mm Hg) calorimetric measurements were begun. Each measurement or "run" consisted of a temperature measuring period, a heating period, and a second temperature measuring period.

To begin a run, the shield heaters were controlled by the variable transformers so that the differential thermocouples indicated zero average temperature difference between the control points on the adiabatic shield and on the calorimeter. (Actually, steady zero values were seldom attained; fluctuations of about 0.1 degree C were common.) When this indicated zero average temperature difference had been attained, the temperature of the calorimeter was measured at five-minute intervals by means of the platinum resistance thermometer and the Mueller bridge.

When the rate of change of temperature with respect to time or "drift" had been determined (it was usually less than 0.003 degrees C per minute) the heating period was begun by throwing the master control switch from the "off" to the "on" position. This simultaneously switched the power from the dummy resistor to the thermometer-heater and motor, and engaged the clutch of the synchronous timer. This switch also disconnected the Mueller bridge from the galvanometer and from the thermometer, to prevent accidental overloading of the galvanometer and to prevent flow of current through the bridge.

The time of starting the heating period was noted. The intended shut-off time was also noted. Heating periods were of 15, 20, 25, 30 and 40 minutes duration, depending on the contents of the calorimeter and the intended temperature rise. At the start of the heating period it was necessary to give the adiabatic shield a burst of power, because the temperature of the adiabatic shield responded to a change of heat input more slowly than the temperature of the calorimeter responded to turning on the power to the thermometer-heater and motor. During a heating period, the adiabatic shield was continually maintained at zero average

temperature differences between the control points on the surface of the calorimeter and on the surface of the adiabatic shield. (This could not be done as well as during the temperature-measuring periods; temperature differences of up to 0.2 degrees C were common.)

At times corresponding to 1/4, 1/2 and 3/4 of the heating period the power supplied to the thermometer-heater and motor was determined. First the potentiometer current was standardized. Then the current through the thermometer-heater and motor was determined by measuring the voltage across the standard 0.10000 ohm resistor which was in series with the thermometer-heater and motor. Next the voltage across the thermometer-heater and motor was determined by measuring the voltage across the standard 10.000 ohm resistor which was in the circuit in parallel with the thermometer-heater and motor. Then the current measurement was repeated. Because the current through the thermometer-heater and motor, and the voltage across them were constantly changing during a heating period, the two current measurements differed, normally by less than 0.05%. The average of the two current readings was assumed equal to the true current at the instant of the voltage reading. The product of this average current and the voltage was recorded as the instantaneous power of the thermometer-heater and motor.

About one minute before the end of the heating period, the power to the adiabatic shield heaters was turned off. This prevented the adiabatic shield temperature from overshooting that of the calorimeter. The heating period was ended by throwing the master switch from the "on" to the "off" position. This simultaneously switched the power from the thermometer-heater and motor to the dummy resistor, disengaged the

clutch of the timer and re-connected the Mueller bridge. The time, and the reading of the timer were noted, and the timer was reset.

After the end of the heating period, the temperature of the adiabatic shield was again controlled to maintain zero average values of the temperature differences between the control points on the surface of the calorimeter and on the surface of the adiabatic shield. Starting 10 minutes after the end of the heating period, temperatures were again recorded at 5 minute intervals, until the drift had been determined. This normally required between 20 and 40 minutes. If only one run was planned, operations ceased when this drift had been found. If several runs were planned, the next heating period was begun immediately. Thus, the second temperature-measuring period of one run served as the first temperature-measuring period of the next.

Unloading the Calorimeter

When C_V as a function of temperature over the planned temperature range had been determined for a given loading, the material was removed from the calorimeter in a fashion similar to the loading procedure. The transfer container was again connected to the calorimeter by means of the T-section of copper tubing. With both the calorimeter and transfer container valves closed, the connecting tubing was evacuated. Then the T-section was closed off from the vacuum pump, and both the transfer container and calorimeter valves were opened. The transfer container was immersed in a dewar of liquid nitrogen, while the calorimeter was, if necessary, warmed. When the transfer container had reached the temperature of the liquid nitrogen, as indicated by the cessation of violent boiling of the liquid nitrogen, and when the calorimeter contained no

more liquid, as indicated by the absence of atmospheric condensation or frost on its bottom, the valve of the transfer container was closed. The transfer container was then disconnected, warmed to room temperature and weighed. The material lost in the two transfer operations, and left in the calorimeter was normally 0.4 to 0.8 grams. For the high-density perfluorocyclobutane loadings involving two or three transfer containers, up to 2 grams were lost.

EXPERIMENTAL RESULTS

The Constant Volume Heat Capacity of Perfluorocyclobutane

The experimental heat capacity results for perfluorocyclobutane are shown in Table I, page 60. The results are presented in the form: gross heat capacity of calorimeter plus contents for a given "run", minus the calibrated heat capacity of the calorimeter, equals the net heat capaqity of the contents. The net heat capacity, divided by the mass of the contents, equals the C_v in calories per gram per degree C. The temperature listed, T_{mean}, for each run is the mean of the temperature interval over which heat was added; the calibration value for the run is that corresponding to T_{mean}. Seven densities were used, ranging from 0.1569 gm/cc (26.2% of the critical density) to 0.5366 gm/cc (89.6% of the critical density). For each density the temperature range was from the saturation temperature to 150°C. The C_v ranged from 0.2164 to 0.2594 gm/cc. The highest C_v corresponded to a $(C_v-C_v^*)/C_v^*$ of 0.25.

The experimental results are plotted on a C_v vs. T plane in Figure 18, page 62. A smooth curve has been drawn through the data points for each density. The worst scatter of the data points from these curves was 0.7%. Except for runs 22 and 28, none of the data points scatter from the curves by more than 0.3%. Also shown in Figure 18 are the values of C_v^* and the boundary of the two phase region, both according to Martin et al.[20]. On Figure 18 and on subsequent data plots the critical temperature and density have been noted because the relation of the data to these parameters is of great interest; the critical temperature and density are those reported by Martin et al.[20]. Figure 19, page 63, is a cross-plot of Figure 18. On it, isotherms have been constructed on a C_v vs. density

TABLE I

THE CONSTANT VOLUME HEAT CAPACITY OF PERFLUOROCYCLOBUTANE

Run #	T_{mean} °C.	(C_g cal./°C.	- Calibration) cal./°C.	= Heat Capacity cal./°C.	cal./gm.°C.
Loading #1 690.71 grams 0.1569 gm./cc.					
21	101.58	256.56	106.21	150.35	0.2177
22	103.45	255.81	106.38	149.45	0.2164
23	114.99	258.50	107.33	151.17	0.2190
24	126.33	261.01	108.26	152.75	0.2212
25	137.41	264.02	109.16	154.86	0.2243
26	146.61	265.33	109.91	155.42	0.2250
Loading #2 848.16 grams 0.1927 gm./cc.					
28	109.18	293.80	106.86	186.94	0.2204
29	119.24	297.35	107.68	189.67	0.2237
30	131.73	300.01	108.68	191.33	0.2257
31	144.05	302.77	109.71	193.06	0.2277
Loading #3 1054.23 grams 0.2394 gm./cc.					
33	110.50	346.39	106.96	239.43	0.2272
34	118.11	346.74	107.58	239.16	0.2269
35	127.20	348.52	108.34	240.18	0.2279
36	136.20	350.08	109.06	241.02	0.2287
37	145.10	352.35	109.81	242.54	0.2301
Loading #4 1410.65 grams 0.3201 gm./cc.					
42	117.32	439.93	107.51	332.42	0.2357
43	126.40	438.39	108.46	329.93	0.2339
44	135.43	441.22	109.01	332.21	0.2356
45	144.40	439.86	109.73	330.13	0.2341
Loading #5 1720.18 grams 0.3902 gm./cc.					
46	114.67	534.16	107.25	426.91	0.2482
47	118.37	526.44	107.58	418.86	0.2436
48	124.01	519.54	108.06	411.48	0.2393
49	131.58	517.35	108.66	408.69	0.2377
50	139.12	517.34	109.31	408.03	0.2373
51	146.69	518.28	109.91	408.37	0.2374

TABLE I (CONT'D)

Run #	T_{mean} °C.	(C_g - Calibration) cal./°C.	Calibration cal./°C.	= Heat Capacity cal./°C.	cal./gm.°C.
Loading #6 1969.16 grams 0.4465 gm./cc.					
52	119.27	598.14	107.70	490.74	0.2492
53	123.01	589.29	107.98	481.31	0.2445
54	127.74	584.04	108.36	475.68	0.2416
55	134.37	581.01	108.91	472.10	0.2398
56	141.97	579.52	109.53	469.99	0.2388
57	147.66	580.36	109.98	470.38	0.2390
Loading #7 2366.1 grams 0.5366 gm./cc.					
64	119.04	721.65	107.66	613.99	0.2594
65	123.56	699.21	108.03	591.18	0.2498
66	129.42	687.27	108.51	578.76	0.2445
67	136.16	681.05	109.06	571.99	0.2417
68	142.95	677.60	109.61	567.99	0.2400

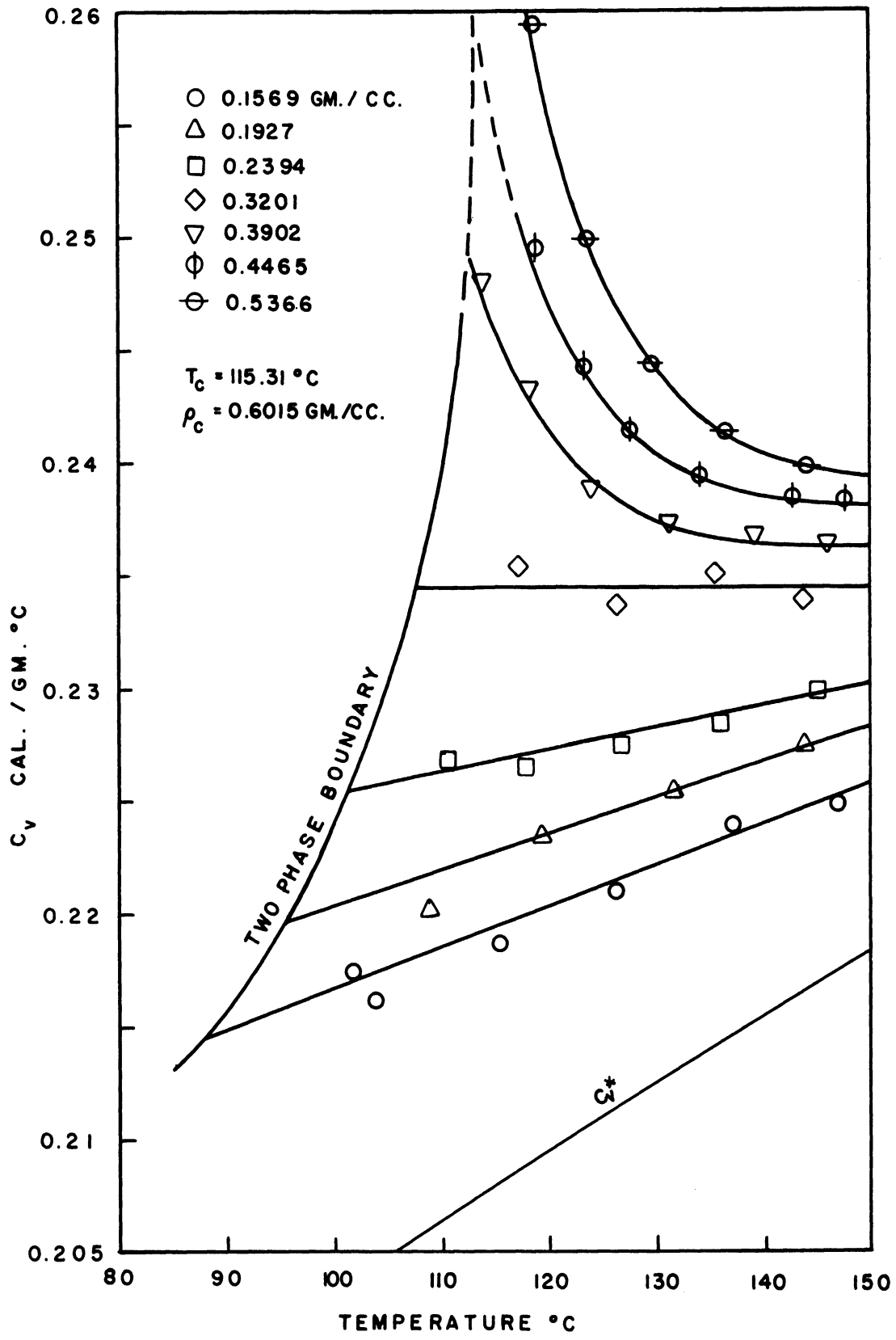

Figure 18. The Constant Volume Heat Capacity of Perfluorocyclobutane

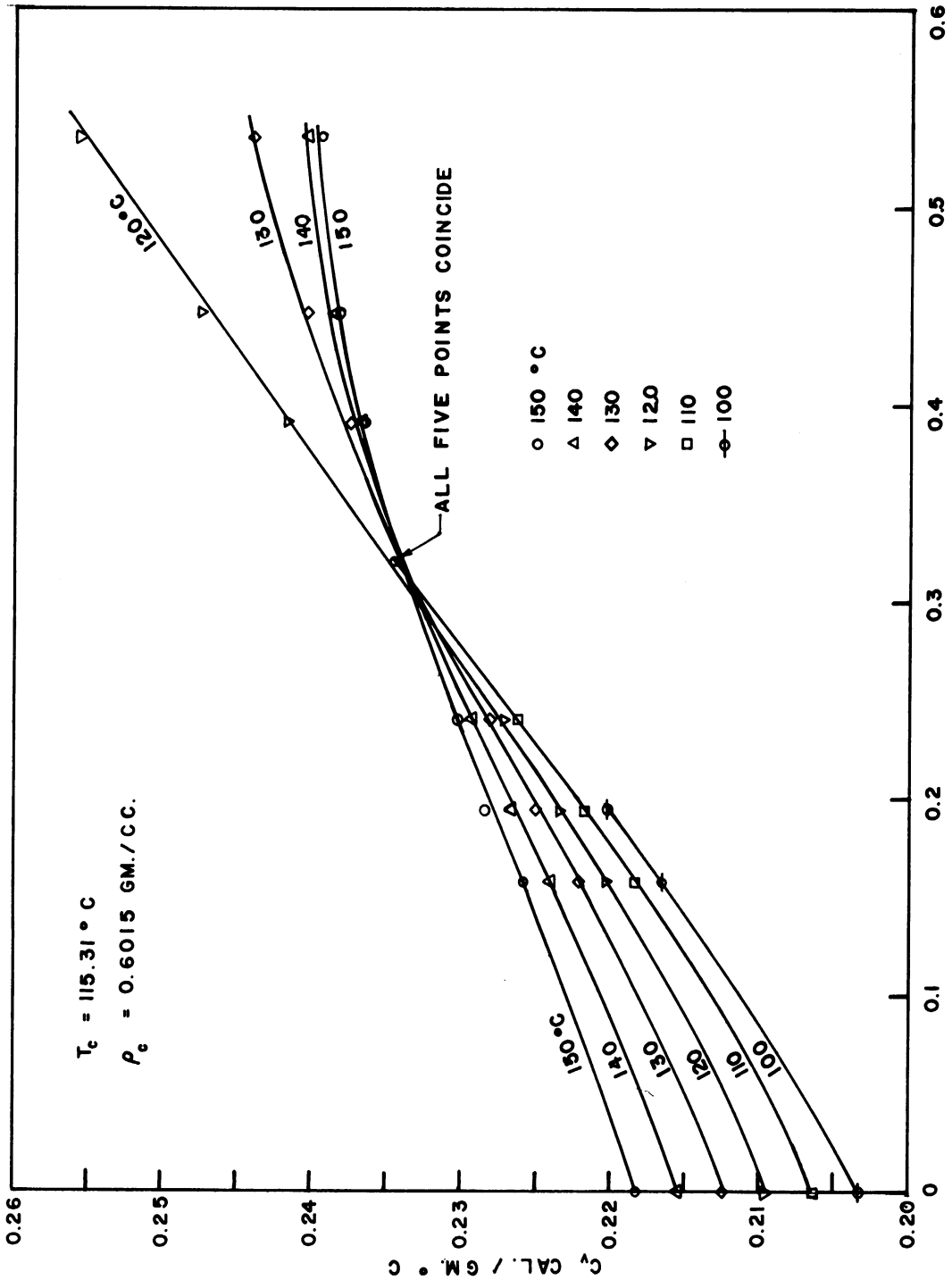

Figure 19. The Constant Volume Heat Capacity of Perfluorocyclobutane
(This is a cross-plot of Figure 18.)

plane. These isotherms were constructed by plotting the values of the various smooth curves of Figure 18, where these curves intersected lines of constant temperature. None of the points plotted on Figure 19, scatters from the isotherms by more than 0.3%. Figure 20, page 65, is similar to Figure 19; in it, however, each isotherm has been translated vertically so that its left end passes through the origin, yielding a plot of C_V-C_V^* vs. density for various temperatures. Both Figure 19 and Figure 20 are influenced by the values of C_V^*. These values were not measured in this research, but are those reported by Martin et al.[20].

The Constant Volume Heat Capacity of Propylene

The experimental heat capacity results for propylene are shown in Table II, page 66. They are presented in the same form as in Table I. Six densities were used ranging from 0.04814 gm/cc (21.8% of the critical density) to 0.1609 gm/cc (72.6% of the critical density). The temperature range for the two lowest densities was from the saturation temperature to 150°C. The temperature range for the two intermediate densities was from the saturation temperature to that temperature at which the calculated pressure was 700 psi. The temperature range for the two highest densities was from the saturation temperature to that temperature at which the calculated pressure was 800 psi. The C_V ranged from 0.3903 to 0.4991 cal/gm degree C. The highest C_V corresponded to a $(C_V-C_V^*)/C_V^*$ of 0.33.

These data are plotted in Figure 21 on a C_V vs. T plane. Also shown are the boundary of the two-phase region calculated from the PVT data of Marchman, Prengle and Motard[21] and the C_V^* reported by Kilpatrick and Pitzer[17]. The critical density and temperature noted are those according to Marchman et al. (There is some question about the critical

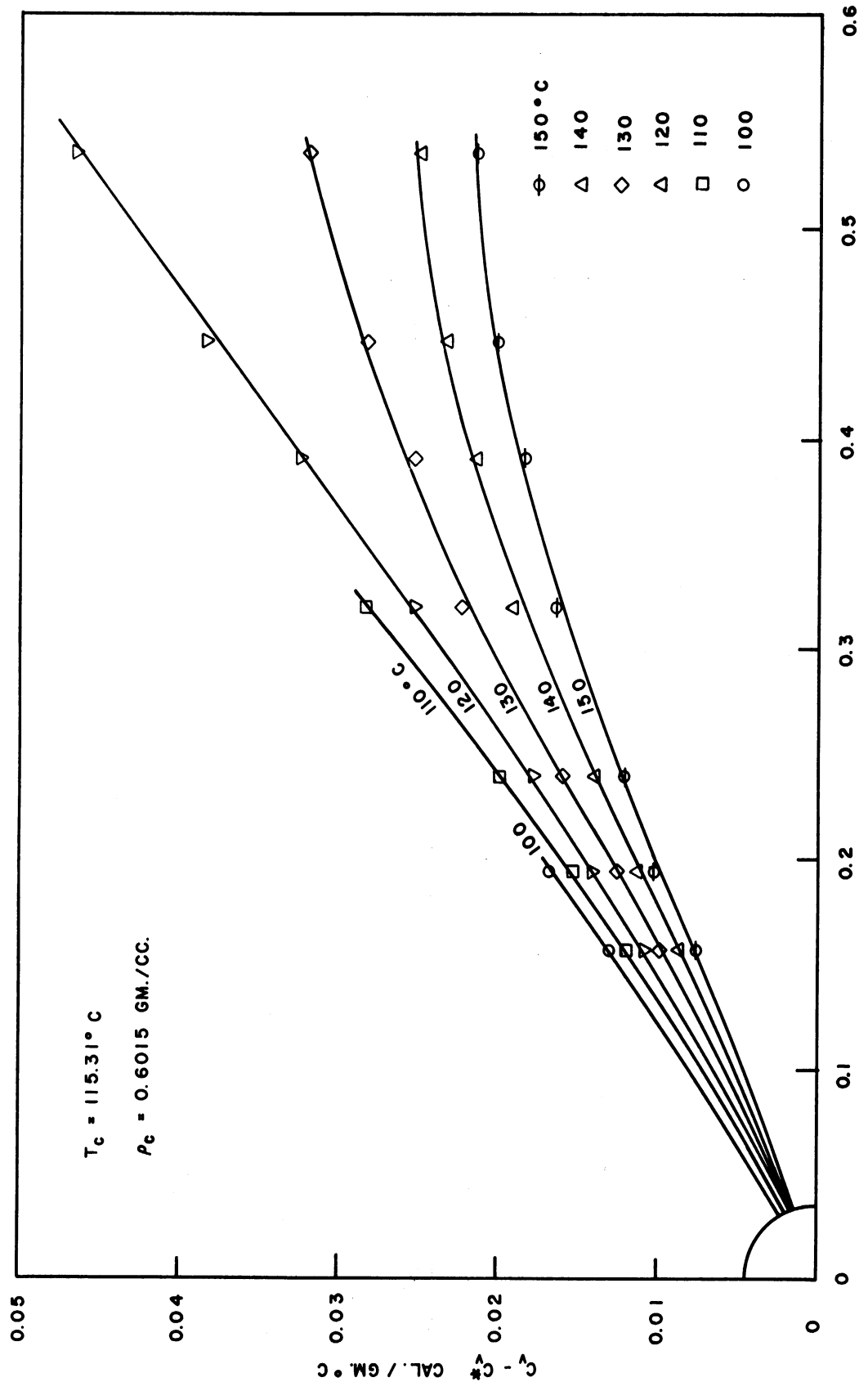

Figure 20. C_v-C_v^* of Perfluorocyclobutane
(This is a modified cross-plot of Figure 18.)

TABLE II

THE CONSTANT VOLUME HEAT CAPACITY OF PROPYLENE

Run #	T_{mean} °C.	(C_g - Calibration) cal./°C.	Calibration cal./°C.	= Heat Capacity cal./°C.	cal./gm.°C.
Loading #1 212.03 grams 0.04814 gm./cc.					
2	67.15	186.16	103.41	82.75	0.3903
3	82.14	188.42	104.63	83.79	0.3952
4	98.45	191.79	105.98	85.81	0.4047
5	111.62	195.23	107.04	88.19	0.4159
6	123.90	197.67	108.06	89.61	0.4226
6a	140.21	201.75	109.38	92.37	0.4357
Loading #2 318.21 grams 0.07219 gm/cc.					
58	75.09	236.45	104.06	132.39	0.4160
59	85.21	237.39	104.90	132.49	0.4163
60	99.93	240.02	106.11	133.91	0.4208
61	117.06	244.48	107.48	137.00	0.4305
62	133.72	249.23	108.84	140.39	0.4412
63	145.92	252.49	109.76	142.73	0.4485
Loading #3 406.94 grams 0.09228 gm./cc.					
69	84.64	283.03	104.80	178.23	0.4380
70	92.91	282.02	105.53	176.49	0.4337
71	103.71	283.06	106.41	176.65	0.4341
72	115.35	285.79	107.36	178.43	0.4385
73	125.32	288.82	108.18	180.18	0.4439
Loading #4 485.80 grams 0.1102 gm./cc.					
74	90.71	323.50	105.34	218.16	0.4486
75	95.75	322.42	105.76	216.66	0.4460
76	101.28	321.81	106.21	215.60	0.4438
77	107.59	322.36	106.71	215.65	0.4439
78	113.37	322.78	107.18	215.60	0.4438

TABLE II (CONT'D)

Run #	T_{mean} °C.	(C_g - Calibration) cal./°C.	Calibration cal./°C.	= Heat Capacity cal./°C.	cal./gm.°C.
Loading #5 619.41 grams 0.1404 gm./cc.					
80	93.17	405.51	105.56	299.95	0.4842
81	99.58	397.82	106.06	291.76	0.4710
82	106.68	395.26	106.64	288.62	0.4659
83	112.47	394.44	107.13	287.37	0.4638
Loading #6 710.26 grams 0.1609 gm./cc.					
84	94.92	460.17	105.68	354.49	0.4991
85	99.51	449.84	106.06	343.78	0.4840
86	104.15	444.63	106.44	338.19	0.4761
87	103.74	445.09	106.41	338.68	0.4768
88	108.41	440.92	106.78	334.14	0.4704

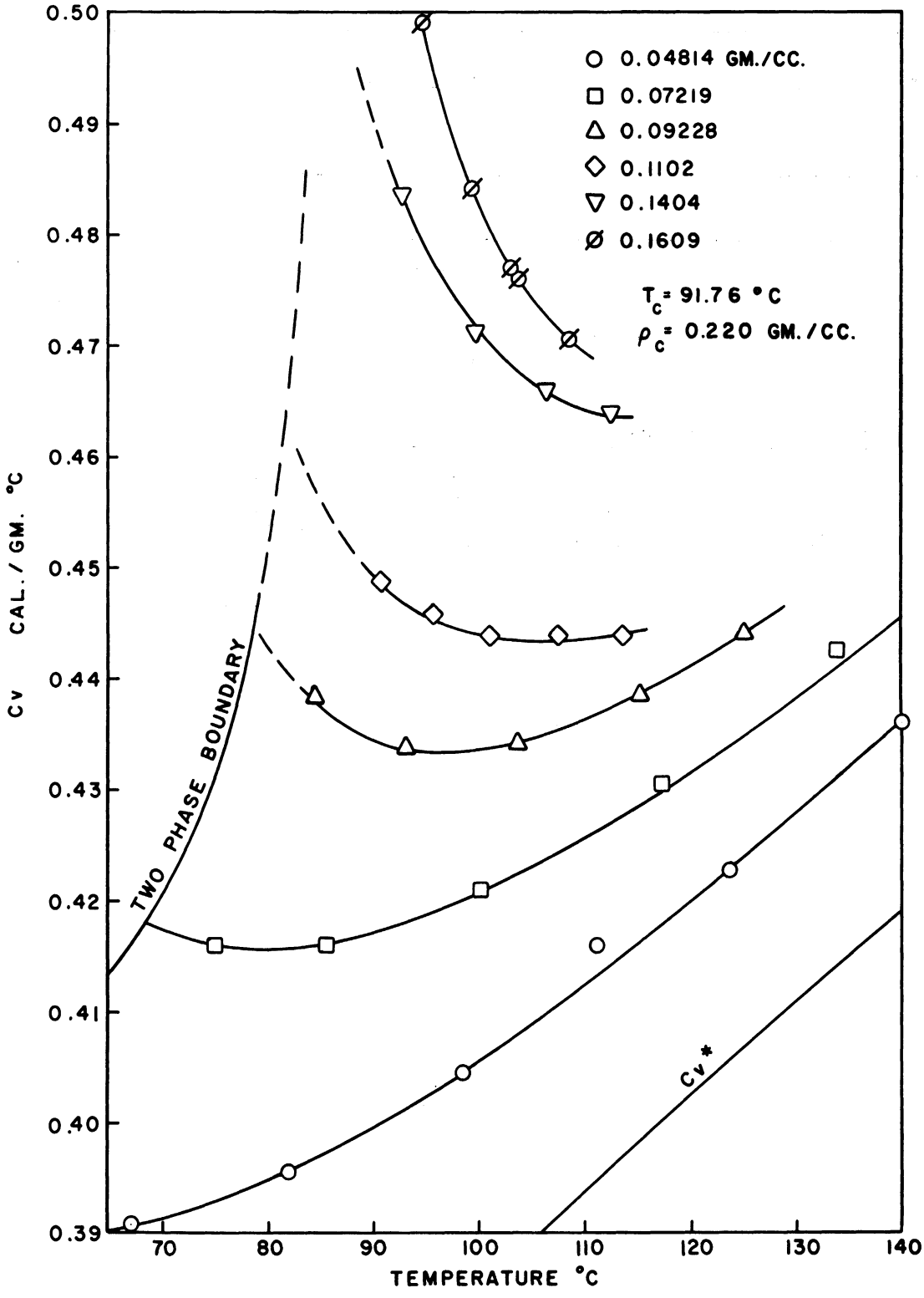

Figure 21. The Constant Volume Heat Capacity of Propylene

density; Marchman et al, report it as 0.220 gm/cc, while Farrington and Sage[12] report it as 0.230 gm/cc. The value of Marchman et al. has been used throughout this research.) A smooth curve has been drawn through the data points for each density. None of the data points differ from the curves by more than 0.4%. Except for Run #5, none differ by more than 0.2%. Figure 22, page 70, is a cross plot of these data, similar to Figure 19. The maximum scatter of the cross-plotted data is 0.5%. Figure 23, page 71, is analogous to Figure 20, showing $C_v - C_v^*$ as a function of temperature and density. As with perfluorocyclobutane, so also in Figures 22 and 23, the shape of the isotherms at low densities is sensitive to the values of C_v^*. These values are those reported by Kilpatrick and Pitzer[17]. On Figures 22 and 23 the isotherms have been drawn at even 10 degree C intervalls, except for the 95°C isotherm which has been drawn only for the four highest densities. This isotherm has been drawn at the high densities, because being only 3.24 degrees C above the critical temperature, it is roughly comparable to the 120°C isotherm for perfluorocyclobutane, which is 4.69 degrees C above the critical temperature. It was not drawn at low densities, because its behavior there is similar to that of the 90°C and 100°C isotherms.

Throughout the calculations, the maximum number of digits which could have been significant has been retained. The data are presented to 0.0001 cal/gm degree C. It is doubtful if the last digit is significant; it was retained because it influenced the placing of the data points on the plots.

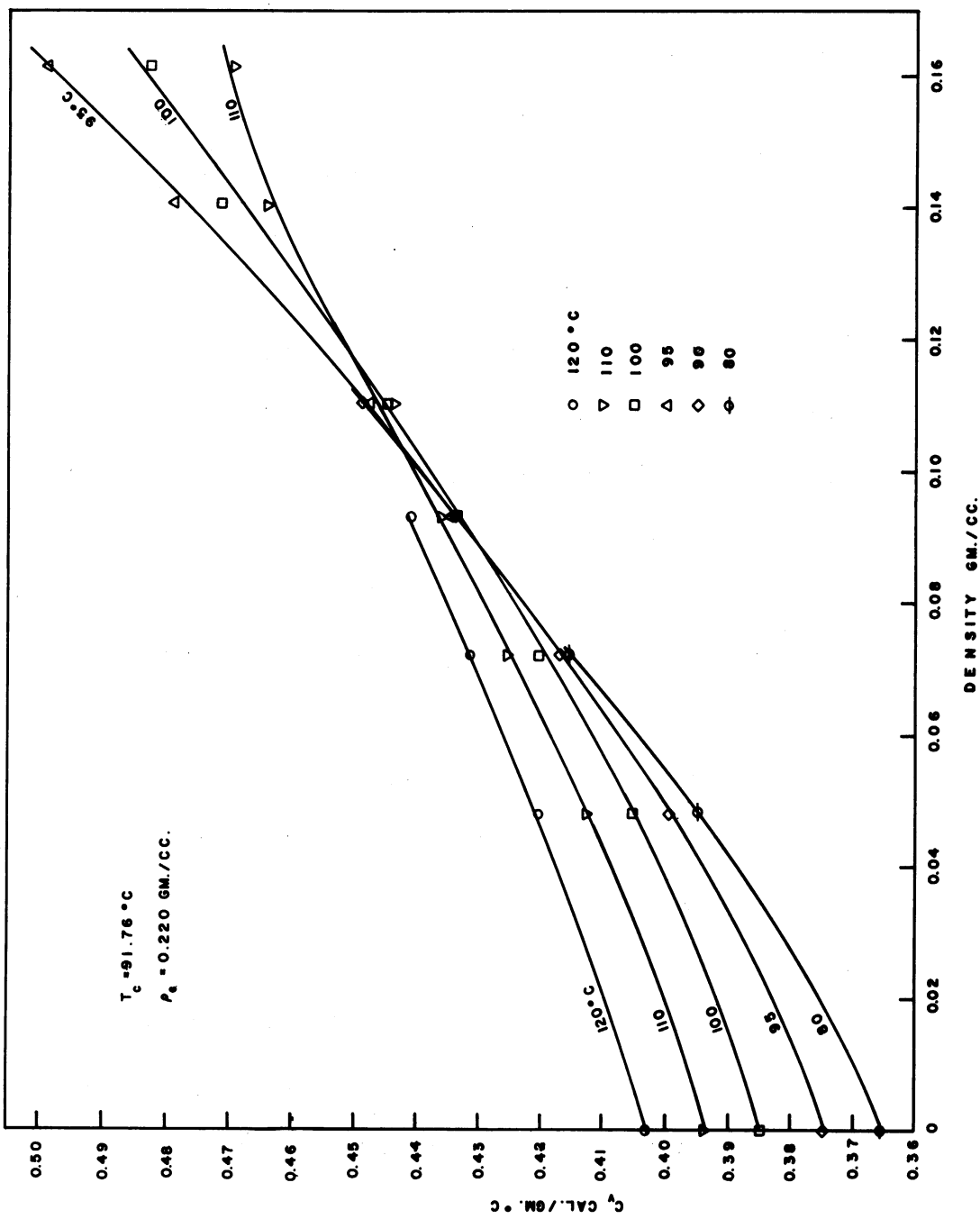

Figure 22. The Constant Volume Heat Capacity of Propylene
(This is a cross-plot of Figure 21.)

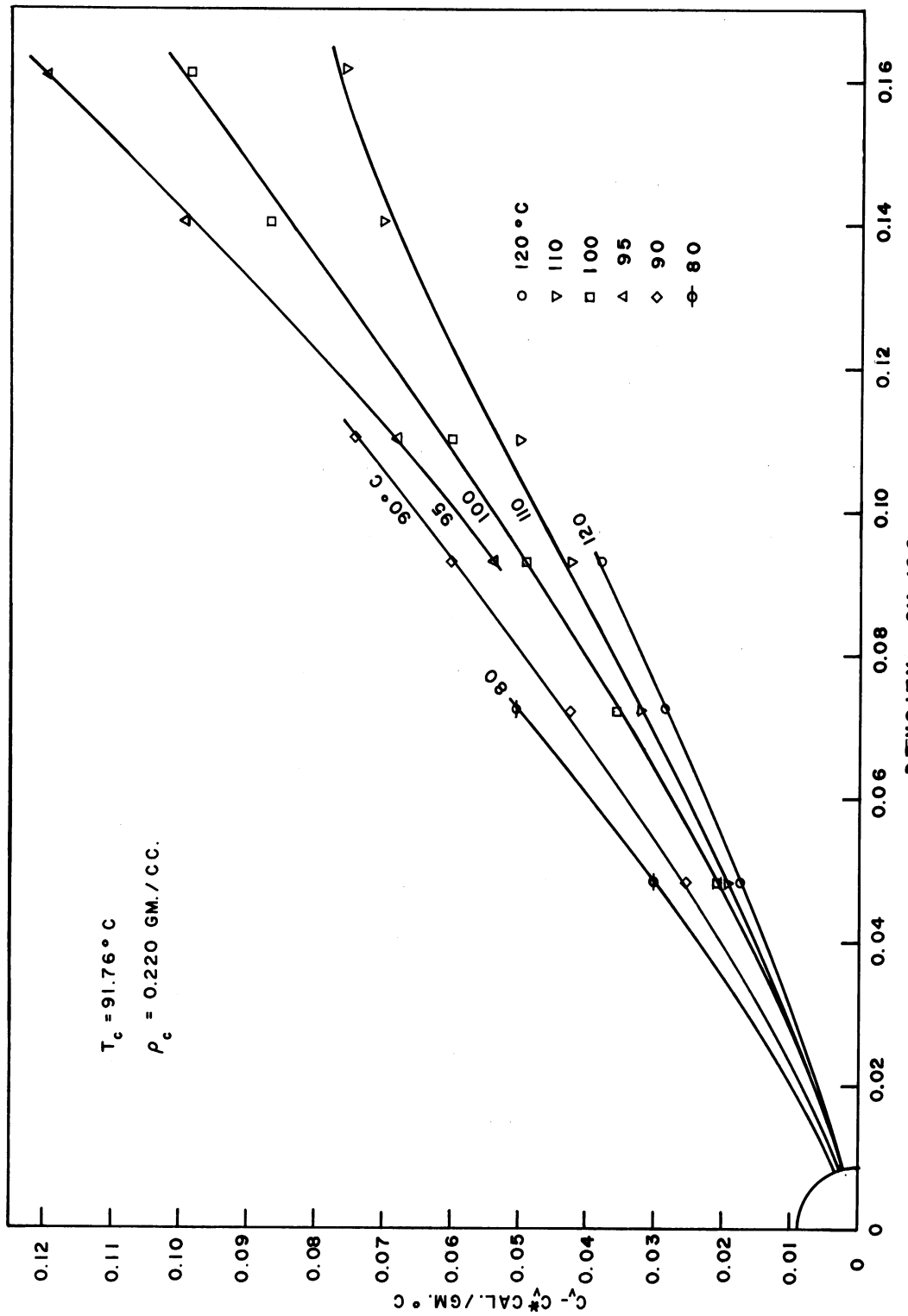

Figure 23. C_v-C_v^* of Propylene
(This is a modified cross-plot of Figure 21.)

METHOD OF CALCULATION AND ESTIMATED ACCURACY

Calculation of the Gross Heat Capacity

For a container of fixed volume, which is in perfectly adiabatic surroundings, and to which energy q is added electrically for a time interval from θ_1 to θ_2, causing an increase in temperature from T_1 to T_2, the gross heat capacity, C_g, is expressed by the relation

$$\int_{T_1}^{T_2} C_g \, dT = \int_{\theta_1}^{\theta_2} q \, d\theta \tag{18}$$

If C_g varies linearly with temperature and q varies linearly with time, then the integrations may be performed, to yield

$$C_{g_{mean}} \Delta T = q_{mean} \Delta\theta \quad \text{or} \quad C_{g_m} = q_{mean} \frac{\Delta\theta}{\Delta T} \tag{19}$$

where the mean values are those at the mean value of temperature and time respectively. The perfectly adiabatic surroundings mentioned above exist only in the fond dreams of calorimetrists; all real calorimeters have heat leakages. To arrive at correct heat capacities, these heat leakages must be taken into account. If the heat leakage rate is known explicitly in watts or calories per minute, then the correction may be in the form of a q_{corr} and Equation (19) may be rewritten

$$C_{g_{mean}} = (q_{mean} + q_{corr}) \frac{\Delta\theta}{\Delta T} \tag{20}$$

where the q's are added algebraically. If, as is more common, the leakage rate is known in the form of an equivalent temperature change T_{corr}

(that change in temperature which would have taken place in time $\Delta\theta$ if no energy had been added electrically), then Equation (19) may be rewritten

$$C_{g_{mean}} = q_{mean} \frac{\Delta\theta}{(\Delta T - \Delta T_{corr})} \qquad (21)$$

where the ΔT's are subtracted algebraically. Throughout this research Equation (21) has been used to calculate C_g. A sample calculation is included in Appendix A, page 113.

Calibration of the Calorimeter Heat Capacity

For any given run, C_g was the sum of the heat capacity of the contents of the calorimeter, plus the heat capacity of the calorimeter itself, plus the heat capacity of those parts of the electrical leads and support strings which received heat from the calorimeter. In order to know the heat capacity of the contents, it was necessary to subtract the heat capacity of the calorimeter, etc. This value was calibrated by filling the calorimeter with materials of known heat capacity and measuring C_g. The details of this procedure and the results of the calibration are shown in Appendix B, page 126.

Estimate of the Accuracy of the Calorimeter

C_g was determined by Equation (21). The uncertainties of measurement of the right-hand quantities resulted in corresponding uncertainties in C_g.

The presence of the motor in series with the heater-thermometer limited the accuracy with which the mean power, q_{mean}, could be determined. The apparent resistance of the motor, [resistance plus (counter

EMF/current)], was not steady, nor was it a steadily varying function of time. It varied erratically, over a relatively small range. The thermometer and balancing resistor in series with the motor minimized this fluctuation, but nonetheless the fluctuation limited the precision of the measurements to about two parts per thousand. The average of three instantaneous power readings was taken as q_{mean}. These readings never varied by more than ten parts per thousand, nor did their average value vary from the instantaneous power at θ_{mean} by more than three parts per thousand. Based on the above, the value of q_{mean} was probably reliable to about three parts per thousand.

The elapsed time, $\Delta\theta$, was measured by an electric timer, which could be read easily to one one-thousandth of a minute. It was dependent on the accuracy of the 60 cycle current supplied it, but since the heating periods were a minimum of 15 minutes long, the percentage fluctuation in number of cycles over that period were very small. The elapsed time measurement was probably reliable to two or three parts in ten thousand.

The temperature change, ΔT, was the difference between two measured temperatures, T_1 and T_2. In the calibration runs and all the runs of propylene loading #1 and perfluorocyclobutane loadings #1 and #2, these temperatures were only read to 0.01 degrees C. Thereafter they were read to 0.001 degrees C. The accuracy of the temperature measurements was probably no better than plus or minus 0.05 degrees C. (See Appendix C, page 130, the thermometer calibration), but because any inaccuracy in the thermometer calibration would be systematic, the differences in temperature were certainly more accurate than the temperatures

themselves. The accuracy of the thermometer for measuring differences of temperatures was probably independent of the size of the temperature difference, over the calibrated range, and was estimated at about one part per thousand. T_1 was read directly, as the temperature just before switching on the power to the thermometer-heater and motor. T_2, however, was not read directly, but was determined by extrapolating the steady drift rate after a heating period back to the time at the end of the heating period. The uncertainty caused by this extrapolation depended on the drift rate. For low drift rates (corresponding to high heat capacities of contents and therefore low ΔT's) it was low: conversely for conditions leading to higher ΔT's it was higher. It was estimated that the uncertainty caused by this extrapolation was probably about two parts per thousand in ΔT. Hence, ΔT was probably reliable to plus or minus three parts per thousand.

The heat leakage correction, ΔT_{corr}, never exceeded 2% of ΔT. The drift rates were generally known to about plus or minus 10%. This corresponded to an uncertainty in $(\Delta T - \Delta T_{corr})$ of about two parts per thousand.

Assuming the worst possible case, that all these uncertainties combined to cause the observed C_g to deviate from the true value in the same direction the maximum error in C_g would be about 0.8%. Assuming further that this maximum error occurred in one direction in all of the calibration runs, and in the other direction in all of the heat capacity runs, the result would be an overall C_v error of 3.2% for the lowest density used, and an overall C_v error of 1.1% for the highest density used. This is the maximum possible error under the most unfavorable

conditions: if the errors were random in direction then the errors in the final results would be much smaller.

The probable errors in density of the experimental gas were smaller than the probable errors in the C_v of the gas. The calibration of the volume at zero gauge pressure and room temperature was certainly accurate to plus or minus one part per thousand. The masses of the contents (except possibly for the calibration runs, for which accurate density values were unimportant) were also known to at least one part in one thousand. The correction for thermal and elastic expansion of the calorimeter was never more than 0.7% of the original volume. The data were reported for the mean value of this correction, for a given loading. (See Appendix A, the sample calculations.) The volume did vary over the course of a series of runs at one density, by up to 0.2%; however, by reporting at the mean value, the error due to this change in volume was restricted to one part per thousand. Therefore, the maximum probable error in density was 0.3%.

DISCUSSION OF THE EXPERIMENTAL RESULTS

The experimental C_v data as represented on a C_v vs. density plane, in Figures 19 and 22, show the following characteristics for both compounds:

1. at low densities all isotherms curve upward slightly; this curvature decreases with increasing temperature;

2. at densities between 1/4 and 1/2 of the critical density all isotherms are straight or nearly straight, and

3. at densities greater than 1/2 of the critical density, isotherms of temperatures within 10°C of the critical temperature are straight or curve upward slightly, while those at higher temperatures curve downward.

The experimental C_v data as presented on a C_v vs. T plane in Figures 18 and 21 show that for both compounds at densities greater than about 1/2 of the critical density C_v increases with decreasing temperature, and for temperatures near the critical temperature C_v increases very rapidly with decreasing temperature.

Extrapolation of the Experimental Data to Zero Density

As noted above, the isotherms on a C_v vs. density plane curve upward at low densities; this curvature decreases with increasing temperature. It must be remembered that the values of C_v at zero density, C_v^*, were not measured in this research, but were taken from the literature. If C_v^* at some temperature were unknown, and an attempt made to determine it from the C_v data presented here, the most natural extrapolation to zero density would be a linear one through the lowest density

C_v points at that temperature. Such an extrapolation would give values of C_v^* which would be 1% to 2% low for perfluorocyclobutane and 2% to 4% low for propylene. There are four possible explanations for this result.

1. The slight upward curvature indicated in Figures 19 and 21 may be correct. Michels and Strijland's C_v data for carbon dioxide, shown in Figure 4, exhibit this sort of curvature. If this curvature is correct, then in order to represent the data correctly, an equation of state may have the form used at low densities by the Beattie-Bridgeman equation, but it may not have the form used at low densities by the Martin-Hou or Benedict-Webb-Rubin equations. These forms are illustrated in Figure 2. In terms of PVT properties, the data suggest that at low densities the value of Equation (12) is positive. The Beattie-Bridgeman equation agrees, while the Martin-Hou and Benedict-Webb-Rubin equations require that it be negative. Since this curvature should be predictable form PVT behavior, it is of interest to attempt to verify this curvature of the experimental C_v isotherms from the PVT data. Unfortunately, such a comparison can only be made by means of some type of equation of state, either numerical or graphical. The PVT data for perfluorocyclobutane have been represented by the Martin-Hou equation[20], and the PVT data for propylene have been represented by both the Martin-Hou[19] and the Benedict-Webb-Rubin equations[21]. The functional form of both of these equations guarantees that no matter how well they represent the experimental PVT data they must predict that the isotherms on a C_v vs. density plane curve downward at low densities, as shown in Figure 2, not upward as shown by the experimental data in Figures 19 and 22. Michels et al.[25], have reported values of the 75°C, 100°C and 125°C isotherms on a C_v vs.

density plane for propylene, calculated from PVT data by the methods discussed in Appendix F, page 139. Their 75°C isotherm shows a distinct upward curvature at low densities; their 100°C isotherm shows a very slight upward curvature at low densities, and their 125°C isotherm shows a very slight downward curvature at low densities. The magnitude of the curvature shown by the 75°C isotherm according to Michels et al, is greater than that of the experimental isotherm; for the 100°C and 125°C isotherms, the curvature of the isotherm according to Michels et al, is less than that of the experimental isotherm. (A graphical comparison of these isotherms is presented in the next section.) The calculated curvature according to Michels et al., shows a decrease with increasing temperature, as does the experimental curvature. Thus, the PVT data, as interpretated by Michels et al, lend some support to the conclusion that the upward curvature of the isotherms at low densities in Figures 19 and 22 is correct.

2. The accuracy of the calorimeter decreases with decreasing density, due to the decrease in the ratio of the heat capacity of contents to heat capacity of the calorimeter. As is seen from Figures 18 and 21, the scatter of the experimental data is greatest at the lowest densities. It is possible that the extrapolation through the low density points could cause the above effect. Because of the problem of decreasing accuracy with decreasing density, it is unlikely that the true behavior of C_v at low densities can be determined with great certainty in the type of calorimeter used in this research.

3. It is possible that the C_v^* values taken from the literature are in error. It is doubtful that they could be in error by more than one percent, so that this is considered an unlikely explanation.

4. It is possible that some systematic error exists in all the C_v measurements which causes them to be low by one to four percent. The author doubts this, but knows no way to absolutely disprove it.

Of the above explanations, the most likely is the first, that that upward curvature shown at low densities is indeed the truth. However, because of the problem of decreasing accuracy of the calorimeter with decreasing density, and the possibility that the C^*_v data might be in error, the above is advanced only as a tentative conclusion. It was never the purpose of this research to devise a calorimeter which would yield the most accurate values of C^*_v, or of low density C_v's, although it was hoped that such values might be obtained as a by-product. The values which one would obtain by a linear extrapolation of the low-density data to zero density, plus some judicious correction for the upward curvature of the isotherms, are probably reliable to plus or minus 2%. This is not comparable to the accuracy obtainable by flow calorimetric measurements, but it is probably more accurate than spectroscopic calculations alone, especially in the case of complex molecules.

Comparison of the Experimental data with State Data As Represented by Various Equations of State

One of the objectives of this research was to provide C_v data over a sufficient range of temperatures and densities to allow the comparison of the experimental values with state data as represented by various equations of state. In making such comparisons, it is necessary to rely on the C^*_v data, because PVT data and equations of state can predict only C_v-C^*_v, not C_v itself. The representation of C_v-C^*_v by several equations of state is discussed in Appendix F, page 139.

The experimental PVT data for perfluorocyclobutane have been correlated by the Martin-Hou equation[20]. The equation constants are shown in Appendix H, page 155. Figure 24, page 82, shows the experimental C_v isotherms exactly as shown in Figure 19. Also shown on this plot are the C_v isotherms predicted by the Martin-Hou equation. This comparison reveals several interesting facts.

1. For densities up to 0.25 gm/cc (42% of the critical density) the experimental and calculated isotherms agree to within 0.5%, although the experimental isotherms curve upward while the calculated isotherms curve downward, as mentioned in the preceeding section.

2. For 150°C the experimental and calculated isotherms agree to within 0.5% over the entire density range. For lower temperatures the differences between the calculated and experimental isotherms increase with increasing density, so that at 120°C and 0.5366 gm/cc the experimental and calculated isotherms differ by 6.7% of the experimental C_v. Except for the 120°C isotherm, which is only 4.69 degree C above the critical temperature, the maximum difference is 2-1/2%.

3. At about 1/2 of the critical density, all of the experimental isotherms coincide. At higher densities the experimental C_v increases with decreasing temperature. Of the calculated isotherms only two, the 120 and 130°C isotherms cross, so that the equation predicts that at the highest densities C_v decreases with increasing temperature at temperatures up to 130°C, then goes through a minimum and increases with further increases in temperature.

4. As discussed previously, the Martin-Hou equation predicts that all of the isotherms will be a family of similar curves. The

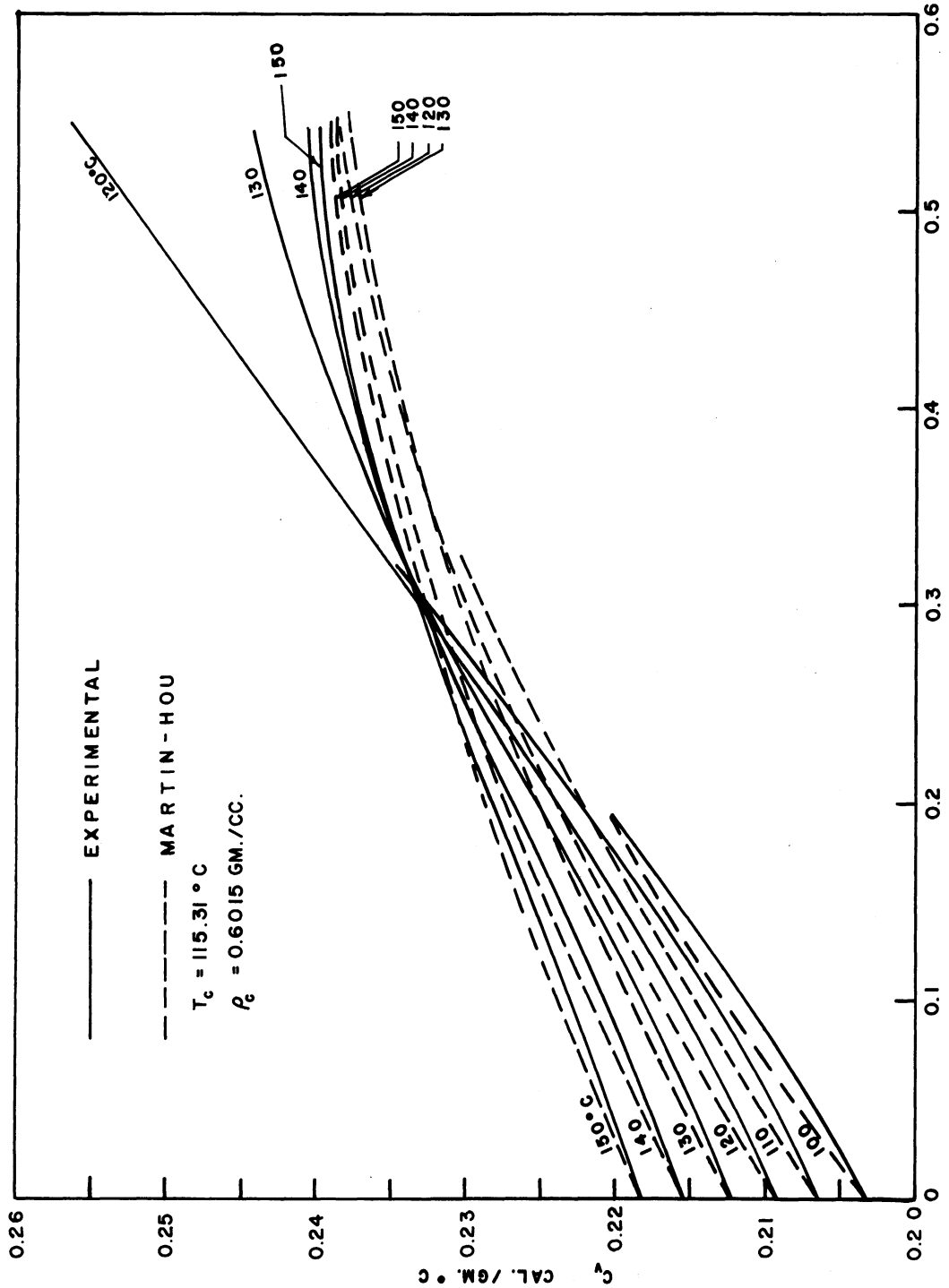

Figure 24. Comparison of the Experimental C_v of Perfluorocyclobutane with the C_v Predicted by the Martin-Hou Equation

experimental isotherms are similar at low densities and at high temperatures, but at higher densities and temperatures near to the critical temperature, this similarity disappears. At high densities the 120°C isotherm is a straight line, while the higher temperature isotherms curve downward. Thus, the functional form of the equation guarantees that it cannot represent both the experimental 120 and 150°C isotherms accurately; in order to do so it must predict a more complicated C_v-C_v^* function, perhaps one of the form

$$C_v - C_v^* = f(T) \cdot f(\rho) \cdot f(\rho, T) \qquad (22)$$

The above facts may be summarized by concluding that the equation predicts the curvature of the isochores on a P-T plot (Figure 1) well at low densities for all temperatures, and well for all densities for high temperatures, but that with increasing density and decreasing temperature, particularly for temperatures within 10°C of the critical temperature the curvature of the isochores on a P-T plot predicted by the equation is significantly less than the curvature which the C_v data implies.

On Figure 25, page 84, the experimental C_v-C_v^* vs. density isotherms shown in Figure 20 are reproduced, and compared with the predictions of the Martin-Hou equation. This is a much more severe test of an equation of state than that made in Figure 24. This plot shows that on a C_v-C_v^* basis, rather than a C_v basis, the difference between the calculated and experimental values is much enlarged, reaching 40% of the experimental value at the highest density and 120°C. If the 120°C isotherm were omitted, the maximum difference would be 21% of the experimental value.

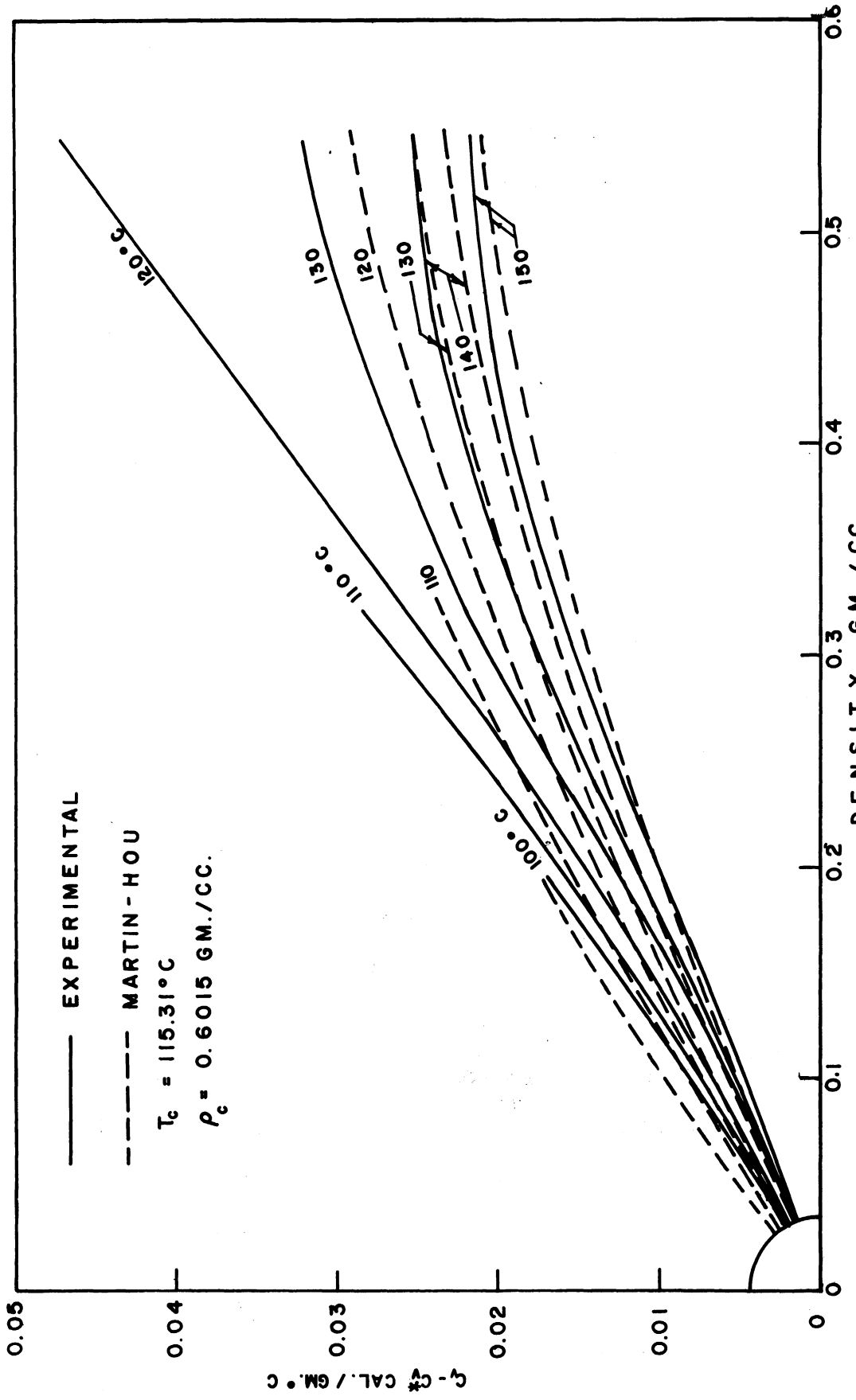

Figure 25. Comparison of the Experimental C_v-C_v^* of Perfluorocyclobutane with the C_v-C_v^* Predicted by the Martin-Hou Equation

The propylene PVT data of Marchman, Prengle and Motard[21] have been represented by both the Martin-Hou[19] and Benedict-Webb-Rubin equations[21]. The equation constants for both equations are shown in Appendix H, page 155. Michels et al.[25], have used their own PVT data to calculate the C_v of propylene by the methods discussed in Appendix F. In Figure 26, page 86, are shown the experimental C_v vs. density isotherms of propylene for 75,100 and 125°C. These are compared with the C_v vs. density isotherms calculated by Michels et al., for the same temperatures. For the 75 and 125°C isotherms over the range covered the difference between the experimental and calculated values is no more than 0.7%. For the 100°C isotherm the maximum difference is less than 1% up to 1/2 of the critical density, and increases from there with increasing density to 2-1/2% at the highest experimental density. The slight discrepancies in the values at zero density are caused by the slight difference between the C_v^* values of Stull and Mayfield[37] which were used by Michels et al., and the C_v^* values of Kilpatrick and Pitzer[17] used in this research. The 75°C isotherm of Michels et al., shows slightly more upward curvature than the experimental isotherm. Both the 100 and 125°C isotherms of Michels et al., are not distinguishable from straight lines in the low density region, although the tabular values reported show that the 100°C isotherm curves upward very slightly at low densities and the 125°C isotherm curves downward very slightly at low densities. Figure 27, page 87, is a plot of the same isotherms on a C_v-C_v^* vs. density plane. The 100°C isotherm according to Michels et al., is virtually straight over the entire density range shown; the experimental isotherm is also straight except at low densities.

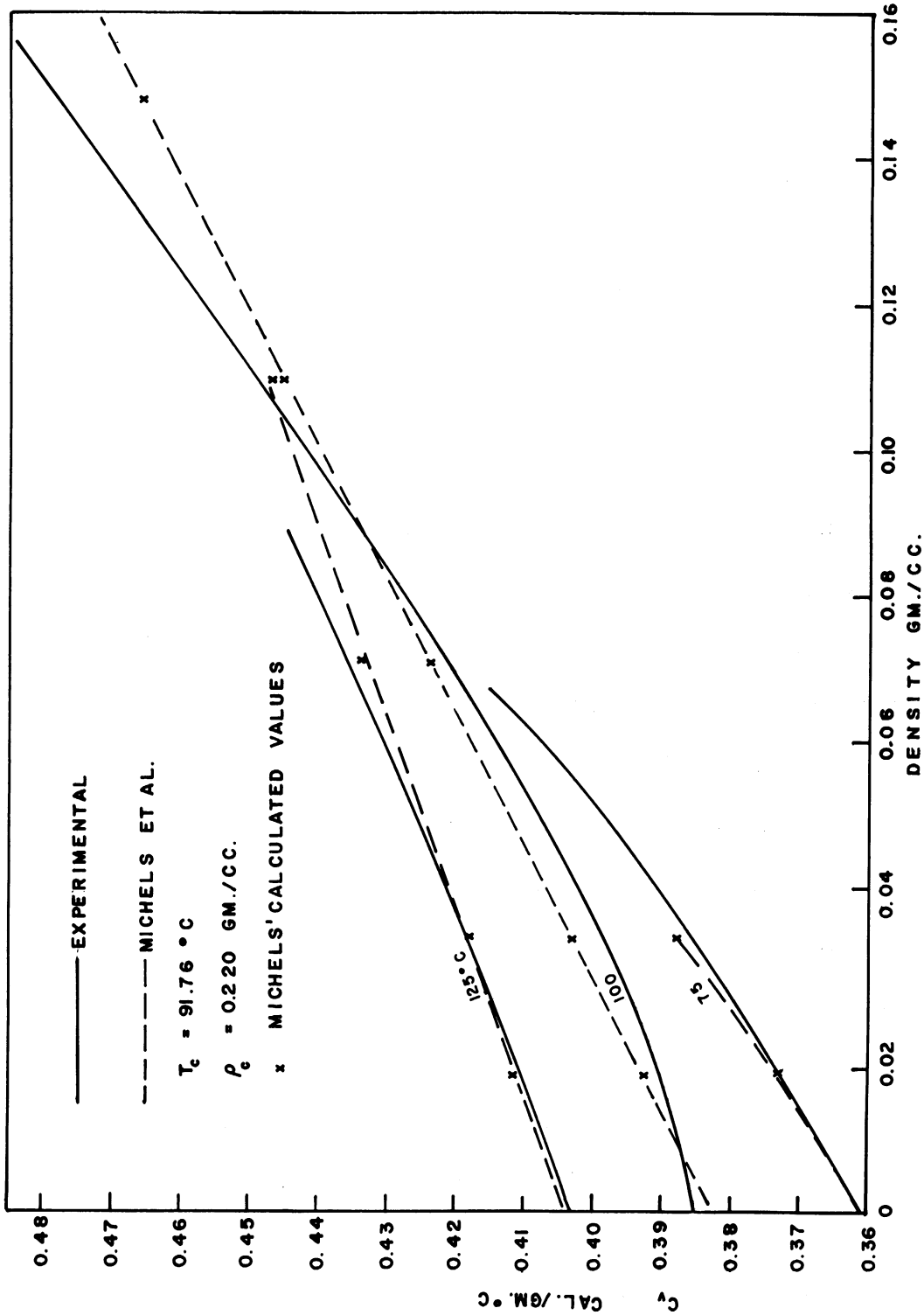

Figure 26. Comparison of the Experimental C_v of Propylene with the Calculated C_v According to Michels et al.

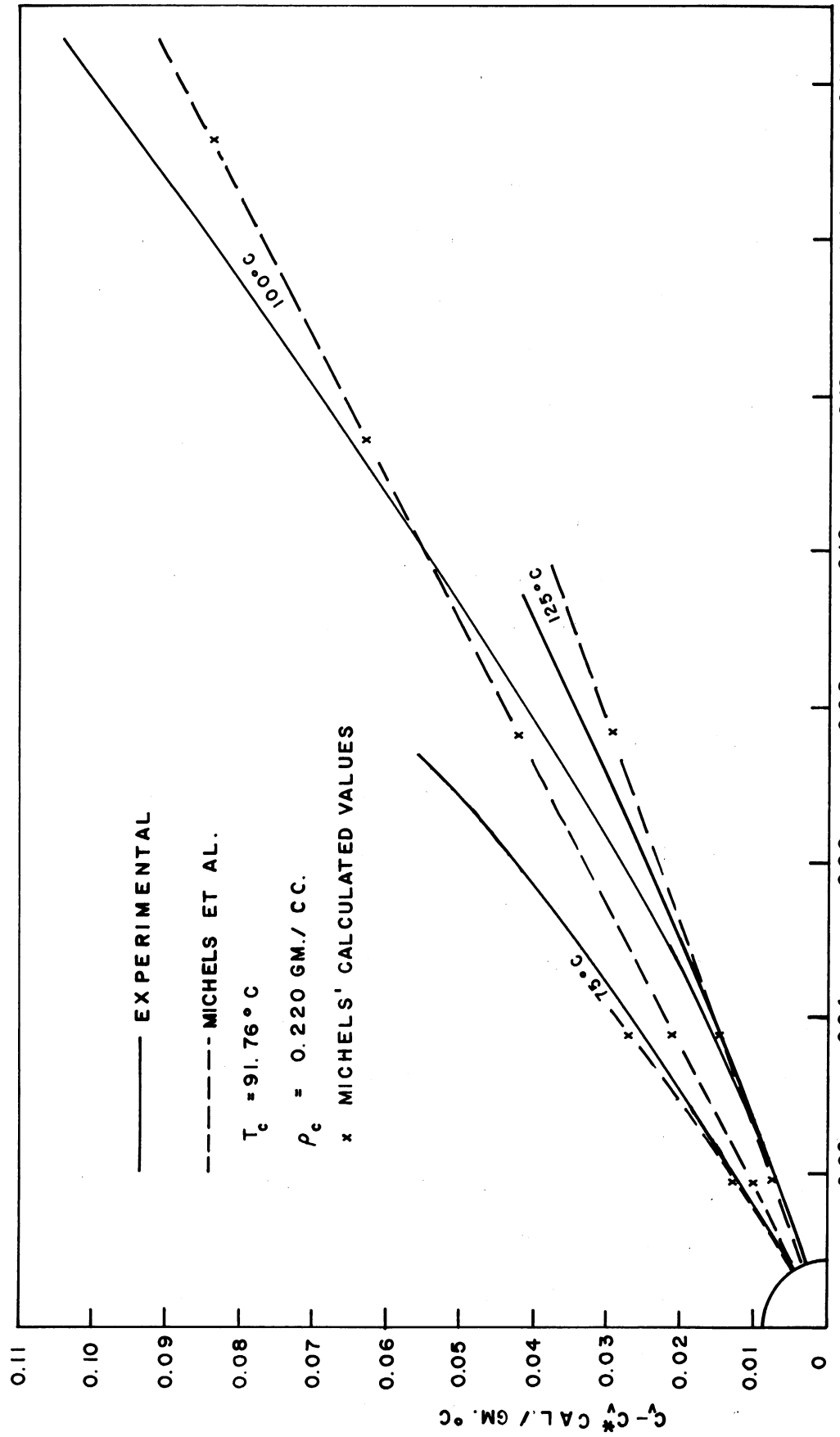

Figure 27. Comparison of the Experimental C_v-C_v^* of Propylene with the Calculated C_v-C_v^* According to Michels et al.

Figure 28, page 89, is a comparison of the experimental C_v isotherms of propylene with the isotherms predicted by the Martin-Hou equation[19]. The agreement between the experimental and calculated isotherms is similar to that in the case of perfluorocyclobutane. Along the 100°C isotherm at the highest density the agreement between the experimental and calculated values is even better than that of the experimental isotherm of C_v with the calculated isotherm according to Michels et al. At lower densities along this isotherm the agreement between the experimental and calculated isotherm is not as good as the agreement of the experimental isotherm and the calculated isotherm of Michels et al., because the Martin-Hou equation requires the isotherms to curve downward at low densities, while the experimental isotherms curve upward, and because the Martin-Hou equation does not predict that the isotherm is straight at any point of the range shown. The maximum disagreement between the experimental and calculated isotherms is 5%. Again the maximum disagreement is found at the highest density and the temperature nearest to the critical temperature. Two features similar to those observed in the comparison of the perfluorocyclobutane data with the Martin-Hou equation are also visible on Figure 28; first, the experimental isotherms show a decreasing C_v with increasing temperature at high density, which is also shown by the calculated isotherms; second, the experimental isotherms are not a family of similar curves at high densities, as the equation of state predicts them to be. This latter feature is shown more clearly on Figure 29, page 90, which is a comparison of the experimental C_v-C$\not{\text{f}}$ isotherms with those predicted by the Martin-Hou equation: the 95°C experimental isotherm curves upward at the highest

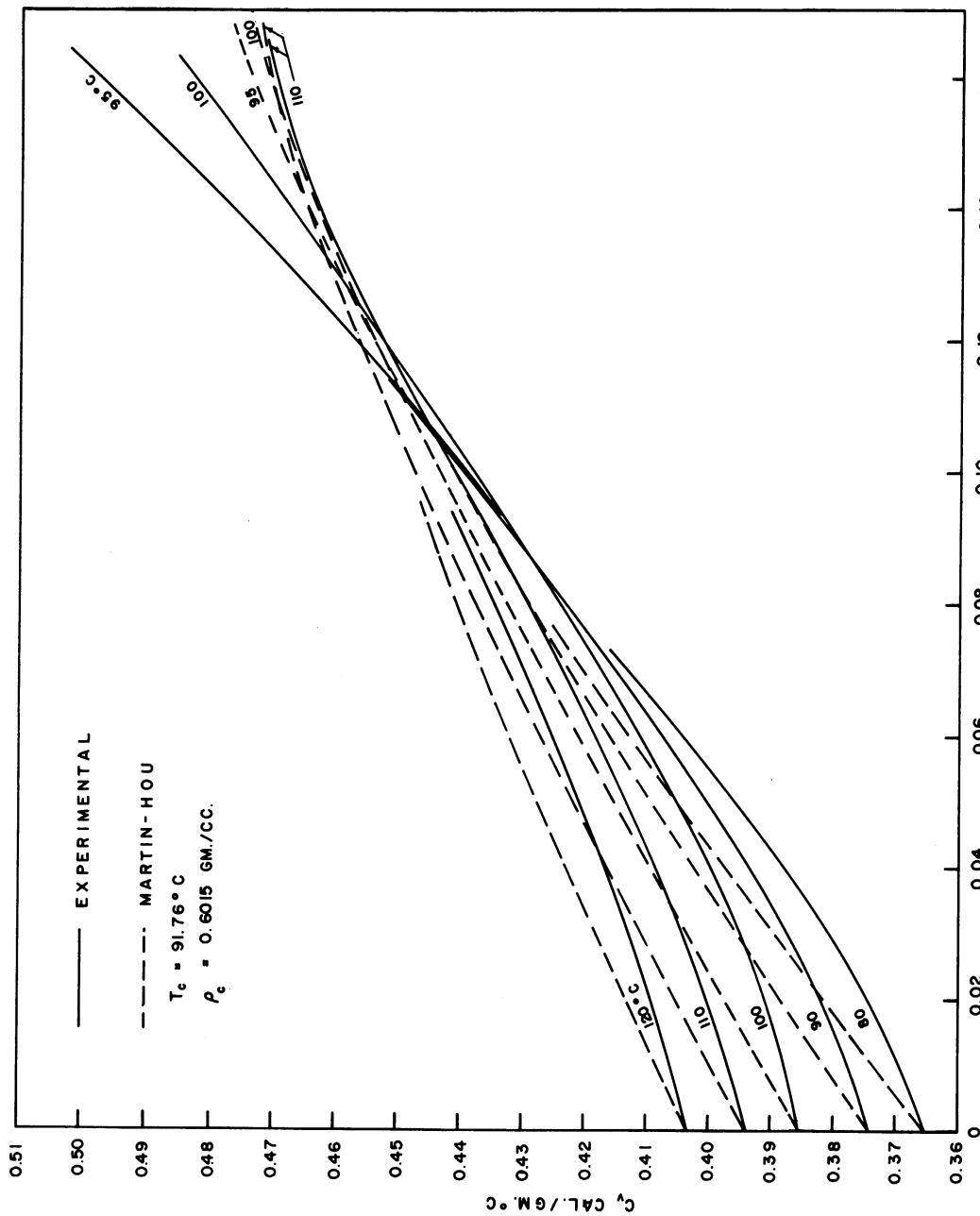

Figure 28. Comparison of the Experimental C_v of Propylene with the C_v Predicted by the Martin-Hou Equation

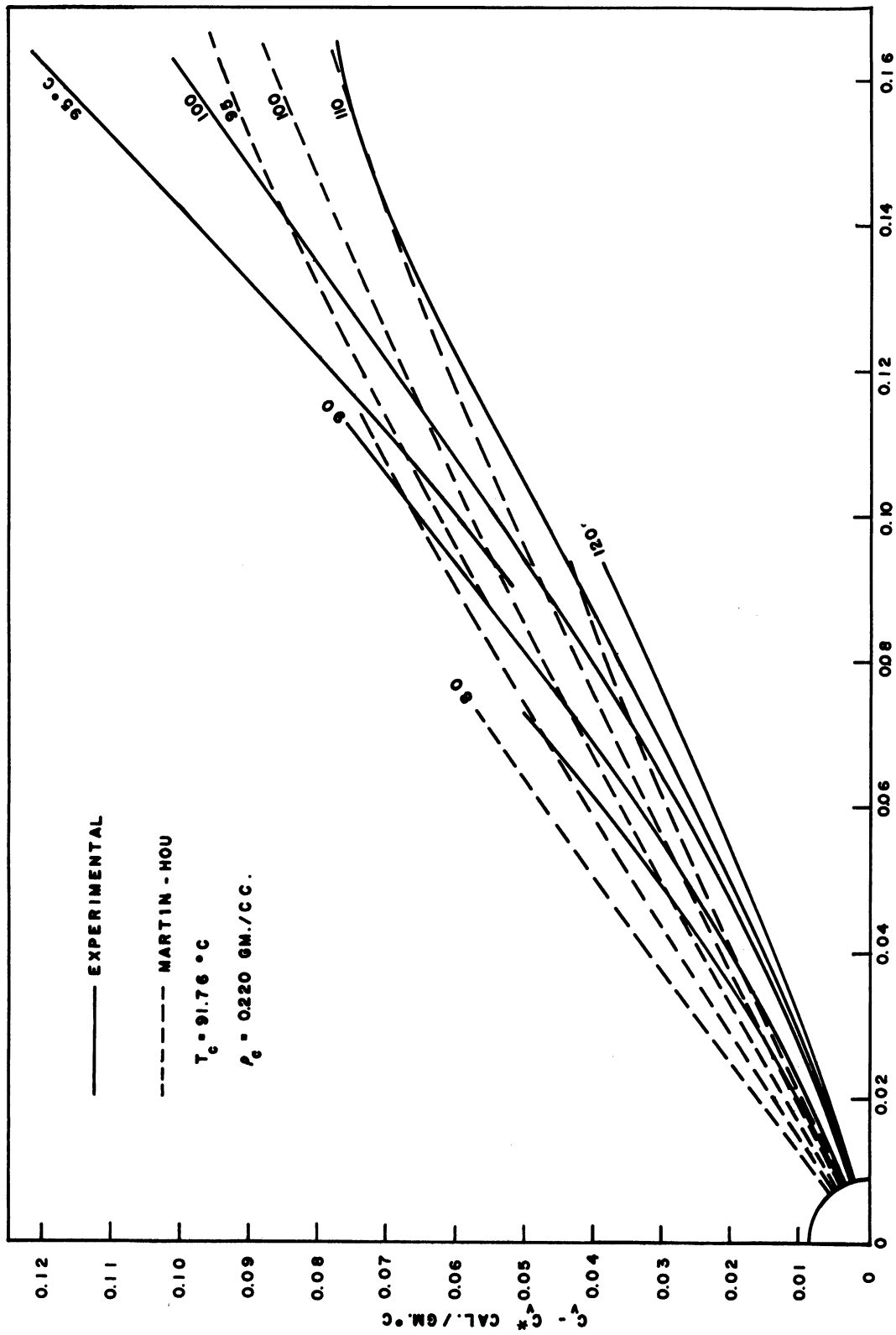

Figure 29. Comparison of the Experimental C_v-C_v^* of Propylene with the C_v-C_v^* Predicted by the Martin-Hou Equation

densities, while the 110°C experimental isotherm curves downward slightly at the same densities.

Figure 30, page 92 and Figure 31, page 93, are comparisons of the experimental C_v and C_v-C_v^* vs. density isotherms of propylene with the same isotherms predicted by the Benedict-Webb-Rubin equation[4] using the constants presented by Marchman, Prengle and Motard[21]. Both this equation and the Martin-Hou equation have been used to represent the same PVT data; nonetheless, the C_v vs. density isotherms predicted by the two equations differ significantly. The Benedict-Webb-Rubin equation predicts much higher values of C_v at densities Below 1/2 of the critical density than does the Martin-Hou equation or the experimental data; the maximum difference between the experimental isotherms and those calculated by the Benedict-Webb-Rubin equation in this region is 4%, compared with 1-1/2% for the Martin-Hou equation. The Benedict-Webb-Rubin equation predicts a greater curvature of the isotherms in the density region of 1/4 to 1/2 of the critical density than does the Martin-Hou equation; the experimental isotherms in this region are straight. At the highest density and 95°C, the difference between the experimental isotherm and that calculated by the Benedict-Webb-Rubin equation is 6.5% compared with 5% for the Martin-Hou equation. The Benedict-Webb-Rubin equation predicts that none of the isotherms cross, hence that C_v increases with increasing temperature over the entire density and temperature range of the data. This latter point is made clearer by a comparison of Figures 29 and 31. The Martin-Hou equation predicts that at the highest densities C_v-C_v^* decreases with increasing temperature more rapidly than the Benedict-Webb-Rubin equation predicts the same decrease. C_v is the sum of C_v^* and C_v-C_v^*. Because C_v^* increases (almost

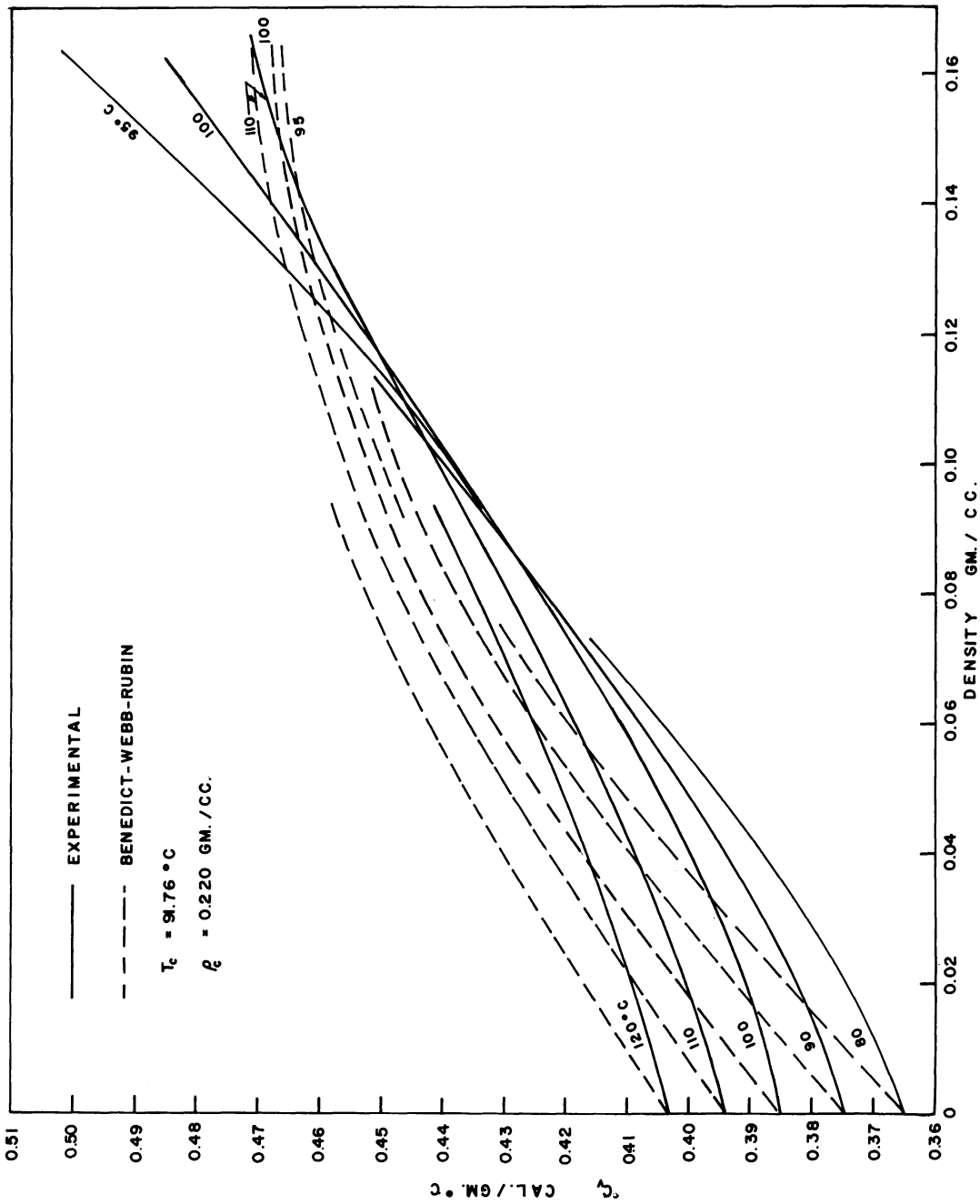

Figure 30. Comparison of the Experimental C_v of Propylene with the C_v Predicted by the Benedict-Webb-Rubin Equation

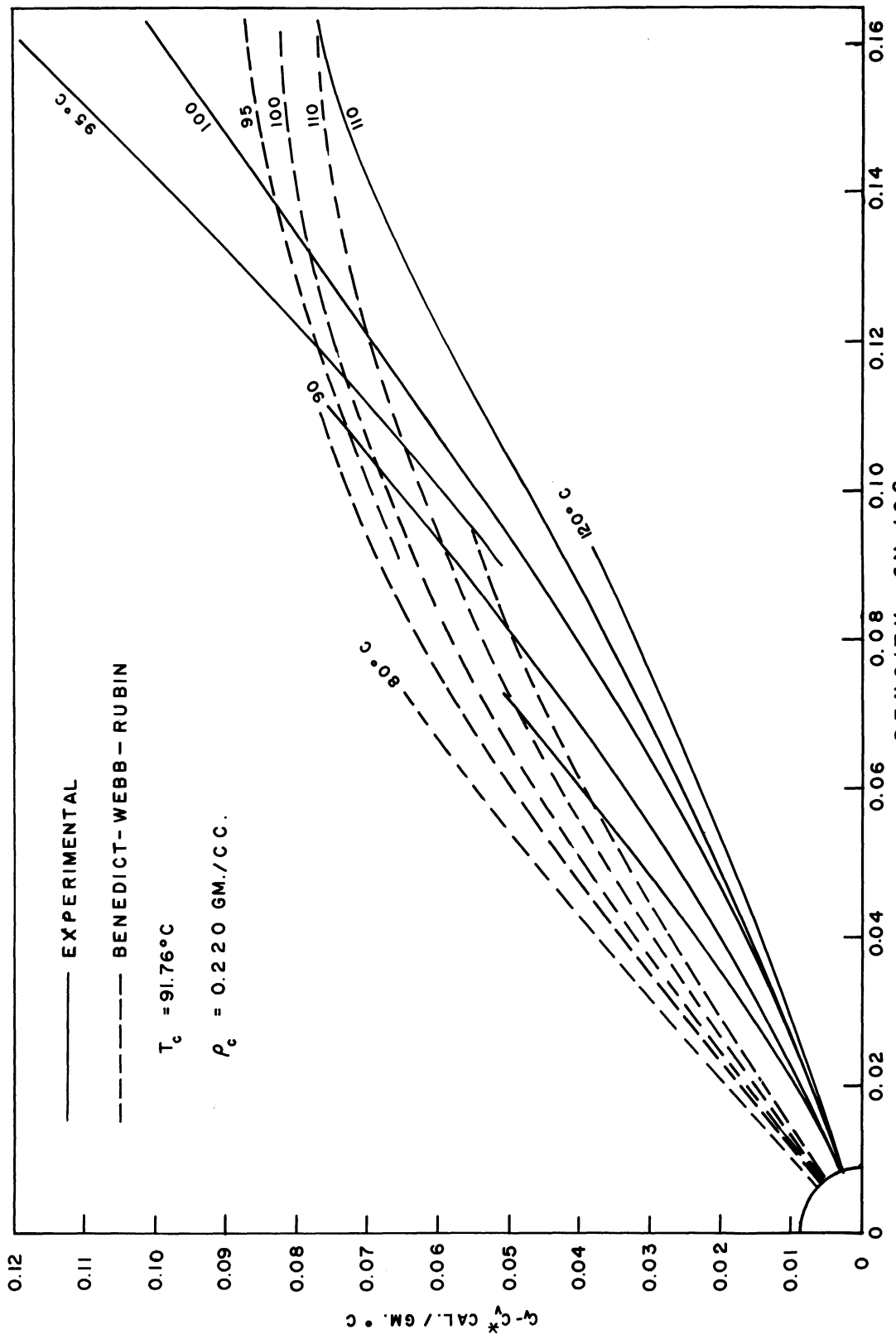

Figure 31. Comparison of the Experimental C_v-C_v^* of Propylene with the C_v-C_v^* Predicted by the Benedict-Webb-Rubin Equation

linearly) with increasing temperature, C_v can only decrease with increasing temperature if C_v-C_v^* decreases with increasing temperature more rapidly than C_v^* increases. At high densities the Martin-Hou equation predicts that C_v-C_v^* decreases rapidly enough with increasing temperature to cause C_v to decrease with increasing temperature, as does the experimental data; the Benedict-Webb-Rubin equation does not predict that C_v-C_v^* decreases with increasing temperature this rapidly. Figure 32, page 95, illustrates this behavior in another way. In it the temperature functions [defined in Equation (7)] used by the Martin-Hou and Benedict-Webb-Rubin equations are compared. The comparison is possible only on a relative basis, because one function has dimension degree K, while the other has dimension (degree K)$^{-3}$. The numerical value of each function has been multiplied by a constant, to make the value of the function equal to 100 at 100°C. As the figure shows, the temperature function used by the Martin-Hou equation,

$$f(T) = T \exp(-kT/T_c) \tag{23}$$

where k is 5.475 for propylene and T is the absolute temperature, changes more rapidly with changes in temperature than does the temperature function

$$f(T) = 1/T^3 \tag{24}$$

where T is the absolute temperature, used by the Benedict-Webb-Rubin equation. (The derivation of these temperature functions is shown in Appendix F, page 139.) Because the value of Equation (23) decreases more rapidly with increasing temperature than the value of Equation (24),

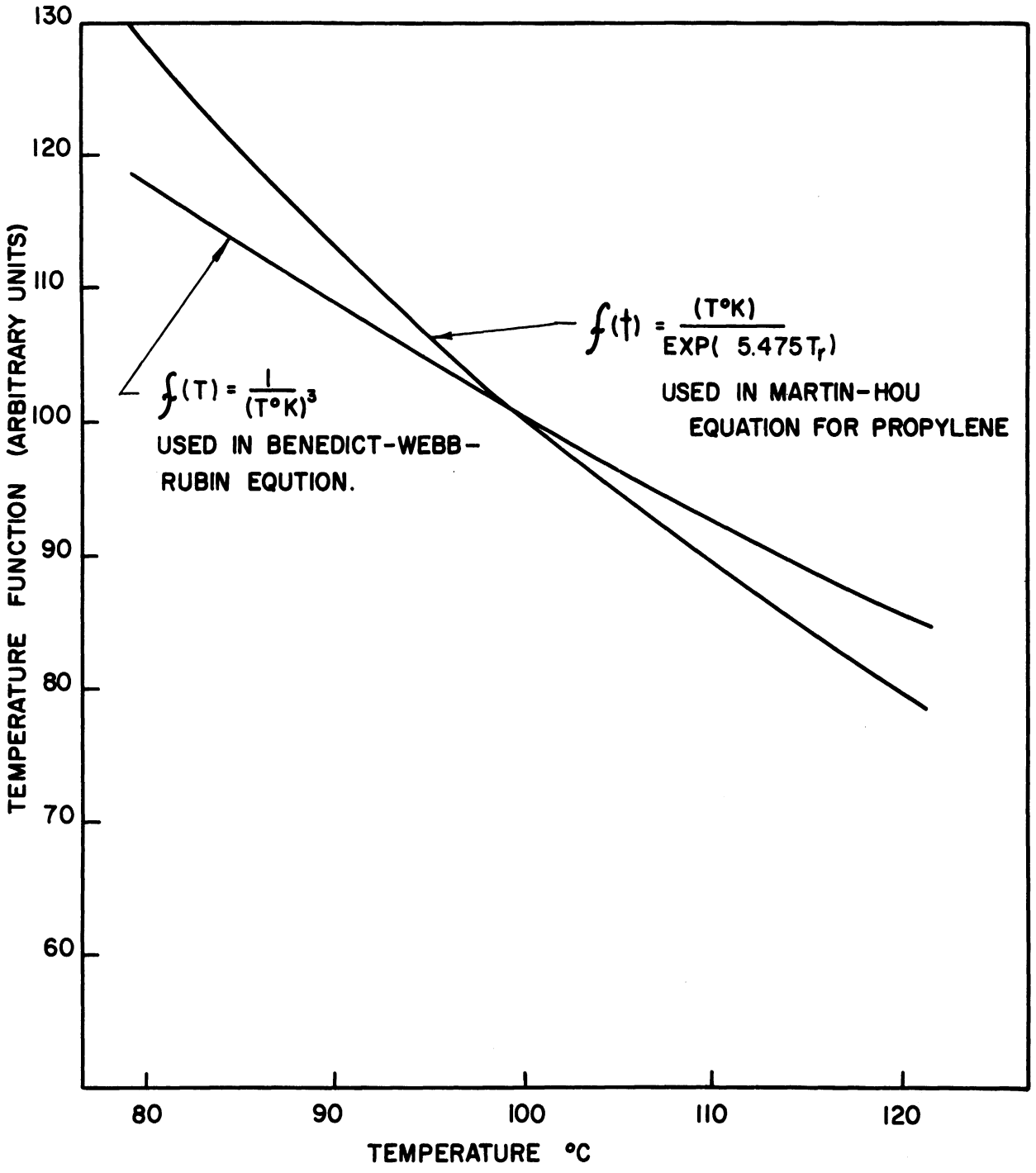

Figure 32. Comparison of the Temperature Functions in Equation (7) Used by Two Equations of State

the Martin-Hou equation is able to represent the variation of C_v with temperature at high densities more accurately than does the Benedict-Webb-Rubin equation. The experimental data suggests that for temperatures between the critical temperature and 20 degrees C above the critical temperature, a temperature function which increases even more rapidly with decreasing temperature than Equation (23) is necessary to represent the experimental data. Because the Beattie-Bridgeman equation has the same temperature function as the Benedict-Webb-Rubin equation, Equation (24), it must predict a similar behavior of C_v as a function of temperature at high densities.

In summary, the comparison of the experimental data with the predictions of equations of state shows:

1. over the range of the experimental data, the maximum difference between the measured and calculated C_v for either compound was 6.7% of the experimental C_v, which corresponded to a difference of 40% in C_v-C_v^*; this maximum difference occurred 4.7 degrees C above the critical temperature and at 89.6% of the critical density; further from the critical state the agreement is better;

2. at densities greater than 1/2 of the critical density, for temperatures less than 10 degrees C above the critical temperature, the isotherms on a C_v vs. density plane are linear or curve slightly upward; at higher temperatures and the same densities they curve downward; an equation of state which predicts that at a given density all isotherms must have the same direction of curvature (upward or downward) cannot correctly represent the C_v data for temperatures within 10 degrees C of the critical temperature and also for higher temperatures;

3. the downward curvature of the isotherms at low densities on a C_v vs. density plane, as predicted by the Martin-Hou and Benedict-Webb-Rubin equations appears to be incorrect, and to force these equations to predict values of C_v which are too high at low densities;

4. neither equation predicts that the isotherms are linear between 1/4 and 1/2 of the critical density; the C_v according to Michels et al., reproduces this feature of the experimental data, and

5. neither equation predicts the change of C_v with increasing temperature at high densities accurately; the Martin-Hou equation predicts a better approximation of it than does the Benedict-Webb-Rubin equation. The C_v as a function of temperature predicted by the Beattie-Bridgeman equation is similar to that predicted by the Benedict-Webb-Rubin equation.

The Constant Volume Heat Capacity Near the Critical Temperature and Density

As mentioned previously, for densities greater than 1/2 of the critical density, C_v increases very rapidly with decreasing temperature, as the temperature nears the critical temperature. For neither compound could the isochores for the two highest densities on the C_v vs. temperature plane be extrapolated with confidence to the two-phase boundary, or even as far as the critical temperature. This behavior is quite similar to that observed by Michels and Strijland and shown in Figure 4, page 17.

When a calorimeter containing a given mass of substance is heated from a temperature below the two-phase boundary to one just above it, held at this temperature for some time period, and then subjected to a heat capacity measurement, it is expected that the measurement

will produce a correct heat capacity. The possibility exists, however, that even after the calorimeter has been held for some time above the temperature corresponding to the two-phase boundary, some liquid may be present. Because the driving forces for the attainment of equilibrium are very small in this region such a condition might persist for some time. If some liquid were present, its subsequent vaporization would cause a very high value to be found for the heat capacity. Such a situation could account for the high C_v values found by Michels and Strijland, and for the "hysteresis" effect found by Pall et al. However, in this research the contents of the calorimeter were vigorously stirred while being heated to above the two-phase temperature, and the same type of behavior was observed. It is unlikely that a liquid could persist above the two-phase temperature under the conditions of this research.

In the section "Prior Work in Constant Volume Calorimetry", two possible explanations for the above phenomenon were suggested:

1. the isochores on a P-T plane in this region may be very strongly curved, which curvature has not been apparent from the available PVT data, or

2. one phase thermodynamic relations may not hold in this region. The first suggestion introduces a further problem. If the isochores are much more strongly curved than the PVT data suggest, then they must intersect the vapor pressure curve at lower temperatures than those commonly reported, i.e., the two-phase boundary must lie at a lower temperature for any given density than is commonly reported.

Examination of Figures 3, 4, 18 or 20 shows that at densities greater than about 1/2 of the critical density, C_v increases very rapidly

with decreasing temperature. The value of C_v at the two-phase boundary is found by extrapolation of the C_v vs. T isochore to T_{sat}, whose value is found from PVT measurements. If the two-phase boundary lies at a lower temperature than has been estimated from the PVT data, then this extrapolation must indicate even higher values of C_v at the two phase boundary than those obtained by extrapolating to the T_{sat} obtained from PVT data.

Remembering the difficulty of any experimental work in this region, it is necessary to be cautious about accepting any experimental work as correct. However, if both the PVT and the C_v data are correct, or even nearly correct, then the logical supposition is that the currently accepted model of the phase behavior of a substance in this region is too simple to represent the truth.

Generalized Constant Volume Heat Capacity Relation

If possible, it is desirable to generalize experimental findings, so that they may be used to estimate properties for substances for which experimental data are not available. For gases such generalization of properties is often made by means of the "correspondence principle". This principle states that the compressibility factor Z, defined by

$$Z = PV/RT \tag{25}$$

is the same for all gases at the same values of the reduced temperature $(\frac{T}{T_C})$ and reduced pressure $(\frac{P}{P_C})$. Accurate PVT data show that this principle in its simple form stated above is only approximately correct, and that Z as a function of reduced temperature and reduced pressure is only the same for gases with similar values of Z_C, and with similar

values of one or more other parameters, e.g., T_C, P_C. According to Equation (25)

$$\left(\frac{d^2P}{dT^2}\right)_\rho = R\rho\left[T\left(\frac{d^2Z}{dT^2}\right)_\rho + 2\left(\frac{dZ}{dT}\right)_\rho\right] \tag{26}$$

and

$$C_V - C_V^* = -RT\int_0^\rho \left[\frac{T}{\rho}\left(\frac{d^2Z}{dT^2}\right)_\rho + \frac{2}{\rho}\left(\frac{dZ}{dT}\right)_\rho\right] d\rho \tag{27}$$

Substituting

$$T = T_C T_R \quad \text{and} \quad \rho = \rho_C \rho_R \tag{28}$$

this becomes

$$C_V - C_V^* = -RT_C T_R \int_0^\rho \left[\frac{T_C T_R}{\rho_C \rho_R}\left(\frac{d^2Z}{d(T_C T_R)^2}\right)_\rho + \frac{2}{\rho_C \rho_R}\left(\frac{dZ}{d(T_C T_R)}\right)_\rho\right] d(\rho_C \rho_R)$$

$$= -RT_R \int_0^{\rho_R} \left[\frac{T_R}{\rho_R}\left(\frac{d^2Z}{dT_R^2}\right)_\rho + \frac{2}{\rho_R}\left(\frac{dZ}{dT_R}\right)_\rho\right] d\rho_R \tag{29}$$

Thus, if two gases obey the "correspondence principle" exactly, then they must have the same $C_v - C_v^*$ (expressed in molar quantities) at any T_r and ρ_r.

According to Martin et al.[20], Z_c of perfluorocyclobutane is 0.2764. According to Marchman et al.[21], Z_c of propylene is 0.2909. (There is some controversy over the Z_c of propylene; Farrington and Sage[12] report that it is 0.2758). According to Martin and Hou[19] another important factor for characterizing gases is the reduced slope of the vapor pressure curve at the critical point

$$M = - \left(\frac{dP_R}{dT_R} \right)_{V,C} \tag{29}$$

The values of this factor are 6.4 for perfluorocyclobutane[20] and 4.68 for propylene[19]. Thus propylene and perfluorocyclobutane cannot obey the "correspondence principle" exactly. In Figure 33, page 102, the values of $C_v - C_v^*$ expressed in cal/gm mole degree C are shown as a function of reduced temperature and reduced density for perfluorocyclobutane and propylene. For a given reduced temperature and density, the value of $C_v - C_v^*$ for perfluorocyclobutane is 1.6 to 2 times that for propylene. Thus, although the "correspondence principle" is a satisfactory approximation for generalizing PVT data, it is not sufficiently accurate to generalize $C_v - C_v^*$ data.

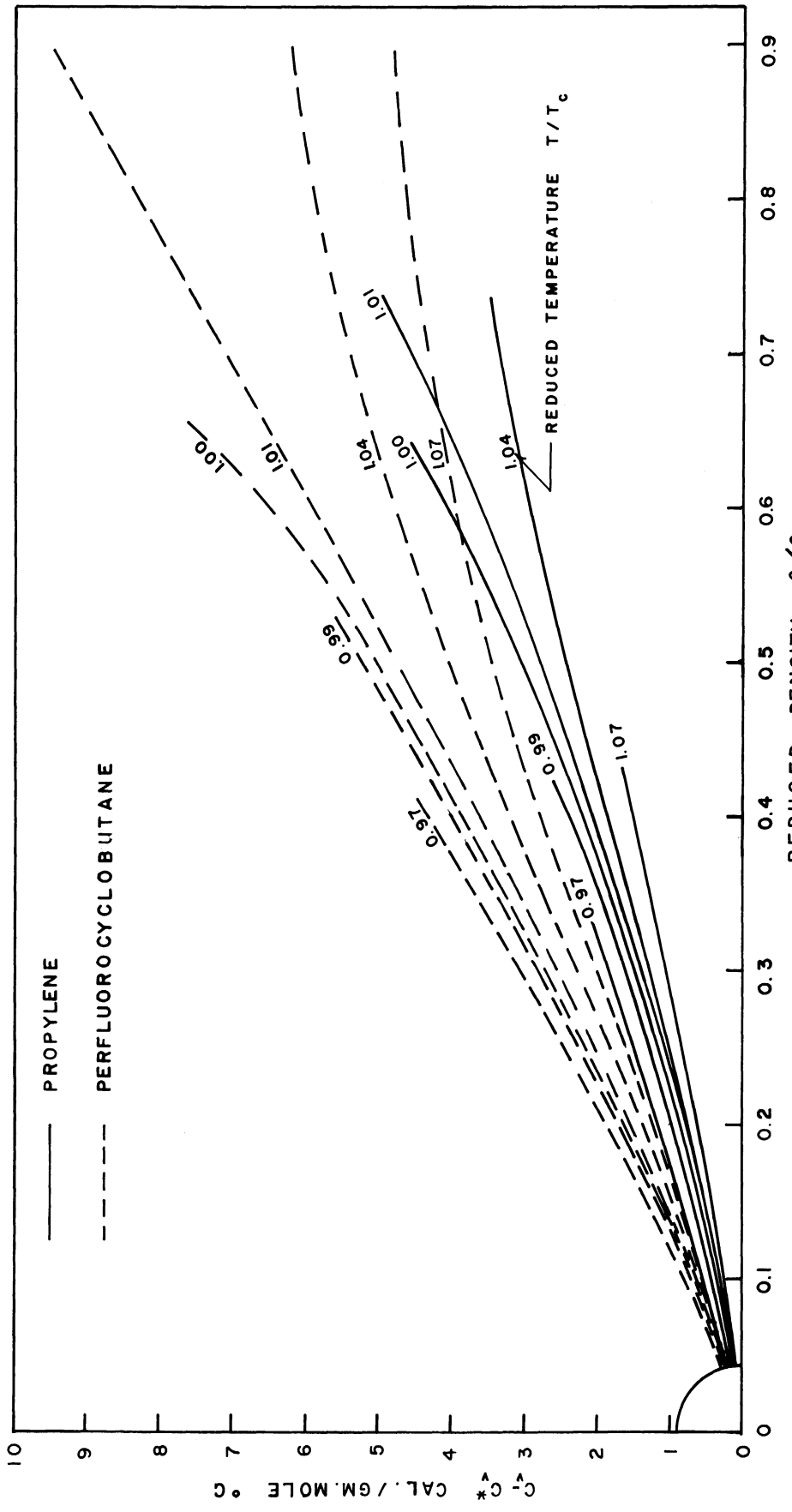

Figure 33. C_v-C_v^* As a Function of Reduced Temperature and Reduced Density

RUPTURE OF THE CALORIMETER

As mentioned previously, the calorimeter was designed to rupture at an internal pressure of 1000 psi. For all of the perfluorocyclobutane densities, and for the first two propylene densities, the upper temperature limit, 150°C, corresponded to a pressure of less than 700 psi. For the next two propylene densities, the upper temperature limit was chosen as that temperature corresponding to a pressure of 700 psi. For the fifth propylene density, the upper temperature limit was chosen as that temperature corresponding to 800 psi. For the sixth propylene density, the upper temperature limit was chosen as that temperature corresponding to 900 psi. During the heating period of what would have been Run #89 the calorimeter ruptured. The calorimeter contained 710.26 grams of propylene, and was at a temperature of about 115°C. The corresponding pressure was about 860 psi. The rupture occurred at a pressure below the design pressure for rupture. The thickness of the weld may have been less than the wall thickness, or the estimate of the yield stress of the steel may have been too high. The yield stress was estimated at 64,500 psi. The stress at rupture was calculated at 55,500 psi. Since this estimate of the yield stress was based on a guess as to the annealing effects of the weld, a 16% error in it would not be surprising.

The rupture caused the instantaneous destruction of the vacuum container and an explosion ensued which broke windows, shifted a cinder-block wall by 6 inches, burned the author on the exposed parts of his body, and generally wrought havoc in the room. The following is the author's analysis of the sequence of events of the explosion, as deduced from the evidence left by it.

1. The calorimeter ruptured. The rupture began at some weak point of the weld joint between the two halves of the calorimeter, and propagated along the weld with great velocity. (At no point did the torn edge of the calorimeter appear to be more than 1/8 inch away from the center of the weld.)

2. The gas was released into the vacuum container in a very short time interval. The calorimeter halves were hurled against the adiabatic shield and flattened neatly. Figure 34, page 105, shows the two halves of the calorimeter after the rupture; from their shape the reader can infer the velocity with which they must have struck the plates of the adiabatic shield.

3. The adiabatic shield was torn apart at the silver-soldered joints, and deformed by the pressure of the gas. Figure 34 also shows the six members of the adiabatic shield and the extent of their deformation.

4. The top of the vacuum container, which was intended to contain the experimental gas in case of a calorimeter rupture, was torn loose. The estimated pressure inside the vacuum container after the rupture was 246 psi. The container was designed to withstand an internal pressure of 250 psi as a static pressure, so that the failure of the top must be laid to inadequate container design.

The four Stupakoff ceramic headers soft-soldered into the wall of the container were expected to act as bursting discs, relieving the pressure before it reached its maximum value. The rupture caused a very sudden pressure rise; three of the four Stupakoff seals did pop out, but they did not lower the pressure rapidly enough to save the top. The

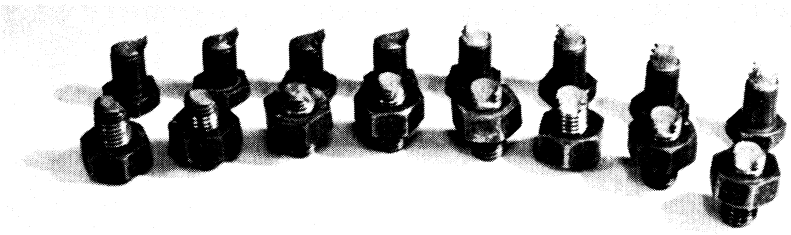

The Cover Bolts

The Adiabatic Shield

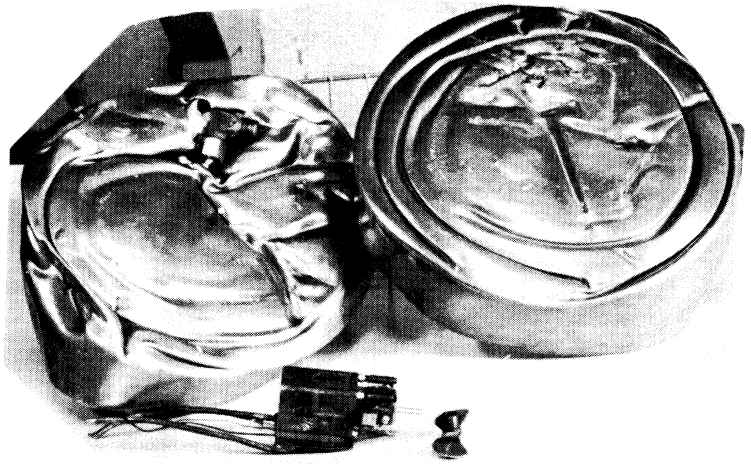

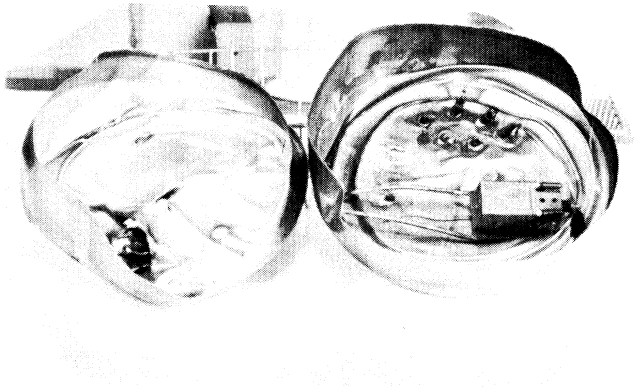

The Calorimeter

Figure 34. Parts of the Calorimeter After the Rupture

forces caused by a sudden application of a pressure are much greater than those caused by the gradual application of the same pressure (See Randall, et al.[32]; the top was not designed to withstand the suddenly applied pressure. In addition to the pressure force, the top was subjected to the force caused by the impact of the top member of the adiabatic shield and the top of the calorimeter upon it; it was not designed to withstand this additional force. Under all the forces acting on it, the top buckled upward, as shown in Figure 35, page 107. Thus its mounting straps applied a very uneven force on the bolts causing severe bending stresses. Figure 34, page 105, shows the eight bolts which had retained the top after the rupture; it is seen from the figure that none of them broke in the clean "cup-and-cone" typical of purely axial loading. Based on the calculated pressure, the top surface area, and the cross sectional area of the bolts, the stress at the minimum cross section of the bolts due to static pressure alone was 34,700 psi. This is more than the commonly prescribed allowable figure, 20,000 psi, but it alone should not have been sufficiently to break the bolts. In summary the errors in design of the top closure were: failure to allow for the effects of a sudden pressure rise, failure to allow for the effects of the kinetic energy of the top of the calorimeter and shield members as they struck the top plate, failure to provide adequate stiffening against bending for the top plate, and worst of all, failure to allow an adequate margin of safety in the static pressure calculations.

5. The propylene rushed out of the vacuum container, mixed with air and detonated. The spark for the detonation may have been supplied by one of the many electrical leads which were severed by the rupture, or by a spark due to the collision of some of the metal parts.

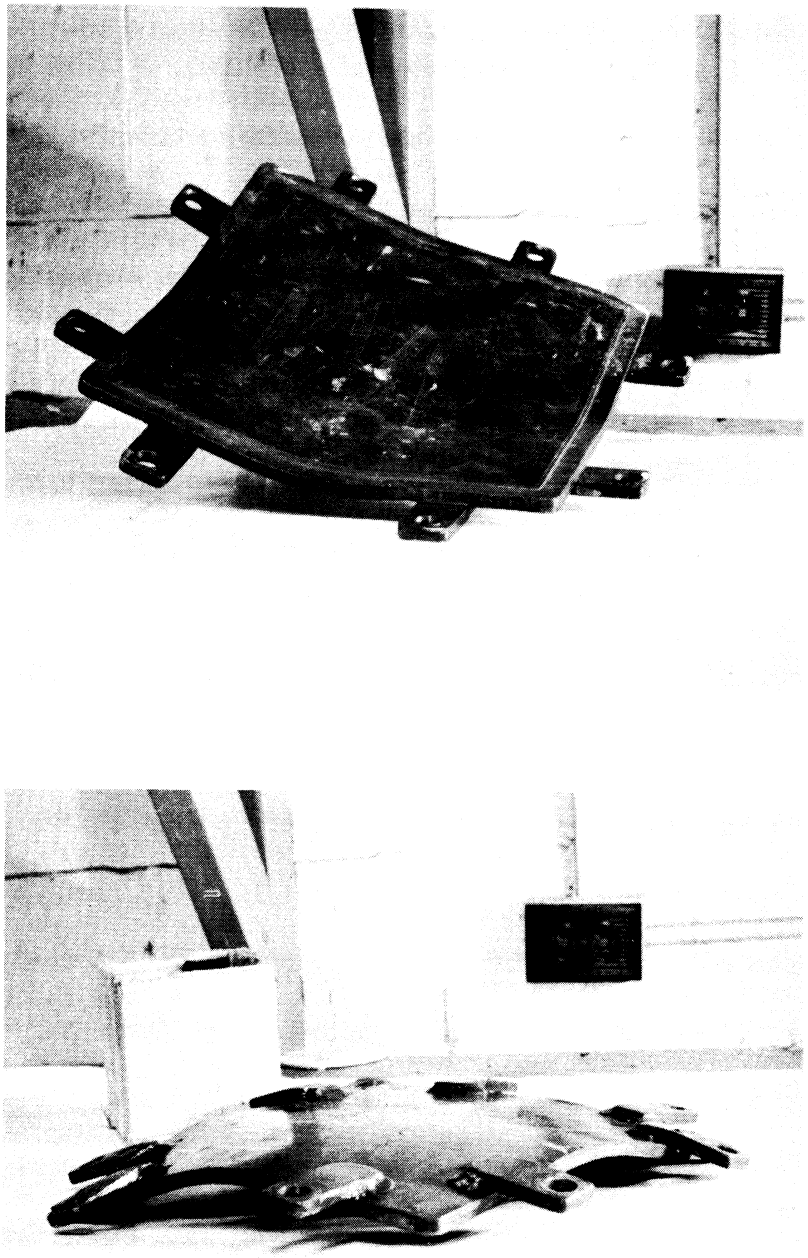

Figure 35. Buckling of the Top Plate of the Vacuum Container

In view of the energy released, the actual damage was fortunately slight. The author, who was operating the apparatus at the time of the rupture, and hence was about three feet from the vacuum container (but was screened from it by the plywood shield) was burned. He was hospitalized for 12 days, primarily as a precaution against possible infection. His doctors have assured him that he will have no scars nor any permanent injuries. Mr. Yu-Tang Hwang, who was studying in the room at the time of the rupture, received minor scratches and burns. Numerous windows were broken, but none of the flying glass struck anyone. The calorimeter, adiabatic shield and vacuum container, were destroyed, but most of the measuring and vacuum systems escaped serious damage.

When this work is resumed, it is recommended that the safety design be based less on containment of the products of a rupture than on the provision of adequate venting and adequate place for the products of a rupture to go. The vacuum container should be strong enough to withstand any internal pressure possible, even if applied suddenly, but it should have adequate bursting discs and vent lines so that any inflammable products of a rupture can be rapidly carried outside of the building. A cylindrical vacuum container would be more desirable than a cubical one, because it would have less top surface area for a given calorimeter volume. As an added precaution, it would be well to build the calorimeter assembly within a test cell, or some other heavy-walled room so that possible safety miscalculations will have less destructive potential. When these requirements have been met, the work can proceed safely.

CONCLUSIONS AND RECOMMENDATIONS

Conclusions

The following are the conclusions drawn from this research.

1. Constant volume calorimetry in thin-walled vessels at moderate pressures is a simple, practical and accurate method of obtaining useful thermodynamic data. This method has been applied successfully for the first time in this research.

2. The experimental data, as represented on a C_v vs. density plane, show the following characteristics:

   a. at low densities all isotherms curve upward slightly; this curvature decreases with increasing temperature;

   b. at densities between 1/4 and 1/2 of the critical density all isotherms are straight or nearly straight, and

   c. at densities greater than 1/2 of the critical density, isotherms of temperatures within 10°C of the critical temperature are straight or curve upward slightly, while those at higher temperatures curve downward.

3. For temperatures close to the critical temperature and densities greater than 1/2 of the critical density, C_v increases very rapidly with decreasing temperature. This behavior would not be expected from the available PVT data.

4. For identical reduced temperatures and reduced densities $C_v - C_v^*$ on a molar basis is 1.6 to 2 times as great for perfluorocyclobutane as for propylene; thus $C_v - C_v^*$ for these gases cannot be generalized by the simple form of the "correspondence principle".

5. The equations of state which have been used to predict C_v from PVT and C_v^* data represent the experimental C_v data with a maximum error of 6.7% for perfluorocyclobutane and 6.5% for propylene. These maximum errors occur for the highest densities used for each compound and for temperatures within 5 degrees C of the critical temperature. For temperatures and densities farther removed from the critical state the agreement between the experimental and calculated C_v is better.

6. The experimental data suggests that the Martin-Hou and Benedict-Webb-Rubin equations of state predict the direction of curvature of the isotherms at low densities on a C_v vs. density plane incorrectly. The Beattie-Bridgeman equation, however, predicts the same direction of curvature as the experimental data.

7. The Beattie-Bridgeman, Martin-Hou and Benedict-Webb-Rubin equations all predict that at a given density, all of the isotherms on a C_v vs. density plane will have the same direction of curvature (upward or downward); the experimental data (as mentioned in Conclusion 2c) show that for temperatures greater than 1/2 the critical density the direction of curvature of the isotherms changes with changes in temperature. Hence these equations cannot accurately represent the C_v data over the experimental density and temperature range.

8. Neither the Martin-Hou nor the Benedict-Webb-Rubin equation accurately represents the relation of C_v to temperature at high densities, but the Martin-Hou equation predicts a better approximation of it than does the Benedict-Webb-Rubin equation. The C_v as a function of temperature predicted by the Beattie-Bridgeman equation is similar to that predicted by the Benedict-Webb-Rubin equation.

Recommendations

When this work is resumed, in addition to the changes recommended for safety reasons, it is recommended that the adiabatic shield and vacuum container be made in a cylindrical form. The cubical shield used in this research was more likely to have non-uniform temperatures than would a cylindrical shield of the same thickness. Furthermore, a cylindrical adiabatic shield should be wound with glass-insulated resistance wire, which would be a more responsive and more uniform heater than were the heating tapes used in this research. With a cylindrical vacuum container, the top closure should be gasketed with an "O-ring" which would be a more satisfactory gasket than the silicone rubber sheet gasket used in this research.

It is also recommended that several calorimeters be constructed to be used at different times, using the same adiabatic shield and control and measuring instruments. The calorimeters should be designed for various pressure ranges. For example, a calorimeter identical with the one used in this research should be used for pressures from 200 to 600 psi. A second calorimeter with a smaller diameter and a thicker wall should be used for the pressure range 500 to 1000 psi, etc. Although such a procedure will entail more construction and calibration, it will allow the measurement of C_v over a wider density range.

The available PVT data suggest (see Price[31] or Woolley et al.[39]) that for temperatures in the range of 2 to 3 times the critical temperature C_v should increase very slightly with increasing density, at constant temperature. At higher temperatures, perhaps 4 to 6 times the critical temperature these data suggest that C_v should again increase

rapidly with increasing density. Thus, in the range of temperatures from 3 to 5 times the critical temperature, $(C_v-C_v^*)_\rho$ should increase with increasing temperature; for the temperatures covered in this research $(C_v-C_v^*)_\rho$ decreased with increasing temperature. It is recommended that the C_v of some low-boiling point material, like hydrogen, helium, argon, nitrogen or oxygen be measured over these temperature ranges to see if this prediction of the PVT data is borne out.

APPENDIX A - SAMPLE CALCULATIONS

Volume of the Calorimeter

The volume of the calorimeter was determined as follows.

1. The calorimeter was evacuated to an indicated pressure of 0.170 mm Hg.

2. The calorimeter was weighed on the Toledo balance in the Highway Department Laboratory. This balance can weigh objects weighing up to 10 kilograms, and be read to plus or minus one gram. The evacuated calorimeter weighed 874 grams.

3. The calorimeter was immersed in water, and its valve opened, allowing the water to fill it. After filling was complete, the valve was left open for 1/2 hour, for the calorimeter to come to thermal equilibrium with the surrounding water. Then the temperature of the water was determined with a mercury-in-glass thermometer to be 23.8°C. The specific gravity of the water was determined with a float hydrometer to be 1.000.

4. The valve of the calorimeter was closed, and the calorimeter removed from the water. The calorimeter was carefully dried, and reweighed. It weighed 5249 grams. Thus, the mass of the water contained was 4375 grams. The water was removed from the calorimeter.

5. The specific volume of water at 23.8°C was found from Perry[30] to be 1.00263 cc/gm. The correction for imperfect evacuation was 740.17/740 = 1.000229. Therefore, the volume of the calorimeter at 23.8°C and zero gauge pressure was (4375 gm)(1.00263 cc/gm)(1.000229) = 4387 cc.

Volume changes due to temperature changes were calculated by the approximate formula

$$\left(\frac{d \ln V}{dT}\right)_P = \text{3(linear coefficient of thermal expansion)} \qquad (30)$$

The value of the linear coefficient of thermal expansion was taken from the ASM Metals Handbook[2] as 5.0×10^{-6} per degree C, for the type of steel used. Therefore

$$\left(\frac{d \ln V}{dT}\right)_P = 1.5 \times 10^{-5} \ ^\circ C^{-1} \qquad (31)$$

For the change in volume with changes in pressure, the following formulae were used:

$$\left(\frac{d \ln V}{dP}\right)_T = 3\left(\frac{d \ln r}{dP}\right)_T \qquad (32)$$

and

$$\left(\frac{d \ln r}{dP}\right)_T = \frac{(0.25)(\text{diameter})}{(\text{wall thickness})(\text{Young's Modulus})} \qquad (33)$$

where r is the radius of the sphere. Inserting 8 inches for the diameter, 0.031 inches for the wall thickness and 30×10^6 psi for Young's Modulus, this becomes

$$\left(\frac{d \ln V}{dP}\right)_T = 0.667 \times 10^{-5} \ psi^{-1} \qquad (34)$$

Because of the small values of these quantities, all second order differentials were ignored, and the following approximation used

$$d \ln V = \left(\frac{d \ln V}{dT}\right)_P dT + \left(\frac{d \ln V}{dP}\right)_T dP \qquad (35)$$

As an example, for propylene loading #6, the two-phase boundary temperature was about 90°C (based on the data of Marchman, Prengle and Motard[21]), and the pressure was 650 psi. Since the calorimeter was surrounded by vacuum, the absolute and gauge pressures were the same. Therefore, according to Equations (31), (34) and (35) the volume correction for this condition was

$$\frac{dV}{V} = (90-24)(1.5\times10^{-5}) + (650)(0.667\times10^{-5}) = 0.0054$$

For the temperature of 110°C at which the last completed run of this loading was ended, the pressure was about 800 psi. The corresponding correction was 0.0066. In the interest of simplicity, all of the runs of any loading were reported at the average density for that loading. The volume chosen to calculate the density was that corresponding to the mean of the corrections, i.e., (4387)(1.0060) = 4413 cc. At no point of the runs of propylene loading #6 did the volume differ from this figure by more than 0.06%. On the other loadings the largest difference between the volume at any point and that used to calculate the density was 0.1%.

Gross Heat Capacity

The gross heat capacity, C_g, was calculated by Equation (21),

$$C_g = q_{mean}\,\Delta\theta/(\Delta T - \Delta T_{corr})$$

As an example, the gross heat capacity calculation of Run #87 is presented herewith.

The primary data are as follows:

The power was switched on to the calorimeter at 12:40.

The power was switched from the calorimeter at 1:00.

The elapsed time, $\Delta\theta$, was 20.004 minutes.

At three times during the heating period the power was measured. The readings were:

Time	Voltage (Volts)	Current (Amps)
12:40	19.23	0.3890
12:50	19.24	0.3886
12:55	19.29	0.3876

At five minute intervals during the two temperature-measuring periods the temperature was measured by means of the platinum resistance thermometer-heater and the Mueller bridge. The following were the sums of the "normal" and "reverse" readings of the bridge, which sums correspond to exactly twice the true resistance of the thermometer-heater.

Time	Ohms
12:30	73.4470
12:35	73.4463
12:40	73.4456
1:10	74.3880
1:15	74.3871
1:20	74.3861
1:25	74.3850
1:30	74.3840

Readings were not commenced until ten minutes after the end of the heating period. This time lapse was necessary for the system to come to thermal equilibrium.

Based on the primary data, the following calculations were made. The thermometer resistance at the start of the heating period, R_1, was equal to one half of the total reading at 12:40, i.e., 36.7228 ohms.

The change in total resistance reading during each five-minute interval before the heating period was -0.0007 ohms. At this temperature, a change of 1 ohm corresponded to a change of 10.06 degrees C, so that a change of -0.0007 ohms in the doubled resistance in five minutes, or a change of -0.0007 ohms in the true resistance in ten minutes corresponded to a drift rate of -0.0007 degrees C per minute. This was $drift_1$. Similarly, the drift rate after the heating period was determined. The values for successive five-minute intervals were: -0.0009 ohms, -0.0010 ohms, -0.0011 ohms and -0.0010 ohms. The average values of -0.0010 ohms per five minutes or -0.0010 degrees C per minute was $drift_2$. Using the value of $drift_2$, the resistance at the end of the heating period was determined by extrapolating the resistance vs. time curve to 1:00. (In all of the data taken with this calorimeter this extrapolation was a simple linear one.) The value obtained was 74.3900 ohms. Dividing this by two, R_2 was found to be 37.1950 ohms. From R_1 and R_2 the corresponding temperatures were found. The thermometer-heater resistance-temperature calibration formula was

$$R = 26.4010\left[1 + 3.8908 \times 10^{-3} T - 3.480 \times 10^{-7} T^2\right] \qquad (36)$$

where R is the resistance in ohms, and T is the temperature in degrees C. This formula is discussed in Appendix C, page 130. Based on this formula, it was found that an R_1 of 36.7228 ohms corresponds to a T_1 of 101.401°C, and an R_2 of 37.1950 ohms corresponds to a T_2 of 106.085°C. Therefore, $\Delta T = (T_2 - T_1)$ was 4.684 degrees C.

From the individual power readings the gross power inputs at the measurement times were 7.480 watts, 7.476 watts and 7.476 watts. The average was 7.477 watts. Not all of this gross power flowed into

the calorimeter. Some of it was dissipated in the voltage measuring circuit, which was in parallel with the thermometer-heater and motor, and some of it was dissipated in the voltmeter, which was also in parallel with the thermometer-heater and motor. Figure 17, page 51, shows these circuit details. The magnitude of this leakage was calibrated as follows: the thermometer-heater and motor were disconnected from the circuit, and the current flowing was measured for various voltages. It was found that all the current data could be represented by considering the two parallel current paths as a single resistor of 2015 ohms plus or minus 5 ohms. Therefore, the power dissipated in the parallel current paths was

$$q_f = IE = (E/R)E = E^2/R = E^2/2015 \quad . \qquad (37)$$

For this run, the average voltage was 19.2 volts, for which the corresponding value of $E^2/2015$ was 0.183 watts. Hence, the mean power supplied to the thermometer-heater and motor was 7.477 watts minus 0.183 watts equals 7.294 watts. The product of the mean power and the elapsed time was 7.294 watts times 20.004 minutes or 145.91 watt minutes. One watt-minute is equal to 14.3403 calories, so that the total heat input Q ($Q = q_{mean}\Delta\theta$) was 2092.3 calories.

From the two drift rates, the change in temperature which would have taken place if no heat had been added was calculated by the formula

$$\Delta T_{corr} = \frac{(drift_1 + drift_2)\Delta\theta}{2} = \frac{-(0.0007 + 0.0010)(20.004)}{2} = -0.017^{\circ}C$$

It was then possible to substitute into Formula (21)

$$C_g = \frac{Q}{(\Delta T - \Delta T_{corr})} = \frac{2092.3 \text{ cal}}{(4.684 + 0.017)^\circ C} = 445.09 \ \frac{\text{cal}}{^\circ C}$$

In Table III, page 120, are listed the values of T_1, T_2, -drift$_1$, -drift$_2$, q_{mean}, $\Delta\theta$, Q, $(\Delta T - \Delta T_{corr})$ and C_g for all of the 89 runs made with this calorimeter.

There were two corrections which could have been made to the above data, both of which were negligible. These would have been for the effects of the expansion work done by the gas on the calorimeter, and for the effects of the adsorption of material on the inside wall of the calorimeter. During run #87 the expansion of the calorimeter was estimated by Equations (31), (34) and (35), to be 0.013% of the original volume of the calorimeter, or 0.57 cc. The true work done was

$$W = \int_{V_1}^{V_2} P \, dV \qquad (38)$$

which could be well approximated by $P_{mean}\Delta v$. The mean value of the pressure was about 775 psi, so that the work done was 0.030 liter-atmospheres or 0.7 calories. This was considered negligible compared with the 2092.3 calories of electrical energy input. According to Fricke[11] the maximum possible energy effect in the transition from the bare to the totally adsorbed state for stainless steel is of the order of 4000 ergs/cm. The inside surface area of the sphere was about 1260 cm^2, so that the maximum conceivable energy effect due to adsorption would have been 5.0×10^6 ergs or about 0.1 calorie.

TABLE III

DETAILED GROSS HEAT CAPACITY DATA

Run #	T_1 °C.	T_2 °C.	- drift$_1$ °C/min.	- drift$_2$ °C/min.	Mean Power Watts	Time Mins.	$Q_{calories}$	$\Delta T - \Delta T_{corr.}$	C_g cal./°C
Propylene Loading #1 212.03 grams. Recovered 210.78 grams.									
1*	52.33	62.56	0.002	0.002	6.768	20.006	1941.7	10.27	189.06
2	62.51	73.80	0.002	0.002	7.354	20.002	2109.3	11.33	186.16
3	73.74	90.35	0.002	0.003	7.304	30.005	3142.8	16.68	188.42
4	90.25	106.44	0.003	0.004	7.261	30.006	3124.3	16.29	191.79
5	106.34	116.86	0.004	0.004	7.213	20.007	2069.5	10.60	195.23
6	116.78	130.96	0.004	0.005	6.579	30.004	2893.8	14.32	197.67
6a**	134.84	145.61	0.005	0.006	7.485	20.451	2195.0	10.88	201.75
Propylene Calibration 17.04 grams. Recovered 16.66 grams.									
7	32.77	49.92	-0.001	0.002	6.397	20.005	1835.1	17.18	106.81
8	49.84	66.65	0.002	0.002	6.395	20.098	1843.1	16.85	109.38
9	66.58	81.93	0.002	0.003	5.951	20.002	1706.9	15.40	110.83
10	82.63	100.05	0.003	0.004	6.844	20.003	1963.2	17.49	112.25
11	99.93	119.95	0.004	0.0065	5.345	30.005	2299.7	20.17	114.02
12	119.77	139.37	0.0065	0.009	5.331	30.005	2293.8	19.83	115.67
13	139.06	151.87	0.009	0.011	5.296	20.007	1519.5	13.01	116.79

*Indicates that some liquid phase was present at the start of the run. Such runs were not presented in Tables I and II because their values do not correspond to C_v's.

**The runs are numbered in chronological order, except run 6a which was actually the first run.

TABLE III (CONT'D)

Run #	T_1 °C.	T_2 °C.	- drift$_1$ °C/min.	- drift$_2$ °C/min.	Mean Power Watts	Time Mins.	$Q_{calories}$	$\Delta T - \Delta T_{corr.}$	C_g cal./°C
Dichlorodifluoromethane calibration 29.65 grams. Recovered 28.16 grams.									
14	29.72	52.32	0.000	0.001	5.520	30.005	2375.0	22.61	105.04
15	52.29	74.25	0.001	0.004	5.483	30.004	2359.1	22.03	107.08
16	74.08	95.41	0.003	0.004	5.438	30.005	2339.9	21.51	108.79
17	95.30	116.12	0.004	0.006	5.402	29.999	2323.9	20.97	110.82
18	115.91	132.84	0.006	0.008	5.357	25.013	1921.5	17.10	112.36
19	132.60	149.14	0.008	0.012	5.311	25.026	1906.0	16.84	113.18
Perfluorocyclobutane Loading #1, 690.71 grams. Recovered 690.20 grams.									
20*	90.15	97.82	0.002	0.002	6.881	20.003	1973.8	7.71	255.98
21	97.78	105.39	0.002	0.003	6.851	20.004	1965.3	7.66	256.56
22	97.58	109.32	0.003	0.003	7.033	30.005	3026.2	11.83	255.81
23	109.24	120.75	0.003	0.003	6.968	30.006	2998.2	11.60	258.50
24	120.67	131.99	0.003	0.004	6.927	30.007	2980.8	11.42	261.01
25	131.86	142.96	0.004	0.004	6.885	30.005	2962.4	11.22	264.02
26	142.86	150.37	0.004	0.005	7.029	20.005	2016.5	7.60	265.33
Perfluorocyclobutane Loading #2, 848.16 grams. Recovered 823.36 grams. (See Note One).									
27*	95.008	104.499	0.001	0.0020	6.522	30.005	2806.2	9.53	294.46
28	104.431	113.934	0.0020	0.0020	6.527	30.012	2809.1	9.562	293.80
29	113.818	124.676	0.0020	0.0023	7.547	30.005	3247.4	10.921	297.35
30	124.606	138.862	0.0023	0.0027	7.507	40.005	4306.5	14.354	300.01
31	138.782	149.326	0.0027	0.0030	7.749	30.003	3217.8	10.628	302.77

*Indicates that some liquid phase was present at the start of the run. Such runs were not presented in Tables I and II because their values do not correspond to C_v's.

TABLE III (CONT'D)

Run #	T_1 °C.	T_2 °C.	- drift$_1$ °C/min.	- drift$_2$ °C/min.	Mean Power Watts	Time Mins.	$Q_{calories}$	$\Delta T - \Delta T_{corr.}$	C_g cal./°C
Perfluorocyclobutane Loading #3 1054.23 grams. 1046.25 recovered.									
32*	101.362	107.475	0.0021	0.0016	7.503	20.006	2166.8	6.150	352.33
33	107.421	113.582	0.0016	0.0018	7.480	20.005	2145.9	6.195	346.39
34	113.511	122.702	0.0018	0.0019	7.451	30.004	3205.9	9.246	346.74
35	122.636	131.753	0.0019	0.0021	7.433	30.003	3198.0	9.126	348.52
36	131.680	140.715	0.0021	0.0027	7.409	30.004	3187.8	9.106	350.08
37	140.634	149.569	0.0027	0.0030	7.386	30.003	3177.8	9.019	352.35
Perfluorocyclobutane Loading #4 1410.65 grams. Recovered 1408.77 grams.									
38*	107.996	112.250	0.0014	0.0015	7.585	20.003	2175.7	4.283	507.98
39*	102.419	105.111	0.0008	0.0022	6.675	20.004	1914.9	2.722	703.48
40*	105.082	108.567	0.0022	0.0013	6.647	30.007	2860.4	3.537	808.69
41*	108.528	112.812	0.0013	0.0013	7.063	20.002	2025.8	4.310	470.02
42	112.767	121.891	0.0013	0.0017	7.043	40.004	4040.3	9.184	439.93
43	121.841	130.961	0.0017	0.0017	7.021	40.005	4027.9	9.188	438.39
44	130.910	139.962	0.0017	0.0023	6.996	40.005	4013.4	9.096	441.22
45	139.205	148.899	0.0023	0.0025	6.970	40.003	3998.3	9.090	439.86
Perfluorocyclobutane Loading #5 1720.18 grams. Recovered 1718.42 grams.									
46	112.814	116.526	0.0013	0.0013	6.961	20.003	1996.7	3.738	534.16
47	116.493	120.253	0.0013	0.0014	6.950	20.003	1993.6	3.787	526.44
48	120.211	127.813	0.0014	0.0016	6.939	40.005	3980.7	7.662	519.54
49	127.768	135.377	0.0016	0.0017	6.922	40.002	3970.7	7.675	517.35
50	135.326	142.908	0.0017	0.0017	6.899	40.005	3957.7	7.047	517.34
51	142.858	150.403	0.0017	0.0018	6.880	40.003	3946.7	7.615	518.28

*Indicates that some liquid phase was present at the start of the run. Such runs were not presented in Tables I and II because their values do not correspond to C_v's.

TABLE III (CONT'D)

Run #	T_1 °C.	T_2 °C.	- drift$_1$ °C/min.	- drift$_2$ °C/min.	Mean Power Watts	Time Mins.	$Q_{calories}$	$\Delta T - \Delta T_{corr.}$	C_g cal./°C
Perfluorocyclobutane Loading #6, 1969.16 grams. Recovered 1851.54 grams. (See Note Two).									
52	117.391	121.149	0.0015	0.0016	7.900	20.005	2266.4	3.789	598.14
53	121.111	124.914	0.0016	0.0015	7.876	20.004	2260.4	3.834	589.29
54	124.871	130.607	0.0015	0.0016	7.850	30.004	3377.5	5.783	584.04
55	130.559	138.231	0.0016	0.0020	7.841	40.016	4499.4	7.744	581.01
56	138.178	145.872	0.0020	0.0020	7.808	40.004	4479.2	7.649	579.52
57	145.759	149.561	0.0020	0.0022	7.777	20.004	2230.9	3.844	580.36
Propylene Loading #2, 318.21 grams. Recovered 317.80 grams.									
58	71.006	79.183	0.0016	0.0016	6.767	20.003	1941.1	8.209	236.45
59	79.132	91.277	0.0016	0.0025	6.736	30.002	2898.1	12.208	237.39
60	91.190	108.676	0.0025	0.0037	7.368	40.004	4226.7	17.610	240.02
61	108.566	125.557	0.0037	0.0047	7.313	40.003	4195.0	17.159	244.48
62	125.414	142.028	0.0047	0.0055	7.307	40.003	4191.6	16.614	249.23
63	141.860	149.997	0.0055	0.0064	7.268	20.003	2084.7	8.257	252.49
Perfluorocyclobutane Loading #7, 2366.91 grams. Recovered 2365.19 grams.									
64	117.008	121.073	0.0010	0.0012	8.235	25.005	2953.0	4.092	721.65
65	121.045	126.075	0.0012	0.0012	8.233	30.002	3542.2	5.066	699.21
66	126.045	132.794	0.0012	0.0014	8.145	40.000	4672.1	6.801	687.27
67	132.751	139.578	0.0014	0.0016	8.176	40.005	4690.4	6.887	681.05
68	139.538	146.349	0.0016	0.0019	8.128	40.003	4662.5	6.881	677.60

TABLE III (CONT'D)

Run #	T_1 °C.	T_2 °C.	- drift$_1$ °C/min.	- drift$_2$ °C/min.	Mean Power Watts	Time Mins.	$Q_{calories}$	$\Delta T - \Delta T_{corr.}$	C_g cal./°C
Propylene Loading #3, 406.94 grams. Recovered 406.41 grams.									
69	80.485	88.803	0.0016	0.0016	8.238	20.004	2363.1	8.349	283.03
70	88.755	97.064	0.0016	0.0022	8.207	20.003	2354.1	8.309	282.02
71	96.998	109.348	0.0022	0.0024	8.169	30.009	3515.4	12.419	283.06
72	109.276	121.421	0.0024	0.0027	8.118	30.005	3493.0	12.222	285.79
73	121.341	129.295	0.0027	0.0030	8.066	20.003	2313.7	8.011	288.82
Propylene Loading #4, 485.80 grams. Recovered 485.27 grams.									
74	88.015	93.410	0.0012	0.0015	8.142	15.004	1751.8	5.415	323.50
75	93.359	98.142	0.0015	0.0016	7.203	15.003	1549.6	4.806	322.42
76	98.094	104.420	0.0016	0.0020	7.193	20.005	2063.4	6.412	321.81
77	104.410	110.757	0.0020	0.0021	7.177	20.005	2058.9	6.387	322.36
78	110.695	116.045	0.0021	0.0020	6.065	20.003	1739.8	5.390	322.78
Propylene Loading #5, 619.41 grams. Recovered 618.86 grams.									
79*	86.898	90.635	0.0006	0.0010	7.265	20.005	2084.3	3.953	527.25
80	90.605	95.727	0.0010	0.0013	7.273	20.004	2086.4	5.145	405.51
81	95.681	103.470	0.0013	0.0013	7.238	30.003	3114.2	7.828	397.82
82	103.426	109.928	0.0013	0.0019	7.211	25.003	2585.8	6.542	395.26
83	109.871	115.063	0.0019	0.0019	7.191	20.005	2062.9	5.230	394.44
Propylene Loading #6, 710.26 grams. No recovery.									
84	92.642	97.201	0.0008	0.0009	7.341	20.004	2105.7	4.576	460.17
85	97.178	101.832	0.0009	0.0009	7.326	20.005	2101.6	4.672	449.84
86	101.804	106.501	0.0009	0.0010	7.309	20.005	2096.8	4.716	444.63
87	101.401	106.085	0.0007	0.0010	7.294	20.004	2092.3	4.701	445.09
88	106.055	110.751	0.0010	0.0014	7.256	20.002	2081.1	4.720	440.92

*Indicates that some liquid phase was present at the start of the run. Such runs were not presented in Tables I and II because their values do not correspond to C_v's.

TABLE III (CONT'D)

Note One: For Perfluorocyclobutane loadings 2 and 3, the recoveries were poor. This was due to the formation of solid perfluorocyclobutane on the inner surface of the transfer cylinder, when it was immersed in liquid nitrogen. The problem was solved by collecting most of the sample in one cylinder, and then completing the recovery into a transfer cylinder containing no more than 50% liquid. The recoveries on the subsequent loadings were satisfactory.

Note Two: After the last run of perfluorocyclobutane loading 6, the calorimeter was left overnight with the shield heaters on. This caused a temperature and pressure rise, and a small leakage through the silver solder joint of the valve to the calorimeter wall. This accounts for the poor recovery. After the recovery the leak was repaired, and work continued.

APPENDIX B - CALIBRATION OF THE CALORIMETER HEAT CAPACITY

The heat capacity of the calorimeter was determined by loading the calorimeter with small amounts of substances of known heat capacity. The gross heat capacity was then measured, and the known heat capacity of the contents subtracted, to find the heat capacity of the calorimeter (plus those parts of the wires and strings which received heat from the calorimeter.) For this calibration the substances used were dichlorodifluoromethane (Freon 12) and propylene. The C_v^* of dichlorodifluoromethane used was that according to Masi[23]. The correction for non-ideality was made by the Martin-Hou equation, using the constants given by McHarness, Eiseman and Martin[18]. The C_v^* of propylene used was that according to Kilpatrick and Pitzer[17]. The corrections for non-ideality were made by the Martin-Hou equation, using the constants given by Martin and Hou[19].

The calibration data are stated in Table IV, page 127. These values are plotted in Figure 36, page 128. The line drawn through the experimental points was considered as the best experimental value, and was used to make the calculations shown in the "Results" section. In this calibration, for none of the data points did the heat capacity of the calibration substance exceed 7% of the heat capacity of the calorimeter. The worst scatter of the calibration points is about 0.8% from the line; most of the points lie within 0.4% of the line.

It was not considered possible to compute the calibration value from published data, because such data are not available for the type of steel used, and because of the difficulty in estimating the heat capacity of the motor. However, as an order of magnitude check,

TABLE IV

CALIBRATION OF CALORIMETER HEAT CAPACITY

Run #	T_{mean} °C.	C_g cal./°C.	- MC_v^* cal./°C.	- $M(C_v - C_v^*)$ cal./°C.	= Calibration cal./°C.
Propylene calibration 17.04 grams					
7	41.25	106.81	5.65	0.09	101.07
8	58.24	109.38	5.91	0.07	103.40
9	74.25	110.83	6.15	0.06	104.62
10	91.34	112.25	6.40	0.05	105.80
11	109.94	114.02	6.70	0.04	107.28
12	129.57	115.67	7.01	0.03	108.63
13	145.46	116.79	7.23	0.03	109.53
Dichlorodifluoromethane calibration 29.65 grams					
14	41.02	104.04	3.88	0.06	101.10
15	63.27	107.08	4.09	0.05	102.94
16	84.75	108.79	4.17	0.04	104.58
17	105.71	110.82	4.27	0.03	106.52
18	124.38	112.36	4.37	0.02	107.96
19	140.89	113.18	4.45	0.02	108.71

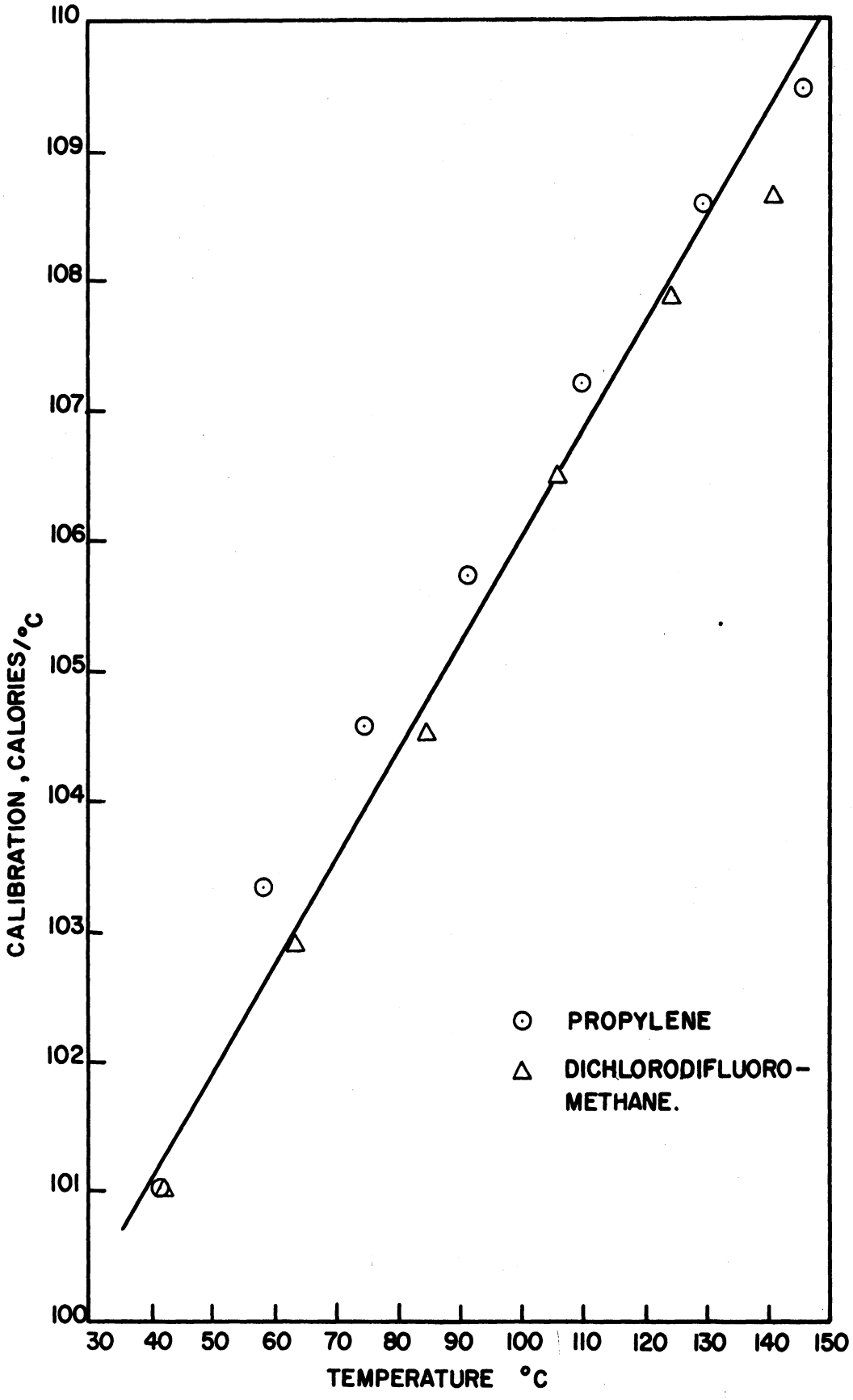

Figure 36. Heat Capacity Calibration of the Calorimeter

the following estimate was made:

The motor weighed 120 grams. This was estimated to be the equivalent of 20 grams of aluminum (the motor housing was aluminum), 50 grams of copper (the windings) and 50 grams of iron (the rotor core, bearings, etc.). The remaining weight of the calorimeter was 754 grams. The approximate heat capacities of the various materials at 100°C are: stainless steel 0.12 cal/gm °C, aluminum 0.22 cal/gm °C, iron 0.11 cal/gm °C, and copper 0.09 cal/gm °C. Multiplying these by the assigned masses of material, and summing, the heat capacity of the calorimeter at 100°C was estimated as 105 calories/degree C. The experimentally determined value was 106 calories/degree C.

APPENDIX C - CALIBRATION OF THE THERMOMETER RESISTANCE

The thermometer-heater was calibrated for use as a platinum resistance thermometer by measuring its resistance at the ice point, and measuring its resistance while it was immersed in an agitated oil bath, whose temperature was measured with a Princo mercury-in-glass thermometer. The Princo thermometers used were #451872, #148202, #456732 and #253157. NBS calibrations dated 1956 were available for these thermometers. The thermometers could be read to about 0.01 degrees C. However, since they were of the total immersion type, and the available oil bath could only be used with an emergent thermometer, emergent stem corrections were necessary. These were made according to the methods suggested by the NBS. The magnitude of the corrections was up to 0.7 degrees C. The temperatures were recorded to 0.01 °C, although their reliability was certainly less than this.

The resistance as a function of temperature was represented by the standard platinum resistance thermometer formula, see Sligh[36],

$$R = R_o\left[1 + aT + bT^2\right] \tag{39}$$

where R is the resistance at a given temperature, R_o is the resistance at the ice point, T is the temperature in degrees C, and a and b are arbitrary constants. Because the ice point determination was considered more reliable than any other measurement, the value of R_o = 26.4010 ohms was considered correct and not subject to the fitting procedure. The constants a and b were determined by fitting the following resistances

and temperatures to Equation (39) by the method of least squares:

Ohms	Degrees C
31.652	51.01
36.350	99.32
37.794	112.12
41.145	145.24
43.645	170.45
46.426	198.71

The values obtained for the constants were $a = 3.8908 \times 10^{-3}$, and $b = -3.480 \times 10^{-7}$.

Using these values, the temperatures predicted by the thermometer equation and the standard glass thermometers were compared as follows:

$T_{platinum}$ °C	T_{glass} °C	$(T_{glass} - T_{plat})$ °C
51.34	51.01	-0.33
99.47	99.32	-0.15
112.02	112.12	0.10
145.41	145.24	-0.17
170.44	170.45	0.01
198.46	198.71	0.24

Although a better agreement could be wished, the above is satisfactory in the light of the probable accuracy of the measurements made with the mercury-in-glass thermometers. It would have been possible to fit the calibration data better by using a more complicated equation, but the gain would not have justified abandoning the standard formula.

APPENDIX D - DERIVATION OF THERMODYNAMIC RELATIONS

The derivations in this appendix are largely a restatement of those contained in unpublished thermodynamics notes by Professor Joseph J. Martin. They are included here for completeness.

Relation Between the Constant Volume Heat Capacity and State Behavior

From the definition of an infinitely small reversible change of the Helmholz Free Energy

$$dF = -SdT - PdV \tag{40}$$

is obtained the Maxwell Relation

$$\left(\frac{dS}{dV}\right)_T = \left(\frac{dP}{dT}\right)_V . \tag{41}$$

Differentiating this expression with respect to T at constant V, yields

$$\frac{d^2S}{dV_T\, dT_V} = \frac{d}{dV_T}\left(\frac{dS}{dT}\right)_V = \left(\frac{d^2P}{dT^2}\right)_V . \tag{42}$$

However

$$\left(\frac{dS}{dT}\right)_V = \frac{C_V}{T} \tag{43}$$

Inserting (43) in (42), yields

$$\left(\frac{dC_V}{dV}\right)_T = T\left(\frac{d^2P}{dT^2}\right)_V . \tag{1}$$

Another form of this relation is obtained by substituting $V = 1/\rho$,

$$-\rho^2\left(\frac{dC_V}{d\rho}\right)_T = T\left(\frac{d^2P}{dT^2}\right)_V . \tag{1}$$

The Relation Between the Constant Volume Heat Capacity and the Speed of Sound

By definition

$$C_P = T\left(\frac{dS}{dT}\right)_P \quad \text{and} \quad C_V = T\left(\frac{dS}{dT}\right)_V. \tag{44}$$

Hence

$$C_P - C_V = T\left[\left(\frac{dS}{dT}\right)_P - \left(\frac{dS}{dT}\right)_V\right]. \tag{45}$$

The entropy may be expressed as a function of pressure and temperature, or as a function of specific volume and temperature. The form of the expression does not affect the value of the total derivative, so that the two total derivatives may be equated

$$\left(\frac{dS}{dT}\right)_P dT + \left(\frac{dS}{dP}\right)_T dP = \left(\frac{dS}{dT}\right)_V dT + \left(\frac{dS}{dV}\right)_T dV. \tag{46}$$

Rearranging

$$dT\left[\left(\frac{dS}{dT}\right)_P - \left(\frac{dS}{dT}\right)_V\right] = \left(\frac{dS}{dT}\right)_V dV - \left(\frac{dS}{dP}\right)_T dP \tag{47}$$

or

$$\left(\frac{dS}{dT}\right)_P - \left(\frac{dS}{dT}\right)_V = \left(\frac{dS}{dT}\right)_V \left(\frac{dV}{dT}\right) - \left(\frac{dS}{dP}\right)_T \left(\frac{dP}{dT}\right). \tag{48}$$

Since the above holds for any reversible change of entropy, we may consider a constant pressure change for which (dP/dT) is zero:

$$\left(\frac{dS}{dT}\right)_P - \left(\frac{dS}{dT}\right)_V = \left(\frac{dS}{dV}\right)_T \left(\frac{dV}{dT}\right)_P . \tag{49}$$

Inserting the Maxwell relation

$$\left(\frac{dS}{dV}\right)_T = \left(\frac{dP}{dT}\right)_V \tag{50}$$

yields

$$\left(\frac{dS}{dT}\right)_P - \left(\frac{dS}{dT}\right)_V = \left(\frac{dP}{dT}\right)_V \left(\frac{dV}{dT}\right)_P . \tag{51}$$

Substituting (51) in (45)

$$C_P - C_V = T\left(\frac{dP}{dT}\right)_V \left(\frac{dV}{dT}\right)_P . \tag{52}$$

This may be written in a more convenient form by substituting

$$\left(\frac{dP}{dT}\right)_V = - \frac{\left(\frac{dV}{dT}\right)_P}{\left(\frac{dV}{dP}\right)_T} \tag{53}$$

to obtain

$$C_P - C_V = -T \frac{\left(\frac{dV}{dT}\right)_P^2}{\left(\frac{dV}{dP}\right)_T} . \tag{54}$$

For gases

$$c^2 = -V^2 \left(\frac{dP}{dV}\right)_S \tag{55}$$

where c is the speed of sound. Also, by definition

$$k = \frac{C_P}{C_V} \tag{56}$$

and

$$\left(\frac{dP}{dV}\right)_S = -\frac{\left(\frac{dS}{dV}\right)_P}{\left(\frac{dS}{dP}\right)_V} = -\frac{C_P\left(\frac{dT}{dV}\right)_P}{C_V\left(\frac{dT}{dP}\right)_V} = -k\frac{\left(\frac{dT}{dV}\right)_P}{\left(\frac{dT}{dP}\right)_V} \tag{57}$$

Substituting

$$\left(\frac{dT}{dV}\right)_P = -\frac{\left(\frac{dP}{dV}\right)_T}{\left(\frac{dP}{dT}\right)_V} \tag{58}$$

into the right-hand member of Equation (57) yields

$$\left(\frac{dP}{dV}\right)_S = k\left(\frac{dP}{dV}\right)_T \tag{59}$$

Inserting (59) into (55)

$$c^2 = -V^2 k \left(\frac{dP}{dV}\right)_T \tag{60}$$

Since

$$C_v \equiv \frac{C_p - C_v}{\frac{C_p}{C_v} - 1} \equiv \frac{C_p - C_v}{k - 1} \tag{61}$$

we may substitute for $(C_p - C_v)$ from Equation (54) and for k from Equation (61) to obtain

$$C_v = \frac{-T\left(\frac{dP}{dT}\right)_v^2 \Big/ \left(\frac{dP}{dV}\right)_T}{-\frac{c^2}{V^2}\left(\frac{dV}{dP}\right)_T - 1} = \frac{TV^2\left(\frac{dP}{dT}\right)_v^2}{c^2 + V^2\left(\frac{dP}{dV}\right)_T}. \tag{62}$$

This may be solved for c^2 as follows

$$c^2 = V^2\left(\frac{T}{C_v}\right)\left[\left(\frac{dP}{dT}\right)_v^2 - \left(\frac{C_v}{T}\right)\left(\frac{dP}{dV}\right)_T\right], \tag{63}$$

which after rearrangement and extraction of the square root yields

$$c = V\left(\frac{dP}{dT}\right)_v \left(\frac{T}{C_v}\right)^{1/2}\left[1 - \frac{\left(\frac{C_v}{T}\right)\left(\frac{dP}{dV}\right)_T}{\left(\frac{dP}{dT}\right)_v^2}\right]^{\frac{1}{2}}. \tag{64}$$

APPENDIX E - CALORIMETER CIRCUIT

The following is extracted from an article by Hoge[13]. It is included here to elucidate the use of a balancing resistor in the heater circuit.

Consider a series circuit consisting of the following three elements: a battery of constant voltage E and zero internal resistance, a balancing resistor of fixed resistance U and a heater of variable resistance R. The power dissipated by the heater is given by

$$q_h = IE_h = \left[\frac{E}{U+R}\right]\left[\frac{RE}{U+R}\right] = \frac{RE^2}{(U+R)^2} \qquad (65)$$

where q_h is the heater power, I is the current in the circuit, and E_h is the voltage across the heater. Then

$$\frac{dq_h}{dR} = \frac{E^2(U-R)}{(U+R)^2} \qquad (66)$$

When R equals U, q_h is a maximum, equal to $E^2/4U$. Furthermore

$$\frac{q_h}{q_{h\,max.}} = \left[\frac{RE^2}{(U+R)^2}\right]\left[\frac{4U}{E}\right] = \frac{4}{\left(2+R/U+U/R\right)} \qquad (67)$$

This latter function is quite insensitive to changes in R/U. For example, setting $q_h/q_{h_{maximum}}$ equal to 0.98 and solving for R/U one finds two values, 0.75 and 1.35. Thus for an 80% increase in R, q_h

goes through a series of values none of which differs from the initial value by more than 2%. From the above it is seen that although the resistance of the thermometer-heater and motor was changing steadily during any heating period, the power dissipated by them changed very slightly.

APPENDIX F - REPRESENTATION OF C_V-C_V^* BY SEVERAL EQUATIONS OF STATE

One of the primary objectives of this research was to compare the experimental values of C_v with those computed from state data by means of various equations of state. In this section, detailed consideration is given to the representation of C_v by several equations of state. From Equation (1)

$$\left(\frac{dC_v}{dV}\right)_T = -\rho^2\left(\frac{dC_v}{d\rho}\right)_T = T\left(\frac{d^2P}{dT^2}\right)_V \tag{1}$$

and the fact that C_v equals C_v^* at zero density or infinite specific volume, it follows that C_v-C_v^* may be calculated by either of the following equivalent relations

$$C_v - C_v^* = -\int_v^\infty T\left(\frac{d^2P}{dT^2}\right)_V dV \tag{68}$$

or

$$C_v - C_v^* = -\int_0^\rho \frac{T}{\rho^2}\left(\frac{d^2P}{dT^2}\right)_\rho d\rho \tag{69}$$

Generally Equation (69) is more convenient to use with equations of state which involve V or ρ, and Equation (68) is more convenient to use with equations of state which involve V-b where b is some constant.

The Dieterici, Berthelot, Beattie-Bridgeman, Benedict-Webb-Rubin and Martin-Hou Equations

All of the early equations of state give zero values for $(d^2P/dT^2)_V$. Thus, these equations (perfect gas equation, Van der Waals

equation, Wohl equation, etc.) predict that $C_v - C_v^*$ is zero for all temperatures and densities. The following five equations are considered in detail, as a representative sample of the many equations which have been proposed. The Dieterici equation[9] is one of the earliest equations which gives a non-zero value of $C_v - C_v^*$; it is

$$P = \frac{RT}{(V-b)} \exp\left(\frac{-a}{RTV}\right) \tag{70}$$

where

$$a = \frac{4R^2T_c^2}{P_c[\exp 1]^2} \quad \text{and} \quad b = \frac{RT_c}{P_c[\exp 1]^2} . \tag{71}$$

According to this equation

$$\left(\frac{d^2P}{dT^2}\right)_V = \frac{a^2 \exp\left(\frac{-a}{RTV}\right)}{RT^3V^2(V-b)} \tag{72}$$

and

$$C_v - C_v^* = \frac{-a^2}{RT^2}\int_V^\infty \frac{\exp\left(\frac{-a}{RTV}\right)}{V^2(V-b)}\, dV . \tag{73}$$

The above integral is integrable only in terms of non-elementary functions. The value of the integrand is always positive, so that the value of the integral is always negative. This equation thus predicts that $C_v - C_v^*$ will be negative and will increase in absolute value with increasing density.

The Berthelot equation[9] which is frequently used by physical chemists, is

$$P = \frac{RT}{(V-b)} - \frac{a}{TV^2} \tag{74}$$

where

$$a = \frac{27\ R^2 T_c^3}{64\ P_c} \qquad \text{and} \qquad b = \frac{V_c}{3} \ . \tag{75}$$

It predicts

$$\left(\frac{d^2P}{dT^2}\right)_V = - \frac{2a\rho^2}{T^3} \tag{76}$$

and

$$C_V - C_V^* = \frac{2a}{T^2}\int_0^\rho d\rho = \frac{2a\rho}{T^2} \ . \tag{77}$$

Thus, this equation predicts that C_V-C_V^* will increase linearly with increasing density and will decrease with increasing temperature proportionally to $1/T^2$.

The Beattie-Bridgeman equation[3] which has been widely used in chemical engineering is

$$P = RT\left[\rho^2 - \frac{c\rho^3}{T^3}\right]\left[\frac{1}{\rho} + B_0 - B_c b\rho\right] - \left[A_0\rho^2 - aA_c\rho^3\right] \tag{78}$$

where a, b, c, A_o and B_o are arbitrary constants. According to it

$$\left(\frac{d^2P}{dT^2}\right)_V = -\frac{6cR\rho^3}{T^4}\left[\frac{1}{\rho} + B_o - B_o b\rho\right] \tag{79}$$

and

$$C_V - C_V^* = \frac{6cR}{T^3}\int_0^\rho \left[1 + B_o\rho - B_o b\rho^2\right] d\rho$$

$$= \frac{6cR}{T^3}\left[\rho + \frac{B_o\rho^2}{2} - \frac{B_o b\rho^3}{3}\right] \tag{80}$$

This equation predicts that C_V-C_V^* will increase with increasing density according to a cubic equation, as shown in Figure 2, and that it will decrease with increasing temperature proportionally to $1/T^3$

The Benedict-Webb-Rubin equation[4] which has been widely applied, especially in vapor-liquid equilibrium calculations is

$$P = RT\rho + \rho^2\left[B_oRT - A_o - \frac{C_o}{T^2}\right] + \rho^3\left[bRT - a\right] + \rho^6 a\alpha + \frac{c\rho^3(1+\gamma\rho^2)\exp(-\gamma\rho^2)}{T^2} \tag{81}$$

where a, b, c, A_o, B_o, C_o and are arbitrary constants. It predicts

$$\left(\frac{d^2P}{dT^2}\right)_V = \frac{6\rho^2}{T^4}\left[-C_o + c\rho(1+\gamma\rho^2)\exp(-\gamma\rho^2)\right] \tag{82}$$

and

$$C_V - C_V^* = \frac{6}{T^3}\int_0^\rho \left[C_0 - c\rho(1+\gamma\rho^2)\exp(-\gamma\rho^2)\right] d\rho$$

$$= \frac{6}{T^3}\left[C_0\rho + \frac{c}{2\gamma}\left\{2\exp(-\gamma\rho^2) - 2 + \gamma\rho^2\exp(-\gamma\rho^2)\right\}\right] \qquad (83)$$

When $\exp(-\gamma\rho^2)$ may be satisfactorily represented by $(1 - \gamma\rho^2 + \ldots)$, which is an excellent approximation whenever $\gamma\rho^2$ is smaller than 0.005, then Equation (83) simplifies to

$$C_V - C_V^* = \frac{6}{T^3}\left[C_0\rho - \frac{c\rho^2}{2} + \ldots\right]. \qquad (84)$$

This equation predicts that C_V-C_V^* will increase with increasing density at low densities according to a parabolic equation as shown in Figure 2, and that it will decrease with increasing temperature proportionally to $1/T^3$.

The Martin-Hou equation[19], which has been used to compute thermodynamic properties of various substances, is

$$P = \sum_{i=1}^{i=5} \frac{A_i + B_i T + C_i \exp(-kT/T_c)}{(V-b)^i} \qquad (85)$$

where the various A_i, B_i, C_i, k and b are arbitrary constants. According to Equation (85)

$$\left(\frac{d^2P}{dT^2}\right)_V = \left(\frac{k}{T_c}\right)^2 \exp\left(\frac{-kT}{T_c}\right) \sum_{i=1}^{i=5} \frac{C_i}{(V-b)^i} \qquad (86)$$

and

$$C_v - C_v^* = -T\left(\frac{k}{T_c}\right)^2 \exp\left(\frac{-kT}{T_c}\right) \int_V \left(\sum_{i=1}^{i=5} \frac{C_i}{(V-b)^i} \right) dV$$

$$= -T\left(\frac{k}{T_c}\right)^2 \exp\left(\frac{-kT}{T_c}\right) \sum_{i=1}^{i=5} \frac{C_i}{(i-1)(V-b)^{(i-1)}} . \qquad (87)$$

In the Martin-Hou equation C_1 and C_4 are zero, and for some gases (e.g., propylene) the constants are only available in the earliest form of the equation in which C_5 was also zero. Therefore in the expanded form

$$C_v - C_v^* = -T\left(\frac{k}{T_c}\right)^2 \exp\left(\frac{-kT}{T_c}\right)\left[\frac{C_2}{(V-b)} + \frac{C_3}{2(V-b)^2} + \frac{C_5}{4(V-b)^4} \right] \qquad (88)$$

or when C_5 is zero

$$C_v - C_v^* = -T\left(\frac{k}{T_c}\right)^2 \exp\left(\frac{-kT}{T_c}\right)\left[\frac{C_2}{(V-b)} + \frac{C_3}{2(V-b)^2} \right] . \qquad (89)$$

C_2 is generally a large negative number, and C_3 a smaller positive number, and at low densities $1/(V-b) \cong \rho$, so that this equation also predicts that $C_v - C_v^*$ will increase with increasing density according to a parabolic equation at low densities, as is shown in Figure 2. The equation also predicts that $C_v - C_v^*$ will decrease with increasing temperature proportionally to $T \exp(-kT/T_c)$.

Michels' Equations

Michels et al.[25], have represented PVT data by equations of the form

$$(PV)_T = A + B\rho^2 + C\rho^2 + D\rho^4 \qquad (90)$$

and

$$(PV)_T = A + B\rho + C\rho^2 + Z\rho^3 + D\rho^4 + Y\rho^5 + E\rho^6 + F\rho^7 + G\rho^8 \qquad (91)$$

In these equations, all of the capital letters are arbitrary constants which are determined by fitting the experimental data. Generally, Equation (90) is used only for densities below 1/5 of the critical density, and the total density range of the experimental data is represented by Equation (91). Note that these equations only describe the PV behavior along specific isotherms; the values of PV between these isotherms must be obtained by interpolation. In the paper on propylene by Michels et al.[25], Equation (90) is applied to 7 isotherms, so that the low density data are fitted by a network involving 28 arbitrary constants. Equation (91) is applied to three isotherms over the density range from zero density to three times the critical density, so that the total range of the data is fitted by a network involving 27 arbitrary constants. Using the constants found in Equation (91), Michels et al., are able to represent PV values for these three isotherms up to three times the critical density with a maximum difference between the calculated and experimental values of 5 parts in 10,000 and an average difference of less than 2 parts in 10,000. The Benedict-Webb-Rubin equation, which has only 9 arbitrary constants including R (see Appendix H), has been

used to represent the propylene PVT data of Marchman, Prengle and Motard up to a density of 1.4 times the critical density. Over this range the maximum difference between the calculated and experimental pressures is 175 parts in 10,000, and the average difference is 20 parts in 10,000[21]. The Martin-Hou equation, which has 11 arbitrary constants incouding R (see Appendix H), has been used to represent the same PVT data of Marchman et al. For the density range up to 1.4 times the critical density, the maximum difference between the experimental and calculated pressures is 100 parts in 10,000. The average difference was not reported[19].

To calculate $C_v - C_v^*$ from the network of constants evaluated for Equations (90) and (91), Michels et al., used two methods. At low densities the data were correlated at various temperatures by a power series of the form of Equation (91). From the variation of the constants with temperature, the necessary second derivative was calculated by

$$\left(\frac{d^2P}{dT^2}\right)_V = \rho^2 \frac{d^2B}{dT^2} + \rho^3 \frac{d^2C}{dT^2} + \rho^4 \frac{d^2Z}{dT^2} + \cdots \quad (92)$$

Using this derivative in Equation (69), $C_v - C_v^*$ was calculated. For higher densities a different method was used. The internal energy was calculated by the relation

$$U = \int_{\text{Lamagat}}^{0} \left(\frac{dU}{d\rho}\right)_{T=0} d\rho + \int_{0\,^\circ C}^{T} C_v^* \, dT + \int_0^{\rho} \left(\frac{dU}{d\rho}\right)_{T=T} d\rho \quad (93)$$

where

$$\left(\frac{dU}{d\rho}\right)_T = \frac{-1}{\rho^2}\left\{T\left(\frac{dP}{dT}\right)_\rho - P\right\} = \frac{-1}{\rho}\left\{T\left(\frac{d(PV)}{d\rho}\right) - PV\right\}. \quad (94)$$

(The somewhat complicated form of Equation (93) is due to the choice of 0°C and a density of 1 amagat as the stantard state of zero internal energy.) From Equation (93), C_v was computed by the relation

$$C_v = \left(\frac{dU}{dT}\right)_v . \tag{95}$$

Differentiation of Equation (93) with respect to T at constant density and rearrangement yields Equation (69), which shows that the two methods are equivalent. In evaluating Equation (94), Michels et al., determined the values of [d(PV)/dT] from a cross-plot of their $(PV)_T$ isotherms at a given density. All of the integrations were performed graphically.

Volume-Explicit Equations of State

All of the equations of state discussed above are pressure-explicit, i.e., they have the form P = f(V,T). Historically, another type of equation has been widely used, the volume-explicit form, V = f(P,T). For equations of even moderate complexity, a volume explicit equation cannot be written in an exact pressure-explicit form, and conversely. In general, volume-explicit equations lead to a very complicated and unwieldly expressions for $C_v - C_v^*$. As an example, we may consider the relatively simple Goodenough equation[9], which is

$$V = c + \frac{RT}{P} - \frac{m}{T^n}\left(1 + 3aP^{1/2}\right) \tag{96}$$

where c, m, n and a are arbitrary constants. The second derivative of pressure with respect to temperature at constant volume is most easily

obtained from the relation,

$$\left(\frac{d^2P}{dT^2}\right)_V = \frac{\left(\frac{dV}{dT}\right)_P\left(\frac{d^2V}{dP_T\,dT_P}\right) - \left(\frac{dV}{dP}\right)_T\left(\frac{d^2V}{dT^2}\right)_P}{\left(\frac{dV}{dP}\right)_T\left(\frac{d^2V}{dT_P\,dP_T}\right) - \left(\frac{dV}{dT}\right)_P\left(\frac{d^2V}{dP^2}\right)_T}. \tag{97}$$

Substituting the values of the Goodenough equation shows

$$\left(\frac{d^2P}{dT^2}\right)_V = \frac{\left\{\left[\frac{R}{P} + \frac{mn}{T^{n+1}}\left(1+3aP^{1/2}\right)\right]\left[\frac{-R}{P^2} + \frac{3mna}{2T^{n+1}P^{1/2}}\right] + \left[\frac{RT}{P^2} + \frac{3am}{2T^nP^{1/2}}\right]\left[\frac{mn(n+1)}{T^{n+2}}\left(1+3aP^{1/2}\right)\right]\right\}}{\left\{-\left[\frac{RT}{P^2} + \frac{3am}{2T^nP^{1/2}}\right]\left[\frac{-R}{P^2} + \frac{3amn}{2T^{n+1}P^{1/2}}\right] - \left[\frac{R}{P} + \frac{mn}{T^{n+1}}\left(1+3aP^{1/2}\right)\right]\left[\frac{3am}{4T^nP^{3/2}} - \frac{2RT}{P^3}\right]\right\}}. \tag{98}$$

In order to use this expression in Equation (68), it is necessary to make the substitution

$$dV_T = \left(\frac{dV}{dP}\right)_T dP_T = -\left(\frac{RT}{P^2} + \frac{3am}{2T^nP^{1/2}}\right)dP_T \tag{99}$$

which yields

$$C_V - C_V^* = -T\int_0^P \left[\text{Equation 98}\right]\left[\frac{RT}{P^2} + \frac{3am}{2T^{1/2}P^{1/2}}\right] dP_T. \qquad (100)$$

The above illustrates the complexity of calculating $C_V - C_V^*$ from a volume-explicit equation of state. From Equation (6), we may infer that it would be approximately as complex to compute $C_p - C_p^*$ from a pressure-explicit equation as it is to compute $C_V - C_V^*$ from a volume-explicit equation. For $C_p - C_p^*$, however, volume-explicit equations give very simple expressions, e.g., the Goodenough equation predicts

$$C_p - C_p^* = \frac{(n+1)(mn)}{T^{n+1}}\left(P + 2aP^{3/2}\right). \qquad (101)$$

The differences between the two types of equations may be summarized by saying that volume-explicit equations are more convenient to use with C_p and enthalpy, while pressure-explicit equations are more convenient to use with C_V and internal energy. In spite of the apparent advantage of volume-explicit equations, that they are more convenient to use with the variables of greatest engineering interest, pressure-explicit equations are in wider use, because the PVT data may be accurately represented in much simpler algebraic form by means of a pressure-explicit equation than by means of a volume explicit equation.

The Second Derivative of C_V with Respect to Density at Constant Temperature

In the "Theoretical Background" section, the simplified values of Equation (12) were given for the Benedict-Webb-Rubin and Martin-Hou

equations. The detailed values may be obtained either by differentiating Equations (83) and (87) twice with respect to density at constant temperature, or by differentiating Equations (82) and (86) once with respect to density at constant temperature, and substituting into Equation (12). For the Benedict-Webb-Rubin equation, the former method yields

$$\left(\frac{dC_v}{d\rho}\right)_T = \frac{6}{T^3}\left[C_0 + \frac{c}{2\gamma}\exp(-\gamma\rho^2)(-2\gamma\rho - 2\gamma^2\rho^3)\right] \tag{102}$$

and

$$\left(\frac{d^2C_v}{d\rho^2}\right)_T = \frac{6c}{T^3}\exp(-\gamma\rho^2)(-1-\gamma\rho^2+2\gamma^2\rho^4). \tag{103}$$

For the Martin-Hou equation, Equation (86) is re-written

$$\left(\frac{d^2P}{dT^2}\right)_V = \left(\frac{k}{T_c}\right)^2 \exp\left(\frac{-kT}{T_c}\right)\left[\frac{C_2\rho^2}{(1-b\rho)^2} + \frac{C_3\rho^3}{(1-b\rho)^3} + \frac{C_5\rho^5}{(1-b\rho)^5}\right] \tag{104}$$

and differentiated once with respect to density at constant temperature to obtain

$$\left(\frac{d^3P}{dT_v^2\, d\rho_T}\right) = \left(\frac{k}{T_c}\right)^2 \exp\left(\frac{-kT}{T_c}\right)\cdot$$

$$\cdot\left[\frac{2C_2\rho}{(1-b\rho)^2} + \frac{3C_3\rho^2}{(1-b\rho)^3} + \frac{5C_5\rho^4}{(1-b\rho)^4} + \frac{2bC_2\rho^2}{(1-b\rho)^3} + \frac{3bC_3\rho^3}{(1-b\rho)^4} + \frac{5bC_5\rho^5}{(1-b\rho)^6}\right]. \tag{105}$$

The values are substituted into Equation (12) to yield

$$T\left[\frac{2}{\rho^3}\left(\frac{d^2P}{dT^2}\right)_\rho - \frac{1}{\rho^2}\left(\frac{d^3P}{dT_\rho^2\, d\rho_T}\right)\right] = T\left(\frac{k}{T_c}\right)^2 \exp\left(\frac{-kT}{T_c}\right) \cdot$$

$$\cdot\left[\frac{-2bC_2 - C_3}{(1-b\rho)^3} \quad \frac{-3C_5\rho^2}{(1-b\rho)^5} \quad \frac{-3bC_3\rho}{(1-b\rho)^4} \quad \frac{-5bC_5\rho^3}{(1-b\rho)^6}\right]. \tag{106}$$

APPENDIX G - TABLE OF NOMENCLATURE

A, B, C, D, E, F, G, Y, Z, a, b, c, k, m, n	Used as arbitrary constants in various equations
c	velocity of sound
C_p	heat capacity at constant pressure
C^*_p	heat capacity at constant pressure and zero pressure
C_v	heat capacity at constant volume
C^*_v	heat capacity at constant volume and zero pressure
C_g	gross heat capacity of calorimeter and contents
$C^{g,l}_{sat}$	heat capacity of a two-phase mixture at constant volume
C^{l}_{sat}	heat capacity of the saturated liquid
d	differential operator
exp	exponential operator

F	Helmholz free energy
f	function
I	electric current
k	C_p/C_v
ln	natural logarithm
M	mass
M	reduced slope of the vapor pressure curve at the critical $M = -\left(\frac{dP_r}{dT_r}\right)_{V,c}$
P	pressure
Q	quantity of energy
q	rate of energy addition
R	resistance
R	universal gas constant
r	radius
S	entropy
T	temperature
U	a fixed resistance
U	internal energy
V	specific volume
v	volume
W	mechanical work
Z	compressibility factor

Greek Letters

α	accommodation coefficient
α, γ, δ	arbitrary constants used in various equations
Δ	finite change operator
θ	time
ρ	density

Subscripts

c	critical
corr	correction
h	heater
i	summation index
mean	mean value over some interval
r	reduced
sat	saturation
1	the beginning of a heating period
2	the end of a heating period

APPENDIX H - CONSTANTS AND CONVERSION FACTORS

The following constants and conversion factors were used throughout this research:

1 calorie = 1 thermochemical calorie = 4.1840 absolute joules
= 0.0412917 liter-atmospheres

1 abs. watt minute = 14.3403 calories

temperature °K = temperature °C plus 273.16°C

temperature °F = 1.8 temperature °C plus 32°F

temperature °R = 1.8 temperature °K

1 atmosphere = 14.70 pounds per square inch

R (The universal gas constant) = 1.987 cal/gm mole degree K
= 0.08205 liter atm/gm mole, degree K

molecular weight of propylene = 42.08

molecular weight of perfluorocyclobutane = 200.04

The Martin-Hou equation constants for propylene[19] are as follows; (Temperature is in degrees K, pressure in atm. and volume in liter/gm mole)

$b = 0.0487575$ $B_4 = 0$

$k = 5.475$ $B_5 = 5.0385878 \times 10^{-6}$

$A_1 = 0$ $C_1 = 0$

$A_2 = -10.2233898$ $C_2 = -153.061055$

$A_3 = 1.219435756$ $C_3 = 21.7717909$

$A_4 = -0.068940713$ $C_4 = 0$

$A_5 = 0$ $C_5 = 0$

(Continued)

$B_1 = 0.082055$

$B_2 = 0.0081804454$

$B_3 = -0.00074168283$ (Note this was misprinted in Reference 19 as +0.00074168283)

The Martin-Hou equation constants for perfluorocyclobutane[20] are as follows: (Temperature is in degrees R, pressure in psia and volume in ft^3/lb)

$b = 0.005655630365$

$k = 5.00$

$A_1 = 0$

$A_2 = -1.782832574$

$A_3 = 2.220141064 \times 10^{-2}$

$A_4 = -2.49243233 \times 10^{-4}$

$A_5 = 1.027671206 \times 10^{-6}$

$B_1 = 0.0536456979$

$B_2 = 0.8288016876 \times 10^{-3}$

$B_3 = -0.7000454923 \times 10^{-6}$

$B_4 = 0$

$B_5 = 0.2444029514 \times 10^{-9}$

$C_1 = 0$

$C_2 = -29.98281801$

$C_3 = 0.6970502981$

$C_4 = 0$

$C_5 = -3.742878007 \times 10^{-5}$

The Benedict-Webb-Rubin equation constants for propylene[21] are as follows: (Temperature is in degrees K, pressure in atm. and volume in liters/gm mole)

$A_0 = 4.01365$

$B_0 = 0.0467375$

$C_0 = 556,093$

$a = 1.065493$

$b = 0.0240732$

$c = 116,990$

$\alpha = 0.000349627$

$\gamma = 0.0162000$

$R = 0.0820544$

BIBLIOGRAPHY

1. Amagat, E. H., Annales de Chimie et de Physique 5e serie, t xxii, pp. 353-389 (1881).

2. American Society for Metals, Metals Handbook, Cleveland, p. 555 (1948).

3. Beattie, J. A. and Bridgeman, O. C., Proc. Amer. Acad. Arts and Sci., 63, pp. 229-308 (1928).

4. Benedict, M., Webb, G. B. and Rubin, L. C., J. Chem. Physics, 8, p. 334 (1940); and 10, p. 747 (1942).

5. Bennewitz, K. and Splittgerber, E., Z. Phys. Chem., 124, pp. 49-68 (1928).

6. Connolly, T. J., Sage, B. H. and Lacey, W. N., Ind. Eng. Chem., 43, p. 946 (1951).
   Note: This is the most recent of a long series of articles on this subject by Sage and various co-workers. It includes a list of the previous articles.

7. Curtiss, C. F., Boyd, C. A. and Palmer, H. B., J. Chem. Phys., 19, p. 801 (1951).

8. Dieterici, C., Ann. der Physik, 12, pp. 144-185 (1903).

9. Dodge, B. F., Chemical Engineering Thermodynamics, McGraw-Hill, N. Y., p. 167 et seq. (1944).

10. Eucken, A. and Hauck, F., Z. Phys. Chem., 134, pp. 161-189 (1928).

11. Fricke, R., Z. Electrochemie, 52, p. 72 (1948).

12. Farrington, P. S. and Sage, B. H., Ind. Eng. Chem., 41, pp. 1734-7 (1949).

13. Hoge, H. J., Review Sci. Inst., 20, pp. 59-61 (1949).

14. Hoge, H. J., J. of Res. NBS, 44, p. 321 (1950).

15. Joly, J., Proc. Roy. Soc., 55, p. 390 (1894).

16. Keenan, J. H., Thermodynamics, John Wiley, N. Y., p. 409 (1941).

17. Kilpatrick, J. E. and Pitzer, K. S., J. of Res. NBS, 37, p. 163 (1946).

18. McHarness, R. C., Eiseman, B. J., Jr. and Martin, J. J., Refrig. Eng., 63, p. 31 (1955).

19. Martin, J. J. and Hou, Y. C., Journ. AIChE, 1, pp. 142-151 (1955).

20. Martin, J. J., Kapoor, R. M., Bray, B. G., Reimus, R. G., Salive, M. L. and Bhada, R. K., Data and Equations for the Thermodynamic Properties of "Freon-C 318" Perfluorocyclobutane, Engineering Research Institute of the University of Michigan, 1956.

21. Marchman, H., Prengle, H. W., Jr. and Motard, R. L., Ind. Eng. Chem., 41, p. 2658 (1949).

22. Masi, J. F., Trans. ASME, 76, pp. 1067-1074 (1954).

23. Masi, J. F., JACS, 74, p. 4738 (1952).

24. Michels, A. and Strijland, J., Physica, 18, pp. 613-628 (1952).

25. Michels, A., Wassenaar, T., Louwerse, P., Lunbeck, R. J. and Wolkers, G. J., Physica, 19, pp. 287-297 (1953).
Note: In order to have a complete description of the calculational procedure used in this paper, it is necessary to refer to both:
Michels, A. and DeGroot, S. R., Appl. Sci. Res., A-1, pp. 94-102 (1948); and
Michels, A., Geldermans, M. and DeGroot, S. R., Physica, 12, pp. 105-117 (1946).

26. Mueller, E. F., Sci. Papers of NBS, #288.

27. Osborne, N. S., Stimson, H. F. and Sligh, T. S., Jr., Sci. Papers of NBS, #503.

28. Partington, J. R. and Shilling, W. G., The Specific Heat of Gases, Ernest Benn Ltd., London, p. 63 (1924).

29. Pall, D. B., Broughton, J. W. and Maass, C., Canadian J. of Research, A-16, pp. 230 and 449 (1938).

30. Perry, J. H., Chemical Engineers Handbook, McGraw-Hill, N. Y., p. 177 (1950).

31. Price, D., Ind. Eng. Chem. Data Series, 1, p. 83 (1956).

32. Randall, P. N., Bland, J., Dudley, W. M. and Jacobs, R. B., Chem. Eng. Prog., 53, p. 547 (1957).

33. Reinganum, M., Ann. der Physik, 18, p. 1008 (1905).

34. Schaefer, K., Fortschritt Chem. Forsch., 1, pp. 61-118 (1949).

35. Schneider, W. G. and Chynoweth, A., J. Chem. Phys., 19, p. 1607 (1951).

36. Sligh, T. S., Jr., Sci. Papers of NBS, #407.

37. Stull, D. R. and Mayfield, F. D., Ind. Eng. Chem., 35, p. 639 (1943).

38. Trautz, M. and Grosskinsky, O., Ann. der Physik, 67, p. 462 (1922).
Note: Several subsequent articles were published, of which the most recent was:
Trautz, M. and Trautz, O., Ann. der Physik, 86, pp. 1-65 (1928).

39. Woolley, H. W., Scott, R. B. and Brickwedde, F. G., J. of Res. NBS, 41, pp. 379-469 (1948).

40. Young, S., Proc. Phys. Soc. London, p. 602 (1894-5).